Numerical and Similarity Analysis on Heat and Mass Transfer of Liquid Film flowing along an Inclined Porous Wall

By

Md. Hasanuzzaman

A dissertation submitted in partial fulfillment of the requirements for the degree of

Doctor of Engineering (Dr. Eng.)

in

Mechanical Engineering

Department of Science and Advanced Technology

Graduate School of Science and Engineering

Saga University, Japan

March 2019

ACKNOWLEDGEMENTS

I begin with the name of Allah, the most Merciful and Beneficent. I am grateful to Almighty **Allah** for the blessings that he has bestowed upon me and for giving me the strength, peace of mind, wisdom and good health to finish this research.

I would like to express my deep gratitude to Professor Dr. Akio Miyara to accept me as Ph.D student in his laboratory. It is my proud privilege and great pleasure to work with him. I am grateful to him for his continuous support, valuable guidance, suggestions and encouragement throughout my research work. I am thankful to him for being an excellent supervisor, great motivator, intellectual magnet, and most important, never be a conservative. I really appreciate all his contributions of time from his busy schedule, support and ideas.

I would like to express my appreciation to Assoc. Prof. Dr. Keishi Kariya for his helpful suggestions, inspirations, support and shearing of his insights throughout my research. Special thanks to Dr. Mohammad Ariful Islam, Professor of Khulna University of Engineering & Technology, Bangladesh to introduce me with Professor Akio MIYARA and for his valuable guidance and suggestions in my research.

I would like to thank "Khulna University of Engineering & Technology" of Bangladesh for allowing my study leave. I would also like to acknowledge the MEXT (Ministry of Education, Culture, Sports, Science and Technology) to grant me with scholarship for this study.

Finally, I also addressed my thanks to all my lab members for their supports (especially, Ishida, Kudho, Sultan, Hasan Ali and Rabeya san). I would like to express my gratitude to all Bangladeshi, international friends and their society for making my Japan life more comfortable and enjoyable. In addition, special thanks to my beloved parents and wife (Jannatul Ferdouse) doing support me throughout my doctoral degree.

ABSTRACT

Interfacial wave behavior and flow characteristics of falling liquid films on an inclined porous wall have been studied by means of a numerical simulation. Basic equations are discretized on a staggered grid fixed on a physical space. Using the Navier-Stokes and Darcy-Brinkman equations in the film and porous layer, respectively, the problem is reduced to study of the evolution equation for the free surface of the liquid film derived through a long-wave approximation. Interfacial boundary conditions are treated with an originally proposed method and the wave behavior can be calculated accurately. Small artificial perturbations given at the inflow boundary grow rapidly and then the amplitude of the waves approaches to developed waves. Calculations have been performed in the wide range of physical parameters, in particular for inclined porous wall. Also, compare the film thickness and the velocity profile between the solid substrate and the porous wall.

Heat and mass transfer for liquid evaporation along a vertical plate covered with a thin porous layer has been investigated. The continuity, momentum, energy and mass balance equations, which are coupled nonlinear partial differential equations are reduced to a set of two nonlinear ordinary differential equations and solved analytically and numerically by using shooting technique in MATLAB. The effect of various parameters like the Froude number, the porosity, the Darcy number, the Prandtl number, the Lewis number and the other driving parameters on the flow, temperature and concentration profiles are presented and discussed. It is clearly viewed that the heat transfer performance is enhanced by the presence of a porous layer. The local Nusselt number and the local Sherwood numbers are computed and analyzed both numerically and graphically.

Similarity solution of heat and mass transfer for the falling film flow on a porous medium in presence of heat generation or absorption has been modeled by Darcy-Brinkman equations and solved by using similarity technique. Heat generation, thermal radiation and chemical reaction effects are considered. By using appropriate transformations, the governing nonlinear partial equations are transformed into coupled nonlinear ordinary differential equations. Graphs are decorated to explore the influence of physical parameters on the non-dimensional velocity, temperature and concentration distributions. The local Nusselt number and the local Sherwood number are computed and analyzed numerically.

Effect of thermal radiation and chemical reaction on heat and mass transfer flow over a moving porous sheet with suction and blowing has been investigated. Thermal radiation and chemical reaction effects are considered. By using appropriate transformations, the governing nonlinear partial equations are transformed into coupled nonlinear ordinary differential equations. Graphs are decorated to explore the influence of physical parameters on the non-dimensional velocity, temperature and concentration distributions. The skin friction, the local Nusselt number and the local Sherwood number are computed and analyzed numerically.

CONTENTS

LIST OF FIGURES

LIST OF TABLES

NOMENCLATURE

b	porosity
C	concentration
C_p	specific heat at constant pressure
C_f	skin friction
D	mass diffusivity
Da	Darcy number
d	thickness of porous layer
f	frequency
Fr	Froude number
Fr_l	Froude number in liquid film
Fr_g	Froude number in gas region
F_W	dimensionless suction/blowing parameter
g	gravitational acceleration
g_x	gravity component in the x-direction
Gr_T	Grashof number
Gr_C	modified Grashof number
h	film thickness
H	Phase change number
K	Permeability of the porous medium
Ka	Kapitza number
k^*	mean absorption coefficient
Kr'	chemical reaction rate of species concentration
Kr_x	chemical reaction parameter
l	variables of the liquid stream
Le	Lewis's number
m_v''	vapor mass flux
Nu_x	Nusselt number
N_R	thermal radiation parameter
p	pressure
Pr	Prandtl number
Pr_l	Prandtl number in liquid film

Pr_g	Prandtl number in gas region
q_l''	latent heat flux
q_s''	sensible heat flux
q_t''	total heat flux
q_r	radiation heat flux
Re	Reynolds number
Re_x	local Reynolds number
R	dimensionless suction/ blowing velocity
R_0	radius of the slender body
Sh_x	local Sherwood number
Sc	Schmidt number
T	temperature
t	time
T_w	temperature at the wall
u	velocity in x-direction
v	velocity in y-direction
$v_w < 0$	suction
$v_w > 0$	blowing or injection
We	Weber number
x	streamwise coordinate
y	transversing coordinate
μ	viscosity
μ_{eff}	effective viscosity
ν	kinematic viscosity
ε	disturbance amplitude
μ_l	dynamic viscosity in liquid film
ρ_l	density in liquid film
α_e	effective thermal diffusivity
ω	mass concentration
ω_i	vapor mass concentration
ρ	density
α_g	thermal diffusivity
ω_i	mass concentration at interface

η	similarity variable
η_l	similarity variable in liquid region
η_g	similarity variable in gas region
Γ	dimensionless inertia coefficient of non-Darcy flow
β_T	thermal expansion coefficient
β_C	solute expansion coefficient
α	thermal diffusivity of the fluid
σ^*	termed as Stafan-Boltzman constant
Δ	heat generation coefficient
δ_x	absorption coefficient

CHAPTER ONE

Introduction

1.1 Background

A falling film is the gravity flow of a continuous liquid film down a solid tube having one free surface. Flow of liquid in thin films is observed in numerous natural occurring phenomena and as well as in practical situation of importance. Due to number of peculiar characteristics, it is discussed in a separate class of flow. There are many researchers to investigate thin film behavior by using analytical, numerical and experimental techniques. Liquid film flows rise in a wide variety of applications in industry for distillation, refrigeration, chemical processing and air conditioning system, power generation and energy production facilities. Comprehensive literature reviews have been presented by Alekseenko et al. [1] and Chang [2]. As well known, the heat and mass transfer of the falling liquid film is enhanced by the interfacial waves. It is, therefore, important for explanation of the enhancement mechanism and for active use of the wave to clarify the wave behavior and flow dynamics.

Actually, solid substrates are rarely smooth, and they often are rather rough or even porous. Such situations are present in the bio-chemical, pharmaceutical, environmental, energy, and food industries. Beavers and Joseph [3] was proposed a pioneering study involving flow at a fluid-porous interface. Saffmann [4] justified theoretically the flows in the fluid and porous layers are described by the Stokes and Darcy equations, respectively, a semiempirical velocity slip boundary condition, was proposed at the interface. It involved a dimensionless slip coefficient which depends on the local geometry of the interface explained by Beavers et. al. [5]. Jeong [6] has been studied the magnitude of the slip velocity on an idealized porous wall or for a fibrous porous structure. However, Neale and Nader [7], and Brinkman, [8] expressed the geometry of the interface is generally unknown, and an alternative model consists in using the Darcy–Brinkman equation in the porous layer. In this case, partial differential equations for each region are of the same differential order and continuity of both velocity and shear stress can be satisfied at the fluid-porous interface.

There are many researchers have been studied instabilities of the interfacial waves intensively with linear, weakly nonlinear and full nonlinear stability analyses. Fulford [9],

Alekseenko et al. [1] and Chang and Demekhin [10] have been studied comprehensive reviews on wave dynamics. Instabilities of the interfacial waves have been studied intensively with linear, weak nonlinear and full nonlinear stability analyses. Interfacial waves can be developed by two ways: (i) disturbing the inlet flow rate or film thickness by periodic disturbance and (ii) by ambient noise (numeric random noise). Periodic disturbance in inlet generates periodic waves in the downstream region. The characteristics of these waves depend on frequency of inlet disturbance. On the other hand, natural waves are noise driven, and waves are selectively amplified as films flow downstream. Natural waves also evolve into solitary waves with fluctuating spacing because of amplification of ambient noise.

In modeling the rough surface as a porous medium, Neogi and Miller [11] jointly eliminated the unboundedness near the contact line and provided a foot of the correct length scale. Davis and Hocking [12] and Starov et al. [13] is imposed continuity of pressure at the interface while boundary conditions for the velocity are described either by using the Beavers and Joseph slip condition Neogi and Miller [11] or by imposing continuity of velocity and shear stress. Davis and Hocking [12] and Starov et al. [13] have been performed a theoretical study in order to characterize the interface conditions for a thin film flow past a porous layer using Reynolds and Darcy equations in the film and the porous layer, respectively. Due to the nature of these equations, Bayada and Chambat [14] have been provided a normal condition for the pressure at the interface. Previously, J. P. Pascal [15, 16] surface have been performed two stability analysis of fluid flow down an inclined isothermal porous. In both cases, Darcy's law was used for momentum transport in the porous layer and therefore viscous diffusion at the interface is not included. The results that depend on the slip coefficient values show the destabilizing effect of the permeability.

Wave formation in the falling film is closely related with the energy. Many energies in the falling film have a significant effect on hydrodynamics. Although a lot of papers is already published to discuss the wave dynamics and instability of falling film, however papers which explain the energy analysis of falling film is seldom. The disturbance kinetic energy of the film flow for a disturbance of arbitrary wave length and identified the various contributions to the disturbance kinetic energy which is analyzed by Kelly et al. [17]. Also, the disturbance kinetic energy of film flowing over oscillating plate using same equations which is discussed by Lin et al. [18] and Lin and Chen [19]. So, wave suppression were the main objectives of those studies. Although energy analysis of falling film is an important

issue which is required to be addressed more elaborately, however still a lacking in complete energy analysis of the falling film. This lacking motivated to do a complete analysis of various energies of the falling film with their wave dynamics.

Fluid dynamics is a subject of widespread interest to researcher and it became an obvious challenge for the scientists, engineers as well as users to understand more about fluid motion. An important contribution to the fluid dynamics is the concept of boundary layer flow introduced first by L. Prandtl [20]. The concept of the boundary layer is the consequence of the fact that flows at high Reynolds numbers can be divided into unequally spaced regions. A very thin layer (called boundary layer) in the vicinity (of the object) in which the viscous effects dominate, must be taken into account, and for the bulk of the flow region, the viscosity can be neglected, and the flow corresponds to the in viscid outer flow. Although the boundary layer is very thin, it plays a vital role in the fluid dynamics. Boundary layer theory has become an essential study now-a-days in analyzing the complex behaviors of real fluids. The concept of boundary layer can be used to simplify the Navier-Stocks' equations to such an extent that the viscous effects of flow parameters are evaluated, and these are useable in many practical problems (viz the drag on ships and missiles, the efficiency of compressors and turbines in jet engines, the effectiveness of air intakes for ram and turbojets and so on).

Effective latent heat transfer mechanism widely utilized in industrial fields such as chemical distillation, air conditioning, cooling towers, drying, and desalination which is liquid film evaporation. With the liquid film exposed to a forced gas stream, the physical scheme consists of a thin liquid film flowing down along a heated plate. Because part of the liquid evaporates into the gas stream, liquid film evaporation possesses a high heat transfer coefficient, low feed rates and other inherent advantages. However, the transport phenomena involve the coupled heat and mass transfer at the liquid film–gas interface because the theoretical analysis of liquid film evaporation problem is inherently complicated. There are many researches with more rigorous treatments of the equations governing the liquid film and liquid–gas interface has been published. The evaporative cooling of liquid film through interfacial heat and mass transfer in a vertical channel was studied by Yan and Lin [21]. The numerical solution for convective heat and mass transfer along an inclined heated plate with film evaporation which presented by Yan and Soong [22]. The free convection boundary layer flow of a Darcy–Brinkman fluid induced by a

horizontal surface embedded in a fluid-saturated porous layer which is explained by Rees and Vafai [23] for the studies of heat and mass transfer for liquid film flow in porous medium. The fluid flow and heat transfer interfacial conditions between a porous medium and a fluid layer which is detailed analyzed by Alazmi and Vafai [24]. The coupled heat and mass transfer in a stagnation point flow of air through a heated porous bed with thin liquid film evaporation studied by Zhao [25]. Also, Zhao [25] assumed the liquid layer was very thin and stationary, and the air stream was idealized as the stagnation point flow pattern to achieve the analytical solution.

Further the boundary layer effects caused by free convection are frequently observed in our environmental happenings and engineering devices. We know that if externally induced flow is provided and flows arising naturally solely due to the effect of the differences in density, caused by temperature or concentration differences in the body force field (such as gravitational field). This type is called `free convection' or 'natural convection' flow. The density difference causes buoyancy effects and these effects act as 'driving forces' due to which the flow is generated.

Khader and Megahed [26] are presented a numerical technique which is the implicit finite difference method to the search for the numerical solutions for the given equations. Their technique reduces the problem to a system of algebraic equations. Recently, M. Hasanuzzaman and A. Miyara [27] have been studied a possible similarity solution of unsteady natural convection laminar boundary layer flow of viscous incompressible fluid caused by a heated (or cooled) axi-symmetric slender body of finite axial length immersed vertically in a viscous incompressible fluid. Thus, it is imperative to reduce the number of variables from the system which reached in a stage of great extent. Similarity solution is one of the important means for the reduction of a number of independent variables with simplifying assumptions and finally the system of partial differential equations reduces to a set of ordinary differential equations successfully. A vast literature of similarity solution has appeared in the area of fluid mechanics, heat transfer, and mass transfer, etc. The similarity solutions in the context of mixed convection boundary layer flow of steady viscous incompressible fluid over an impermeable vertical flat plate were discussed by Ishak et al. [28]. Ramanaiah et al. [29] studied the similarity solutions of free, mixed and forced convection problems in a saturated porous media.

Suction (or blowing) is one of the useful means in preventing boundary layer separation. The effect of suction consists in the removal of decelerated particles from the boundary layer before they are given a chance to cause separation. The surface is considered to be permeable to the fluid, so that the surface will allow a non-zero normal velocity and fluid is either sucked or blown through it. In doing this however, no-slip condition $u_w = 0$ at the surface (non-moving) shall continue to remain valid. Suction or blowing causes double effects with respect to the heat transfer. On the one hand, the temperature profile is influenced by the changed velocity field in the boundary-layer, leading to a change in the heat conduction at the surface. On the other hand, convective heat transfer occurs at the surface along with the heat conduction for $v_W \neq 0$. A summary of flow separation and its control are found in Chang [30, 31]. The study of natural convection on a horizontal plate with suction and blowing is of huge interest in many engineering applications, for instance, transpiration cooling, boundary layer control and other diffusion operations.

1.2 Objective of this present study

In this thesis, we studied two types of studies which are numerical simulation as well as similarity analysis.

First is numerical simulation:

For numerical simulation, wavy falling liquid films are simulated with a finite difference method of which algorithm is based on MAC method. Although the adaptive grid has the advantage for the free boundary condition as mentioned before, an originally proposed advanced technique for the fixed grid is employed in the present simulation. Neglecting the interfacial shear stress is only an assumption for the present numerical simulation. Waves are generated by temporal periodic small-amplitude disturbances with a specific frequency at the flow inlet. Calculations have been performed in the wide range of physical parameters, in particular for vertical and slightly inclined films. The simulation code is developed by extending the previous work by Miyara [32] for hydrodynamics of wavy falling film.

Second is similarity analysis:
For similarity analysis, to find a possible similarity solution of heat and mass transfer for liquid evaporation along a vertical plate covered with a thin porous layer. We are attempted

to investigate the effects of several involved parameters on the velocity, temperature and concentration fields. The numerical results including the velocity, temperature and concentration fields are to be presented graphically for different selected values of the established dimensionless parameters. The local skin friction, local Nusselt number and the local Sherwood numbers are computed numerically and graphically as well as analyzed.

To investigate the effect of heat generation or absorption, thermal radiation and chemical reaction on the velocity, temperature and concentration fields in the thin liquid film on a porous medium. Mathematical modelling is developed under the considerations of heat generation or absorption, thermal radiation and chemical reaction stratification effects. The effects of various emerging parameters on velocity, temperature as well as concentration fields are presented graphically. The local Nusselt number and the local Sherwood numbers are computed and analyzed both numerically and graphically.

Also, to investigate the effect of thermal radiation and chemical reaction on heat and mass transfer flow over a moving porous sheet with suction and blowing. Under the consideration of thermal and chemical reaction stratification effects the Mathematical modelling is developed. The effects of various emerging parameters on the velocity, temperature and concentration fields are presented through graphically and tables. The local Nusselt number and the local Sherwood numbers are computed numerically and analyzed.

1.3 Outline of the thesis

This thesis is composed of Seven Chapters.

Chapter One: An introduction of basic principles of boundary layer theory, natural convection flows, suction and blowing phenomena with historical review of earlier researches and background of our problem are presented in chapter one.

Chapter Two: Chapter two provides the numerical simulation of wavy liquid film flowing along inclined porous wall. To observe the effect of various parameters on the film thickness along the downstream. Also, compared the film thickness and velocity between solid substrate and porous wall.

Chapter Three: Chapter three also provides numerical simulation of wavy liquid film. In this chapter included energy equation. To observe the effect of the various parameters on the

film thickness along the downstream. Also, compared the velocity between solid substrate and porous wall.

Chapter Four: In chapter four we constructed a physical model and corresponding governing equations with the boundary conditions. Then we used a similarity technique which is converted partial differential equations into ordinary differential equations. Under the considered condition, the numerical solutions with graphs has also given here for some selected values of the established parameters. Moreover, the local skin friction, the local Nusselt number and the local Sherwood numbers are computed numerically and analyzed.

Chapter Five: To investigate the effect of heat generation or absorption, thermal radiation and chemical reaction on the velocity, temperature and concentration fields in the thin liquid film on a porous medium. Mathematical modelling is developed under the considerations of heat generation or absorption, thermal radiation and chemical reaction stratification effects. The effects of various emerging parameters on velocity, temperature as well as concentration fields are presented graphically. The local Nusselt number and the local Sherwood numbers are computed and analyzed both numerically and graphically.

Chapter Six: In this chapter, we also developed a physical model and corresponding predicted governing equations with the boundary conditions. Also, the partial differential converted into the ordinary differential equations by using the similarity transform. The effect of thermal radiation, chemical reaction and other parameters on velocity, temperature and concentration, respectively. Moreover, the local skin friction, the local Nusselt number and the local Sherwood numbers are computed numerically and analyzed.

Chapter Seven: In chapter seven, the conclusions gained from this present work and brief descriptions for further works related to our present research are discussed.

References

[1] Alekseenko S.V., Nakoryakov V.E., Pokusaev B.G., 1994. Wave Flow of Liquid Films, Begell House, New York.

[2] H.-C. Chang, 1994. Wave evolution on a falling film, Annu. Rev. Fluid Mech. 26, 103.

[3] G. S. Beavers and D. D. Joseph, 1967. Boundary conditions at a naturally permeable wall, J. Fluid Mech. 30, 197.

[4] P. G. Saffman, 1971. On the boundary condition at the surface of a porous medium, Stud. Appl. Math. 50, 93.

[5] G. S. Beavers, E. M. Sparrow, and R. A. Magnuson, 1970. Experiments on coupled parallel flows in a channel and a bounding porous medium, J. Basic Eng. 92, 843.

[6] J. T. Jeong, 1884. Slip boundary condition on an idealized porous wall, Phys. Fluids 13.

[7] G. Neale and W. Nader, 1974. Practical significance of Brinkman's extension of Darcy's law: Coupled parallel flow within a channel and a bounding porous medium, Can. J. Chem. Eng. 52, 475.

[8] H. C. Brinkman, 1947. A calculation of the viscous force exerted by flowing fluid on a dense swarm of particles," Appl. Sci. Res. A1, 27.

[9] Fulford, G. D., 1964. The flow of liquid in thin films. Adv. Chem. Eng. 5, 151.

[10] Chang H-C, Demekhin, E.A., 2002. Complex wave dynamics on thin films. Elsevier,

[11] P. Neogi and C. A. Miller, 1983. Spreading kinetics of a drop on a rough solid surface, J. Colloid Interface Sci. 92, 338.

[12] S. H. Davis and L. M. Hocking, 1999. Spreading and imbibition of viscous liquid on a porous base," Phys. Fluids 11, 48.

[13] V. M. Starov, S. R. Kosvintsev, V. D. Sobolev, M. G. Velarde, and V. G. Zhdanov, 2002. Spreading of liquid drops over saturated porous layers, J. Colloid Interface Sci. 246, 372.

[14] Bayada and M. Chambat, 1995. On interface conditions for a thin film flow past a porous medium, SIAM J. Math. Anal. 26, 1113.

[15] J. P. Pascal, 1999. Linear stability of fluid flow down a porous inclined plane, J. Phys. D 32, 417.

[16] J. P. Pascal, 2006. Instability of power-law fluid flow down a porous incline, J Non-Newtonian Fluid Mech. 133, 109.

[17] Kelly, R. E., Goussis, D. A., Lin, S. P., Hsu, F. K., 1989. The mechanism for surface

[18] Lin, S. P., Chen, J. N., Woods, D. R., 1996. Suppression of instability in a liquid film flow. Phys. Fluids 8 (12), 3247-3252.

[19] Lin, S. P., Chen, J. N., 1998. The mechanism of surface wave suppression in film flow down a vertical plane. Phys. Fluids 10 (8), 1787-1792.

[20] Prandtl, L., 1904, "Uber Flussigkeitsbewegungen bei sehr kleiner Intern.", Math. Congr. Heidelberg, 484 – 491.

[21] W.M. Yan, T.F. Lin, 1991. Evaporative cooling of liquid film through interfacial heat and mass transfer in a vertical channel—II. Numerical study, Int. J. Heat Mass Transfer 34,1113–1124.

[22] W.M. Yan, C.Y. Soong, 1995. Convection heat and mass transfer along an inclined heated plate with film evaporation, Int. J. Heat Mass Transfer 38, 1261–1269.

[23] D.A.S. Rees, K. Vafai, 1999. Darcy–Brinkman free convection from a heated horizontal surface, Numer. Heat Transfer, Pt A 35, 191–204.

[24] B. Alazmi, K. Vafai, 2001. Analysis of fluid and heat transfer interfacial conditions between a porous medium and a fluid layer, Int. J. Heat Mass Transfer 44, 1735–1749.

[25] T.S. Zhao, 1999. Coupled heat and mass transfer of a stagnation point flow in a heated porous bed with liquid film evaporation, Int. J. Heat Mass Transfer 42 861–872.

[26] Khader M. M., Megahed Ahmed M., 2013. Numerical simulation using the finite difference method for the flow and heat transfer in a thin liquid film over an unsteady stretching sheet in a saturated porous medium in the presence of thermal radiation, Journal of King Saud University – Engineering Sciences 25, 29 – 34.

[27] Md. Hasanuzzaman and Akio Miyara, 2017. Similarity solution of natural convective boundary layer flow around a vertical slender body with suction and blowing, J. Mech. Cont. & Math. Sci., 11, 8-22.

[28] Ishak A., Nazar R., and Pop I., 2007, “Duall solutions in mixed convection boundary-layer flow with suction or injection”, IMA Journal of Applied Mathematics, 1 – 13.

[29] Ramanaiah G. Malarvizhi G., 1989, “Unified treatment of similarity solutions of free, mixed and forced convection problems in saturated porous media”, Proc. Of Sixth Int. Conf. on Numerical Method in Thermal Problems, Swansea, U.K.,431 – 439.

[30] Chang, P. K., 1970, “Separation of flow”, Pergamon Press, Oxford.

[31] Chang, P. K., 1976, “Control of flow Separation”, Hemis-phere Publ. Corp., Washington, D. C.

[32] Akio Miyara, 2000. Numerical simulation of wavy liquid film flowing down on a vertical wall and an inclined wall, Int. J. Therm. Sci. 39, 1015–1027.

CHAPTER TWO

Numerical Simulation of Wavy Liquid Film Flowing Along an Inclined Porous Wall

2.1 Introduction

Waves generated on an interface of a thin falling liquid film down an inclined or vertical wall have been studied extensively because of the scientific interests and very wide application in the fields of engineering. Liquid layers flowing on a solid wall and possessing a free surface can be described by a film thickness evolution equation obtained through a long-wave approximation of the Navier–Stokes equations (Chang, [2] and Oron et al., [3]). Most works consider a smooth solid impervious substrate and therefore a no-slip and no-penetration boundary conditions for the fluid velocity at the fluid/substrate interface is adopted. In that case, Benney [4] showed that past a critical Reynolds number the base flow is unstable to a long-wave instability. However, Benney-type equations even with stabilizing surface tension have only a limited validity range since they lead to blow-up of solutions in finite time, which is not the case when solving the full Navier–Stokes equations (Rosenau at el., [5] and Salamon at el., [6], Oraon and Gottlieb, [7] and Scheid at el., [8]). The hydrodynamic stability of a falling film on a porous substrate is a currently developing subject because of its application to several technology processes, for instance food manufacturing, and because of its relevance to geophysical problems, such as rill flows and surface waves over soil systems. Comprehensive literature reviews have been presented by Alekseenko et al. [1] and Chang [2]. As well known, the heat and mass transfer of the falling liquid film is enhanced by the interfacial waves. It is, therefore, important for explanation of the enhancement mechanism and for active use of the wave to clarify the wave behavior and flow dynamics.

A pioneering study involving flow at a fluid-porous interface was performed by Beavers and Joseph [9]. The flows in the fluid and porous layers are described by the Stokes and Darcy equations, respectively, a semiempirical velocity slip boundary condition, justified theoretically by Saffmann [10], was proposed at the interface. It involved a dimensionless slip coefficient which depends on the local geometry of the interface (Beavers, [11]). Recently, the magnitude of the slip velocity has been studied on an idealized porous wall

(Jeong, [12]) or for a fibrous porous structure (James and Davis, [13] and Levy, [14]). However, the geometry of the interface is generally unknown, and an alternative model consists in using the Darcy–Brinkman equation in the porous layer (Neale and Nader [15], and Brinkman, [16]). In this case, partial differential equations for each region are of the same differential order and continuity of both velocity and shear stress can be satisfied at the fluid-porous interface.

Many researchers have been studied instabilities of the interfacial waves intensively with linear, weakly nonlinear and full nonlinear stability analyses. The linear analyses (Benjamin [17], Yin[18], Bankoff [19], Penev at el. [20], Marschall and Lee [21], Pierson and Whitaker [22], and Solorio and Sen [23], are, however, limited only to the initial stage of wave inception and the weakly nonlinear analyses (Benney [24], Lin[25], Gjevik [26], Nakaya and Takaki [27], Nakaya [28], Unsal and Thomas [29], and Pumir et al. [30]) are developed to study the evolution subsequent to wave inception. Although the full nonlinear solution (Pumir et al. [30] and Joo et al. [31]) based on the long-wave boundary layer equations has been obtained numerically, finite-amplitude permanent waves are assumed, and the stationary equations are solved in a frame of reference translating with the wave velocity. Three-dimensional instabilities have been studied by Joo and Davis [32] and Chan et al. [33]. All the analytical studies, however, focus only on the wave instability and the evolution behavior, and the flow characteristics in the liquid film have not been discussed sufficiently. Two stability analysis of fluid flow down a inclined isothermal porous surface have been previously performed (Pascal [34], and Pascel [35],). In both cases, Darcy's law was used for momentum transport in the porous layer and therefore viscous diffusion at the interface is not included. The results that depend on the slip coefficient values show the destabilizing effect of the permeability.

The finite difference method is also widely used [36–40]. Most of researchers employed an adaptive grid fitted to the free surface because the adaptive grid has an advantage to apply easily the exact free boundary conditions. Nagasaki and Hijikata [36] employed the adaptive grid. They calculated variations from small amplitude sinusoidal disturbance to fully developed solitary wave, composed of a big wave and small waves, under the periodic boundary condition. They recognized the existence of a circulation flow in the big wave. In order to modify the temporal film thickness variation, a constant mean film thickness in the whole calculation region was applied. This method, however, seems to be impertinent to the falling film, because the mean film thickness under constant flow rate condition may be changed depending on the variation of the mean velocity. They mentioned the increase of the

mean flow rate with the development of the wave. Therefore, it is necessary to develop the alternative appropriate correction method for the temporal film thickness variation. Kiyata et al. [37] calculated variations of wave shape with the similar manner of Nagasaki and Hijikata [36]. They calculated the initial stage of wave evolution and compared the calculated wave evolution with the linear stability theory. Stuhlträger et al. [38], [39] solved a wavy condensate film with a self-modified MAC method under an outflow boundary condition proposed by Shapiro and O'Brien [41]. In their calculation, the velocity profile at the interface is approximated by a parabolic function and the interfacial boundary condition treated insufficiently.

In the present study, wavy falling liquid films are simulated with a finite difference method of which algorithm is based on MAC method. Although the adaptive grid has the advantage for the free boundary condition as mentioned before, an originally proposed advanced technique for the fixed grid is employed in the present simulation. Neglecting the interfacial shear stress is only an assumption for the present numerical simulation. Waves are generated by temporal periodic small-amplitude disturbances with a specific frequency at the flow inlet. Calculations have been performed in the wide range of physical parameters, in particular for vertical and slightly inclined films. The simulation code is developed by extending the previous work by Miyara [40] for hydrodynamics of wavy falling film.

2.2 Model and Governing Equations

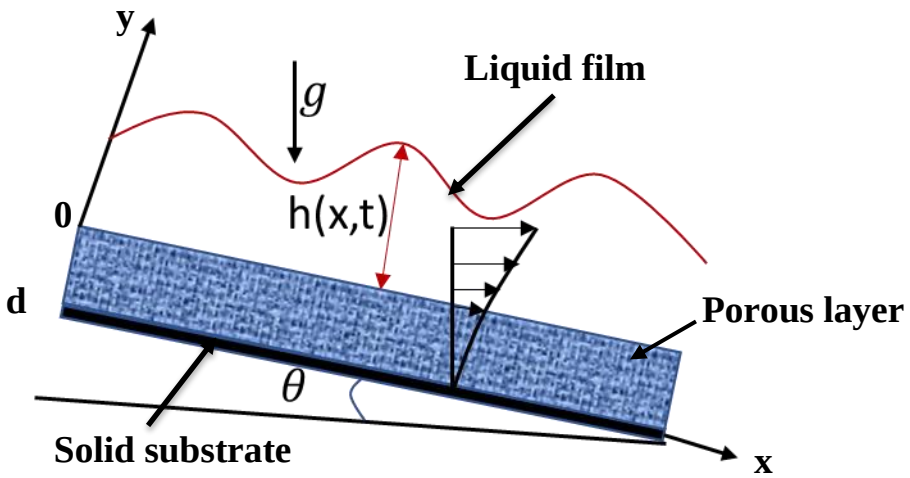

Figure 2.1: physical model and coordinates for a two-dimensional falling liquid film down an inclined porous wall.

We consider a two-dimensional incompressible Newtonian liquid fluid flowing over an inclined porous wall, saturated by the same liquid from the side of the substrate (Figure 2.1). Note that we consider a porous layer of a finite constant thickness *d* on a nonporous outer wall.

The hydrodynamics of falling can be expressed by following continuity equation and Navier-Stokes equations.

Continuity equation

$$\frac{\partial u'}{\partial x'} + \frac{\partial v'}{\partial y'} \tag{2.1}$$

Navier-Stokes equations

$$\rho\left(\frac{\partial u'}{\partial t'} + u'\frac{\partial u'}{\partial x'} + v'\frac{\partial u'}{\partial y'}\right) = -\frac{\partial p'}{\partial x'} + \mu\left(\frac{\partial^2 u'}{\partial x'^2} + \frac{\partial^2 u'}{\partial y'^2}\right) + \rho g\, sin\theta \tag{2.2}$$

$$\rho\left(\frac{\partial v'}{\partial t'} + u'\frac{\partial v'}{\partial x'} + v'\frac{\partial v'}{\partial y'}\right) = -\frac{\partial p'}{\partial y'} + \mu\left(\frac{\partial^2 v'}{\partial x'^2} + \frac{\partial^2 v'}{\partial y'^2}\right) - \rho g\, cos\theta \tag{2.3}$$

In the following, buoyancy will be neglected since we consider sufficiently thin films. The liquid film flow inside the porous substrate is described using the Darcy-Brinkman equation (Goyeau et al. [45], Whitaker, [46] and Bousquet et al., [47]).

$$\frac{\partial \tilde{u}'}{\partial x'} + \frac{\partial \tilde{v}'}{\partial y'} = 0 \tag{2.4}$$

$$\frac{\rho}{b}\frac{\partial \tilde{u}'}{\partial t'} = -\frac{\partial \tilde{p}'}{\partial x'} + \mu_{eff}\left(\frac{\partial^2 \tilde{u}'}{\partial x'^2} + \frac{\partial^2 \tilde{u}'}{\partial y'^2}\right) - \frac{\mu}{K}\tilde{u}' + \rho g\, sin\theta \tag{2.5}$$

$$\frac{\rho}{b}\frac{\partial \tilde{v}'}{\partial t'} = -\frac{\partial \tilde{p}'}{\partial y'} + \mu_{eff}\left(\frac{\partial^2 \tilde{v}'}{\partial x'^2} + \frac{\partial^2 \tilde{v}'}{\partial y'^2}\right) - -\frac{\mu}{K}\tilde{v}' - \rho g\, cos\theta \tag{2.6}$$

where $\tilde{u}'$ and $\tilde{v}'$ are the filtration velocities in the x and y-directions, *k* is the permeability, *b* is the porosity, ρ is the density, and μ_{eff} represents the effective viscosity. Following Whitaker [46], the reduced viscosity is given by $\frac{\mu}{\mu_{eff}} = \frac{1}{b}$. The flow in the porous wall is assumed to be slow enough to neglect inertial (Bousquet et al., [47]).

Definitions of dimensionless coordinates and variables are as follows:

$$x = \frac{x'}{\delta_0}, \;\; y = \frac{y'}{\delta_0}, \qquad t = \frac{\varepsilon u_0}{\delta_0} t' \tag{2.7}$$

$$u = \frac{u'}{u_0}, \;\; \tilde{u} = \frac{\tilde{u}'}{u_0}, \;\; v = \frac{v'}{u_0}, \;\; \tilde{v} = \frac{\tilde{v}'}{u_0} \tag{2.8}$$

$$p = \frac{p'}{\rho u_0^2}, \qquad \tilde{p} = \frac{\tilde{p}'}{\rho u_0^2}, \quad h = \frac{h'}{\delta_0} \tag{2.9}$$

where δ_0 is the mean thickness of the film and ε is the ratio of the length scales $\frac{\delta_0}{L} \ll 1,$, L denotes the characteristic length scale for a surface deformation, $\delta = \frac{d}{\delta_0}$ is the dimensionless thickness of the porous substrate.

Above continuity equation and Navier-Stokes equations are converted into dimensionless by assuming constant physical properties.

Continuity equation

$$\frac{\partial u}{\partial x} + \frac{\partial v}{\partial y} = 0 \tag{2.10}$$

Navier-Stokes equations

$$\frac{\partial u}{\partial t} + u\frac{\partial u}{\partial x} + v\frac{\partial u}{\partial y} = -\frac{\partial p}{\partial x} + \frac{1}{Re_0}\left(\frac{\partial^2 u}{\partial x^2} + \frac{\partial^2 u}{\partial y^2}\right) + \frac{1}{Fr_{x0}} \tag{2.11}$$

$$\frac{\partial v}{\partial t} + u\frac{\partial v}{\partial x} + v\frac{\partial v}{\partial y} = -\frac{\partial p}{\partial y} + \frac{1}{Re_0}\left(\frac{\partial^2 v}{\partial x^2} + \frac{\partial^2 v}{\partial y^2}\right) + \frac{1}{Fr_{y0}} \tag{2.12}$$

While in the porous layer they take the form

Continuity equation

$$\frac{\partial \tilde{u}}{\partial x} + \frac{\partial \tilde{v}}{\partial y} = 0 \tag{2.13}$$

Navier-Stokes equations

$$\frac{1}{b}\frac{\partial \tilde{u}}{\partial t} = -\frac{\partial \tilde{p}}{\partial x} + \frac{1}{Re_0}\left(\frac{\partial^2 \tilde{u}}{\partial^2 x} + \frac{\partial^2 \tilde{u}}{\partial^2 y}\right) - \frac{1}{Da\, Re_0}\tilde{u} + \frac{1}{Fr_{x0}} \tag{2.14}$$

$$\frac{1}{b}\frac{\partial \tilde{v}}{\partial t} = -\frac{\partial \tilde{p}}{\partial y} + \frac{1}{Re_0}\left(\frac{\partial^2 \tilde{v}}{\partial^2 x} + \frac{\partial^2 \tilde{v}}{\partial^2 y}\right) - \frac{1}{Da\, Re_0}\tilde{v} + \frac{1}{Fr_{y0}} \tag{2.15}$$

where $\mathrm{Re}_0 = \frac{\rho u_0 \delta_0}{\mu}$ is the Reynolds number and $Da = \frac{k}{\bar{h}^2}$ is the number representing the dimensionless permeability. Hence, the porosity is not necessarily related to the Darcy number and its influence on the stability of the film will be studied independently of the dimensionless permeability.

The following relation between u_0 and δ_0 is given by:

$$u_0 = \frac{\rho \delta_0^2 \, sin\alpha}{2\mu} \tag{2.16}$$

From this above equation, the dimensionless parameters are satisfied the following relations:

$$Fr_{x0} = \frac{1}{2} Re_0, \qquad Fr_{y0} = \frac{1}{2} Re_0 tan(\pi - \theta) \tag{2.17}$$

2.3 Boundary Conditions

2.3.1 Wall Surface

Boundary conditions of the velocity at the wall surface are given as follows:

$$\tilde{u} \neq 0, \quad \tilde{v} \neq 0 \quad \text{at} \quad y = 0 \tag{2.18}$$

Pressure at the wall surface is obtained by substituting equation (2.18) into the Navier–Stokes equation of *y*-direction (2.15):

$$\frac{\partial \tilde{p}}{\partial y} = \frac{1}{Re_0} \frac{\partial^2 \tilde{v}}{\partial^2 y} + \frac{1}{Fr_{y0}} \tag{2.19}$$

2.3.2 Interface

With the following kinematic boundary condition, the temporal variation of the film thickness is calculated:

$$\frac{\partial h}{\partial t} = \tilde{v} - \tilde{u} \frac{\partial h}{\partial x} \tag{2.20}$$

On the other hand, by integrating the continuity equation (2.13) between the limits *y*=0 *to y=h.*

$$\int_0^h \frac{\partial \tilde{u}}{\partial x} dh + \tilde{v}_{y=h} = 0 \tag{2.21}$$

From the differential and integral calculus,

$$\frac{\partial}{\partial x}\int_0^h \tilde{u}dy = \tilde{u}_{y=h}\frac{\partial h}{\partial x} + \int_0^h \frac{\partial \tilde{u}}{\partial x}dy \tag{2.22}$$

Consequently, from equations (2.20)– (2.22) we obtain the following equation:

$$\frac{\partial}{\partial x}\int_0^h \tilde{u}dy + \frac{\partial h}{\partial t} = 0 \tag{2.23}$$

Because calculated film thickness of new time step does not satisfy mass conservation due to truncation error, a correction of the new film thickness is required.

Including the effects of pressure, surface tension, and momentum, the force balance normal to the interface is obtained and the pressure at the interface is calculated with the following equations:

$$p = \frac{-\frac{\partial^2 h}{\partial x^2}}{We_0\left[1+\left(\frac{\partial h}{\partial x}\right)^2\right]^{\frac{3}{2}}} + \frac{2}{Re_0\left[1+\left(\frac{\partial h}{\partial x}\right)^2\right]}\left[\frac{\partial \tilde{u}}{\partial x}\left(\frac{\partial h}{\partial x}\right)^2 - \left(\frac{\partial \tilde{u}}{\partial y}+\frac{\partial \tilde{v}}{\partial x}\right)\frac{\partial h}{\partial x} + \frac{\partial \tilde{v}}{\partial y}\right] \tag{2.24}$$

where We_0 is the Weber number, defined as

$$We_0\frac{\rho u_0^2 \delta_0}{\sigma} \tag{2.25}$$

By using equation (2.16), We_0 can be rewritten as

$$We_0 = Re_0^{\frac{5}{3}}\left(\frac{1}{2}Ka\ sin\alpha\right)^{\frac{1}{3}} \tag{2.26}$$

where Ka is the Kapitza number, defined as

$$Ka = \frac{g\mu^4}{\rho\sigma^3} \tag{2.27}$$

By neglecting the shear stress from the vapor phase, the force and momentum balance in the tangential direction becomes as follows:

$$\left(\frac{\partial \tilde{u}}{\partial y}+\frac{\partial \tilde{v}}{\partial x}\right)\left[1-\left(\frac{\partial h}{\partial x}\right)^2\right]-2\frac{\partial h}{\partial x}\left(\frac{\partial \tilde{u}}{\partial x}-\frac{\partial \tilde{v}}{\partial y}\right) \tag{2.28}$$

2.3.3 Inflow Boundary

At the inflow boundary, the film thickness is disturbed with the following equation.

$$h = 1 + H + F(t) \tag{2.29}$$

Two types of waves are modeled in this simulation: periodic force waves and natural waves. Periodic force waves are modeled by giving following periodic disturbance in the inflow boundary.

$$F(t) = \varepsilon\, sin(2\pi f t) \tag{2.30}$$

where ε is the disturbance amplitude and *f* is the dimensionless frequency, defined as

$$f = \frac{f'\delta_0}{u_0} \tag{2.31}$$

f' is the frequency with dimension Hz.

Nusselt solution is used to give an average film thickness and velocity profiles at inflow boundary. The amplitude of the disturbance wave is given as $\varepsilon = 0.05$. The magnitude of the amplitude affects wave growth rate while effects on the fully developed waves are small.

Natural waves are modeled by giving following random noise (white noise) in the inflow boundary in similar manner.

$$F(t) = \int_0^\infty \hat{F}(\omega)\, exp(-i\omega t)d\omega = \int_0^\infty \left|\hat{F}(\omega)\right| exp(i\alpha(\omega) - i\omega t)d\omega \tag{2.32}$$

where ω is angular frequency and $\alpha(\omega)$ is the phase of the complex amplitude $\hat{F}(\omega)$. Eq. (2.32) is approximated with *M* frequency units of width $\Delta\omega = \omega^*/M$. Where ω^* is some high frequency cutoff.

$$F(t) = \sum_{k=1}^{M} \left|\hat{F}(\omega)\right| exp(i\alpha(\omega_k) - ik\,\Delta\omega t)\Delta\omega \tag{2.33}$$

The phase $\alpha_k = \alpha(\omega_k)$ is taken from a random number generator from the range $\alpha_k \in [0, 2\pi]$ and $\left|\hat{F}(\omega)\right|$ can be arbitrarily specified.

2.3.4 Outflow Boundary

At outflow boundary, the following equations are employed for *x*-direction velocity $\tilde{u}$ and pressure $\tilde{p}$

$$\frac{\partial \tilde{u}}{\partial x} = 0, \qquad \frac{\partial \tilde{p}}{\partial x} = 0 \tag{2.34}$$

From the above equations, the continuity equation, and the wall boundary condition, *y*-direction velocity $\tilde{v}$ becomes $\tilde{v} = 0$.

2.3.5 Initial Condition

At t=0, the film thickness is one in the whole simulation region. Initial values of velocities and pressure are given from the Nusselt theory.

2.4 Numerical Simulation Method

2.4.1 Wall Surface and Film Inside

The algorithm of the present calculation is based on the MAC method. Inside the liquid film and at the wall surface, the convection terms and the diffusion terms of the basic equations are discretized by the third-order upwind scheme and the second-order central-difference scheme, respectively. Near the film surface, where the third-order upwind scheme cannot be applied, the donor cell method is employed.

2.4.2 Interface

At the closest grid points to the interface, the donor cell method and the second-order central-difference scheme are also employed. However, values at the grid points outside of the liquid film, which are shown as open symbols in Figure 2.2, are unknown, though they are necessary. The values of $u_{i,J+1}$, which are at outside grid points, are extrapolated with the following scheme by using the values inside the film and the interfacial boundary condition, equation (2.28):

$$u_{i,J+1} = u_{i,J} + \frac{1}{2}\left(\left.\frac{\partial u}{\partial y}\right|_{J} + \left.\frac{\partial u}{\partial y}\right|_{J+1}\right)\Delta y$$

$$= u_{i,J} + \frac{1}{2}\left[\left.\frac{\partial u}{\partial y}\right|_{J} + \left.\frac{\partial u}{\partial y}\right|_{h} + \frac{\Delta y'}{3\Delta y/2 - \Delta y'}\left(\left.\frac{\partial u}{\partial y}\right|_{h} - \left.\frac{\partial u}{\partial y}\right|_{J-1}\right)\right]\Delta y \qquad (2.35)$$

Where $\left.\partial u/\partial y\right|_h$ is calculate from equation (2.28). The *x*-direction surface velocity $u_{s,i}$ is obtained by interpolating from $u_{i,J}$ and $u_{i,J+1}$. $u_{i+1,J}$ is extrapolated from $u_{i,J}$ and u^*, which is calculated from $u_{s,i}$ and $u_{s,i+1}$.

$v_{(i),(J)}$ is calculated from the following equation:

$$\frac{u_{i+1,J} - u_{i,J}}{\Delta x} + \frac{v_{(i),(J)} - v_{(i),(J-1)}}{\Delta y} = 0 \qquad (2.36)$$

Then *y*-direction surface velocity $v_{s,(i)}$ is interpolated from $v_{(i),(J)}$ and $v_{(i),(J-1)}$.

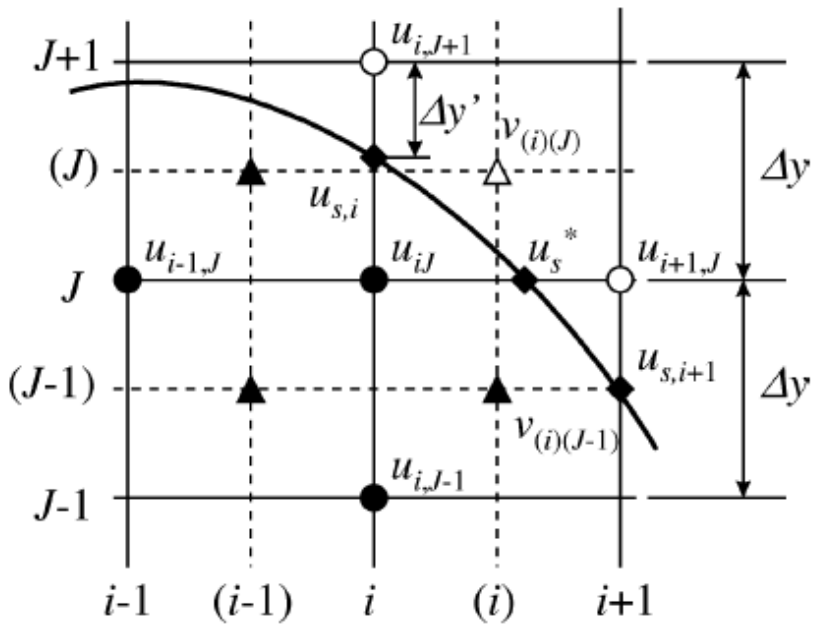

Figure 2.2. Staggered grid fixed on the physical space near the interface

2.4.3 Film Thickness

The temporal film thickness variation is calculated from the kinematic boundary condition equation (2.20). Considering the movement of a particle which reaches a grid point (*i*) at new time step *n*+1 as shown in Figure 2.3, equation (2.20) may be rewritten and a new film thickness at the point (*i*) calculated with the following equation:

$$\tilde{h}_{(i)}^{n+1} = h_{(i)}^{n} + v^{*}\Delta t - \left(h_{(i)}^{n} - h^{*} \right) \tag{2.37}$$

The calculated film thickness, however, does not satisfy the mass conservation at new time step because of the truncation error. Although Nagasaki and Hijikata (1989) corrected the film thickness with the constant volume condition, this method is inappropriate to the falling film since it causes increase of the mean flow rate. By using equation (21) derived from continuity equation, the correction value can be obtained as follows:

$$\Delta h = -\left(\tilde{h}_{(i)}^{n+1} - h_{(i)}^{n} \right) - \left[\int_{0}^{\tilde{h}} \tilde{u}\,dy\Big|_{i+1} - \int_{0}^{\tilde{h}} \tilde{u}\,dy\Big|_{i} \right] \frac{\Delta t}{\Delta x} \tag{2.38}$$

Therefore, the new film thickness which satisfies the mass conservation is

$$h_{(i)}^{n+1} = \tilde{h}_{(i)}^{n+1} + \Delta h \tag{2.39}$$

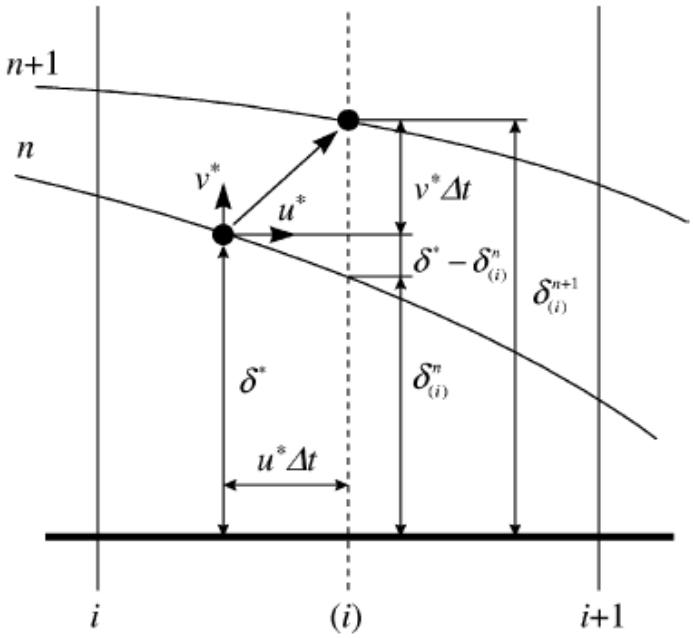

Figure 2.3: Temporal variation of film thickness

2.5 Simulation Results and Discussions

2.5.1 Effects of Wave Frequencies

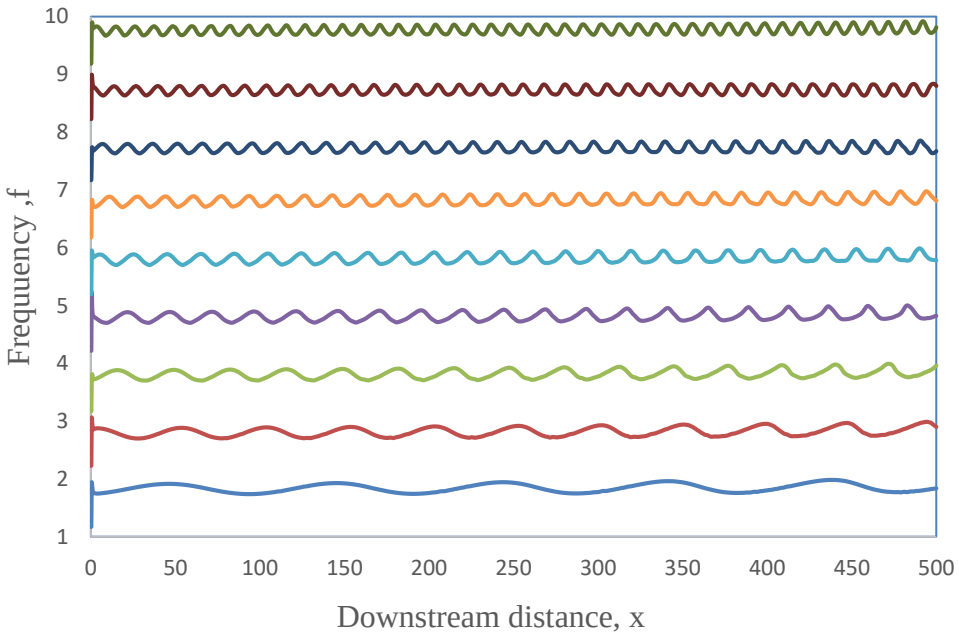

Figure 2.4. Developed waves generated by different inlet disturbance frequencies under the conditions of $\mathrm{Re}_0 = 100,\ We_0 = 0.503,\ \varepsilon = 0.03,\ Da = 100, b = 0.1$

Figure 2.4 shows wave shapes developed from different inlet disturbance frequencies. For all the conditions, the inlet disturbances quickly develop to saturated wave of which wave length and amplitude are almost constant along the downstream. In the case of low frequency, wave front is steeper than wave rear. On the other hand, high frequency wave is symmetry.

2.5.2 Effects of Reynolds Numbers

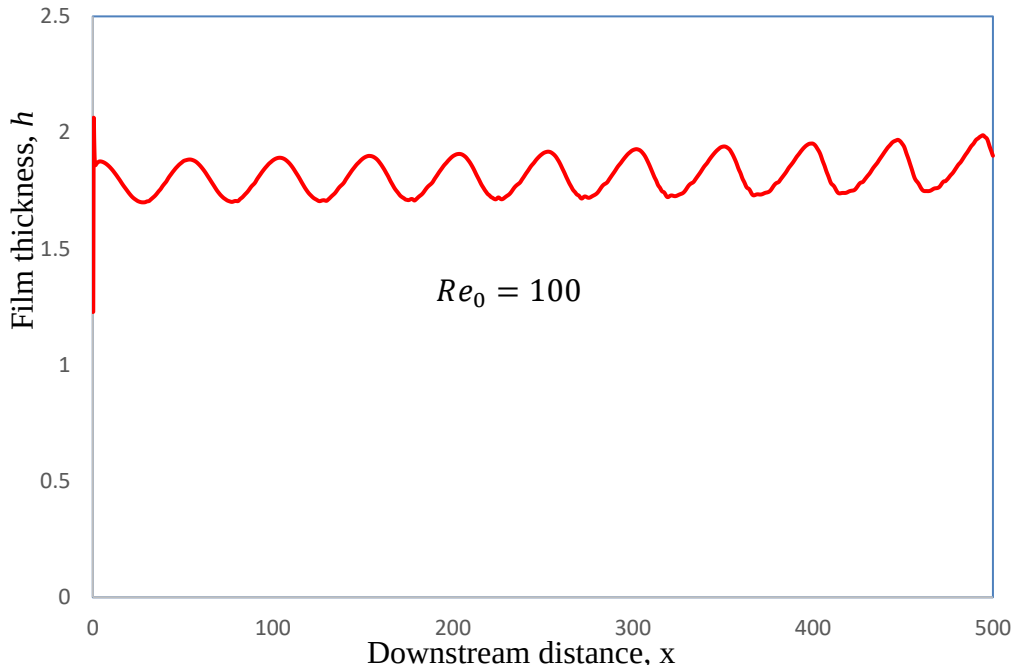

Figure 2.5 (a): Effects of Reynolds number $Re_0 = 100$ on the wave behavior with the fixed values of $We_0 = 0.503, \varepsilon = 0.03, Da = 100, f = 0.02$ and $b = 0.1$

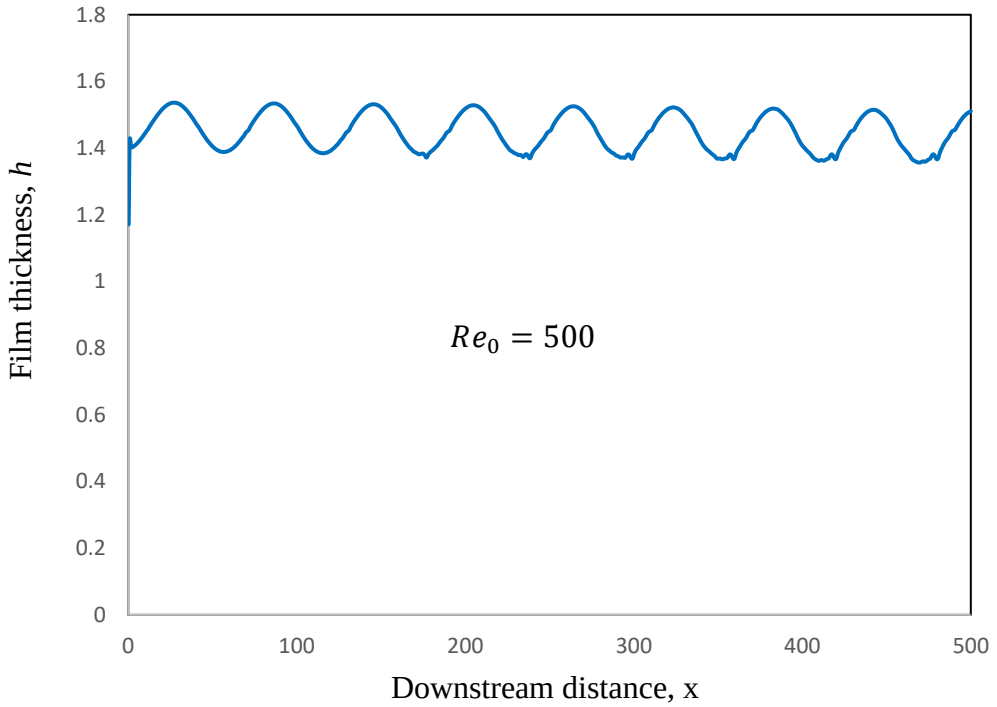

Figure 2.5 (b): Effects of Reynolds number $Re_0 = 500$ on the wave behavior with the fixed values of $We_0 = 0.503, \varepsilon = 0.03, Da = 100, f = 0.02$ and $b = 0.1$

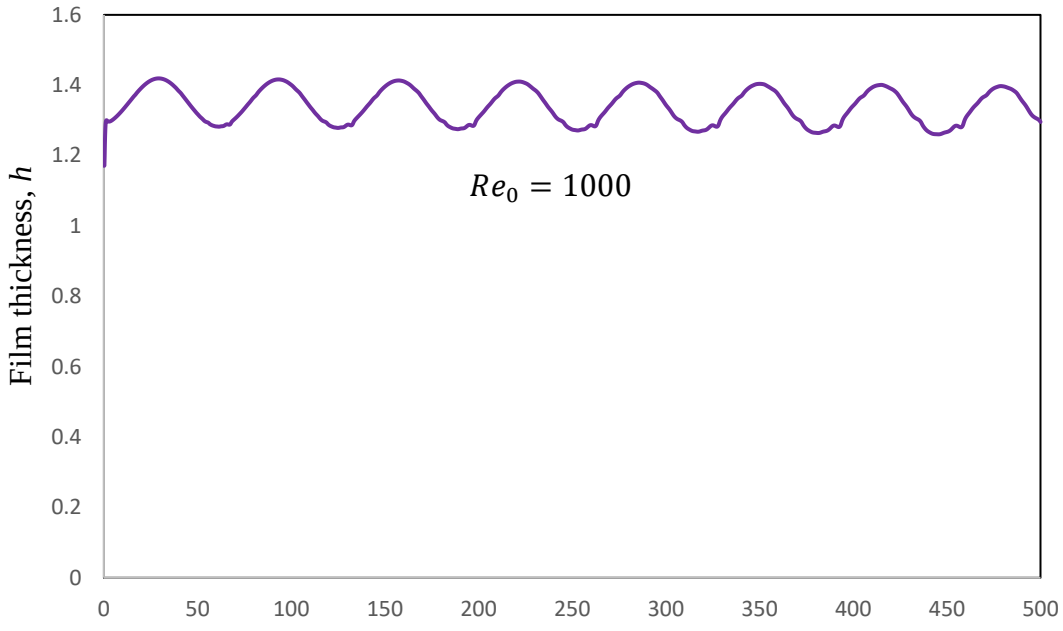

Figure 2.5 (c): Effects of Reynolds number $Re_0 = 1000$ on the wave behavior with the fixed values of $We_0 = 0.503, \varepsilon = 0.03, Da = 100, f = 0.02$ and $b = 0.1$

Influence of the Reynolds number Re_0 on the wave shape are shown in Figure 2.5 (a), (b) and (c). The Reynolds number is changed from 100 to 1000, and the other parameters are constant. The wave peak height decreases with increase of Re_0 . Also, the starting wave peak height decrease with the increase in Reynolds number Re_0.

2.5.3 Effects of Froude Numbers

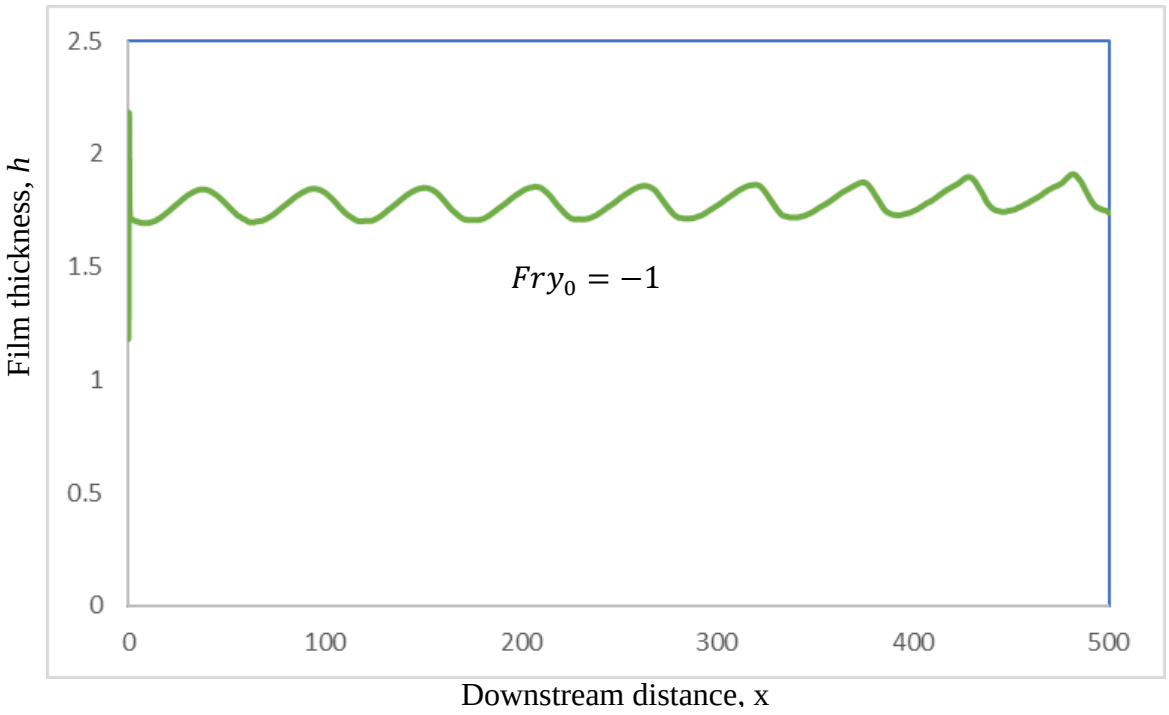

Figure 2.6 (a): Effects of Froude number $Fry_0 = -1$ on wave behavior for $Re_0 = 100, We_0 = 0.503,\ \varepsilon = 0.03, Da = 100, f = 0.02$ and $b = 0.1$

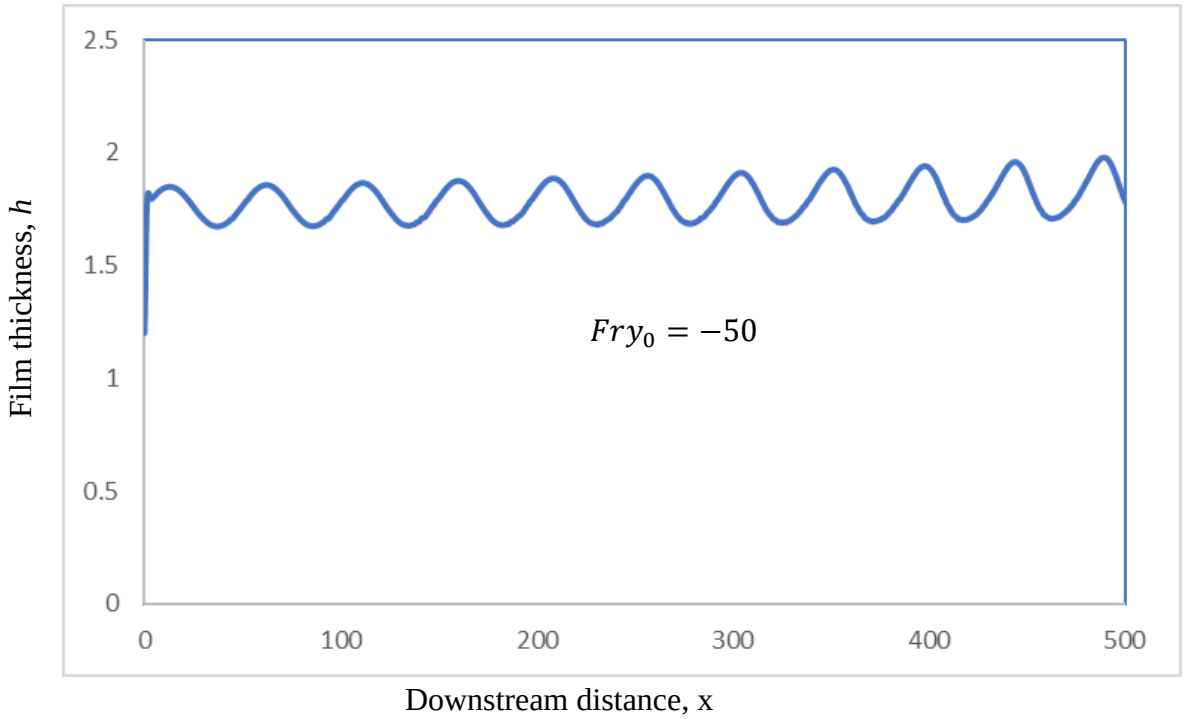

Figure 2.6 (b): Effects of Froude number $Fry_0 = -50$ on wave behavior for $Re_0 = 100, We_0 = 0.503,\ \varepsilon = 0.03, Da = 100, f = 0.02$ and $b = 0.1$

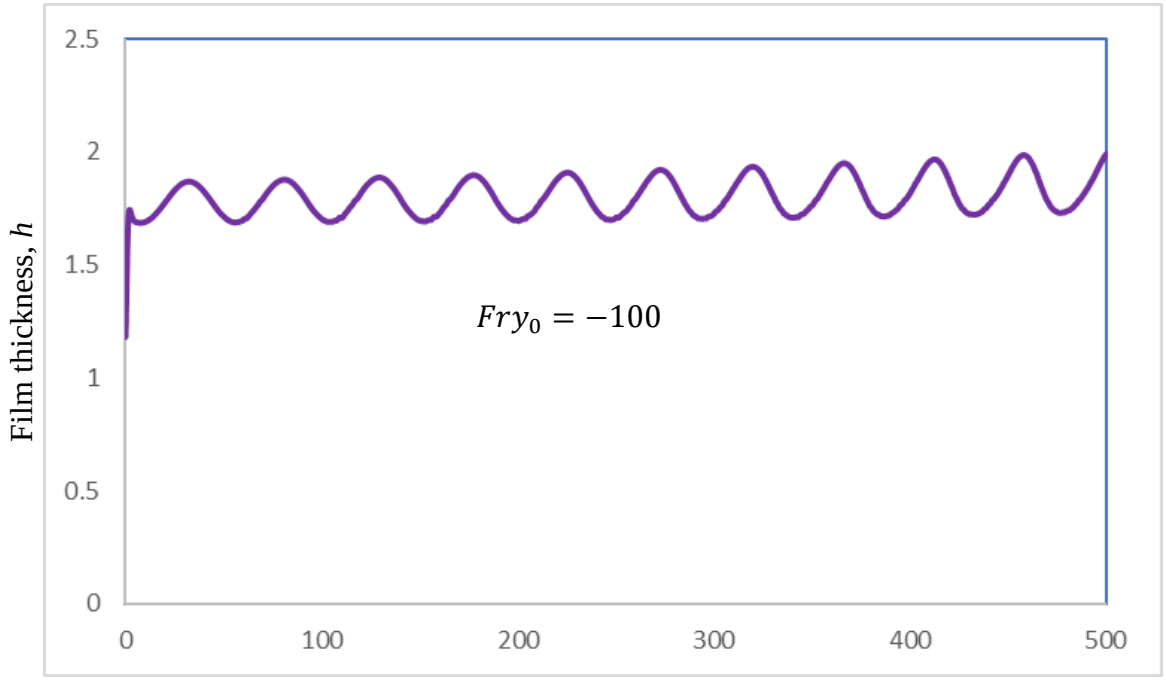

Figure 2.6 (c): Effects of Froude number $Fry_0 = -100$ on wave behavior for $Re_0 = 100, We_0 = 0.503,\ \varepsilon = 0.03, Da = 100, f = 0.02$ and $b = 0.1$

Influence of the Froude number Fry_0 on the wave shape are shown in Figure 2.6 (a), (b) and (c). The Froude number is changed from -1 to 100, all the other parameters are constants. The wave peak height decreases with decrease Fry_0. The starting wave height increase with increase Fry_0.

2.5.4 Effects of Porosities

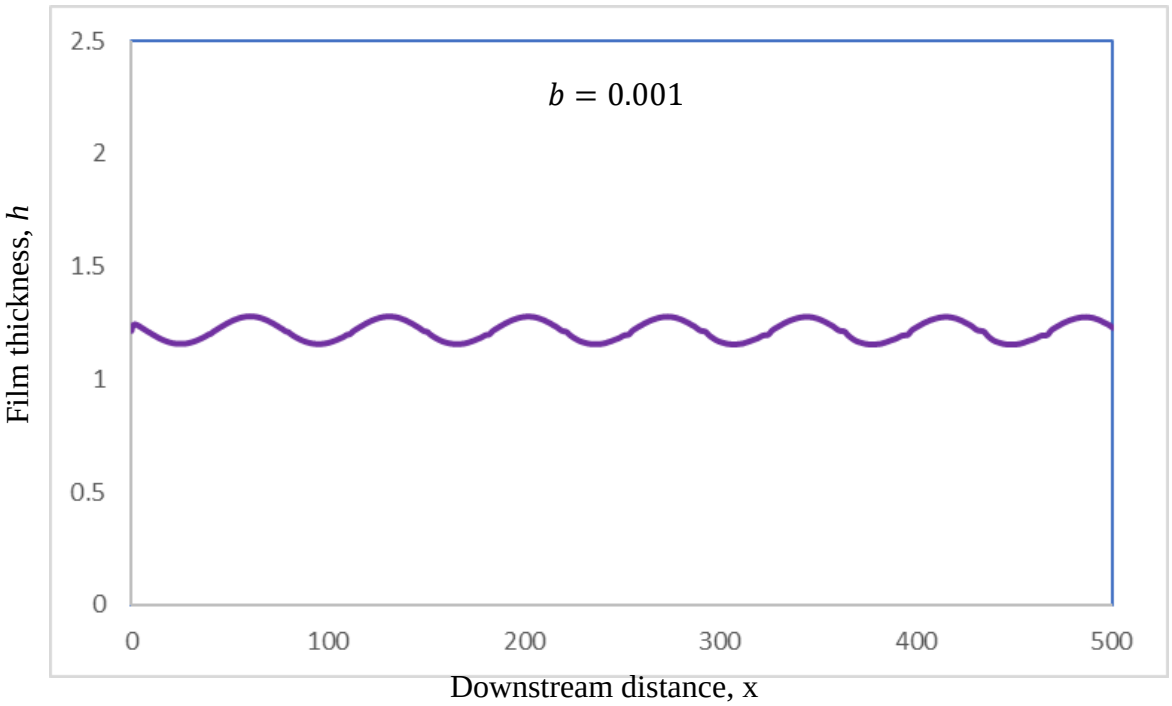

Figure 2.7 (a): Effects of porosity $b = 0.001$ on wave behavior for $Re_0 = 100, We_0 = 0.503,\ \varepsilon = 0.03, Da = 100, f = 0.02$ and $Fry_0 = -0.5$

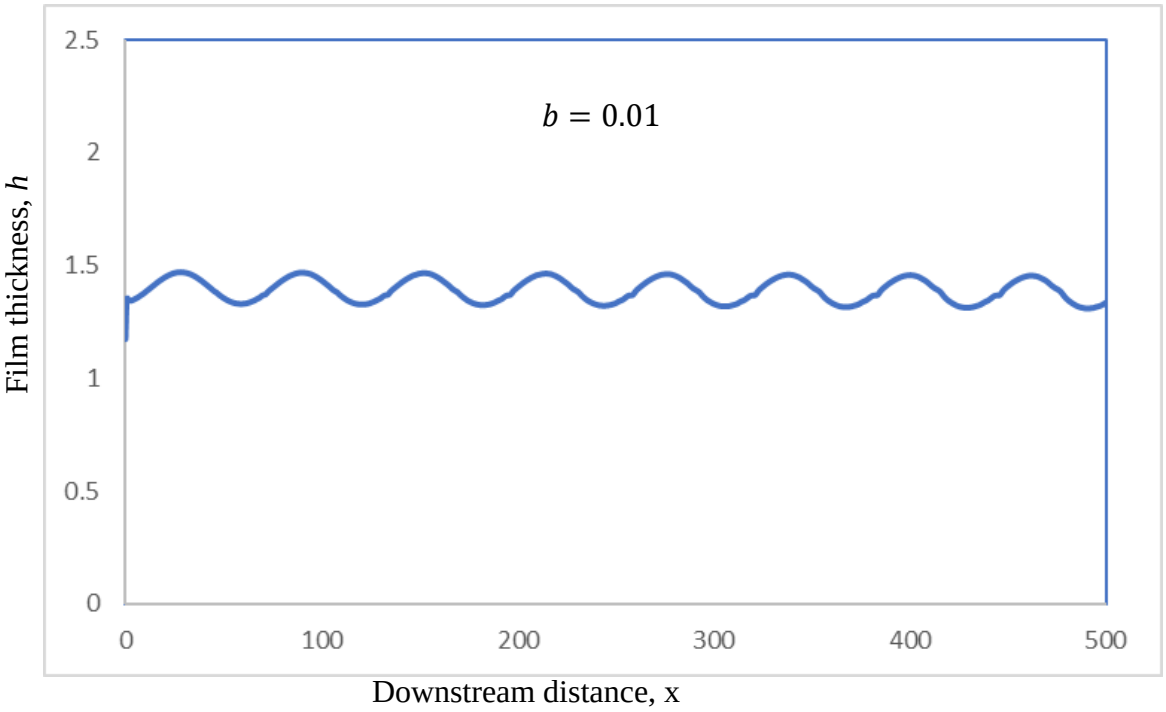

Figure 2.7 (b): Effects of porosity $b = 0.01$ on wave behavior for $Re_0 = 100, We_0 = 0.503,\ \varepsilon = 0.03, Da = 100, f = 0.02$ and $Fry_0 = -0.5$

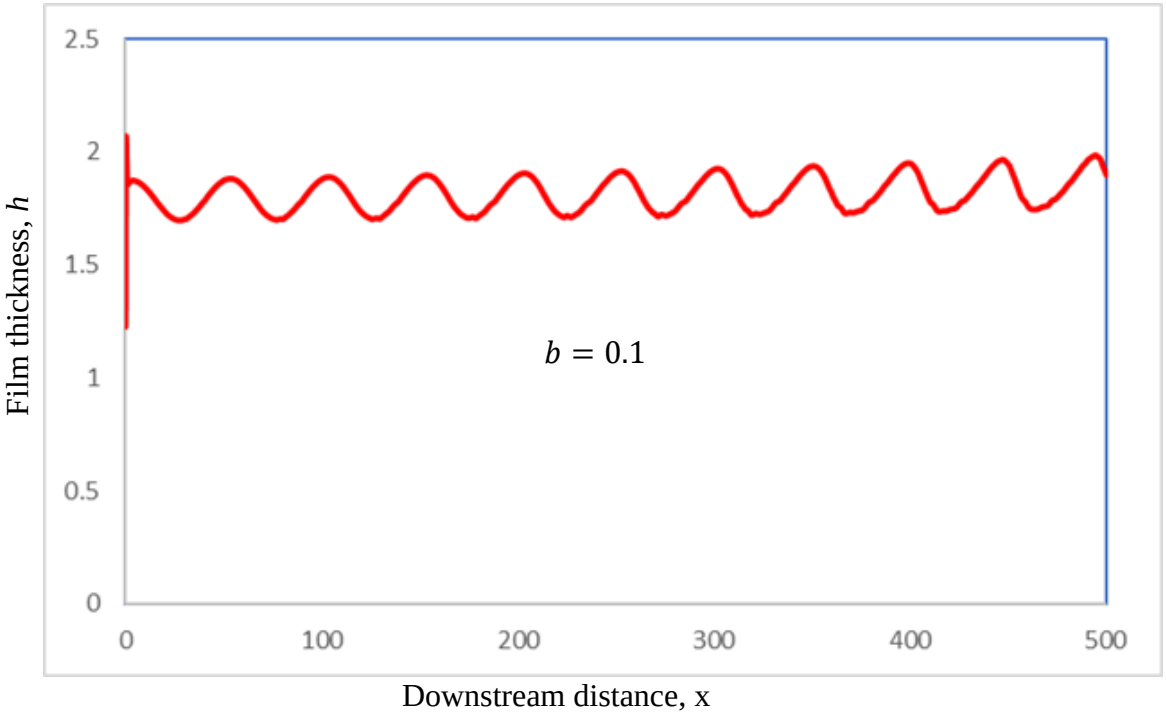

Figure 2.7 (c): Effects of porosity $b = 0.1$ on wave behavior for $Re_0 = 100, We_0 = 0.503,\ \varepsilon = 0.03, Da = 100, f = 0.02$ and $Fry_0 = -0.5$

Influence of the porosity b on the wave shape are shown in Figure 2.7(a), (b) and (c). The porosity is changed from 0.001 to 0.1, and the other parameters are constant. The wave peak height increases with increase the porosity b. Also, the starting wave height increases with increase the porosity. Moreover, for the low porosity the wave front is steeper than the wave rear.

2.5.5 Effects of Weber Numbers

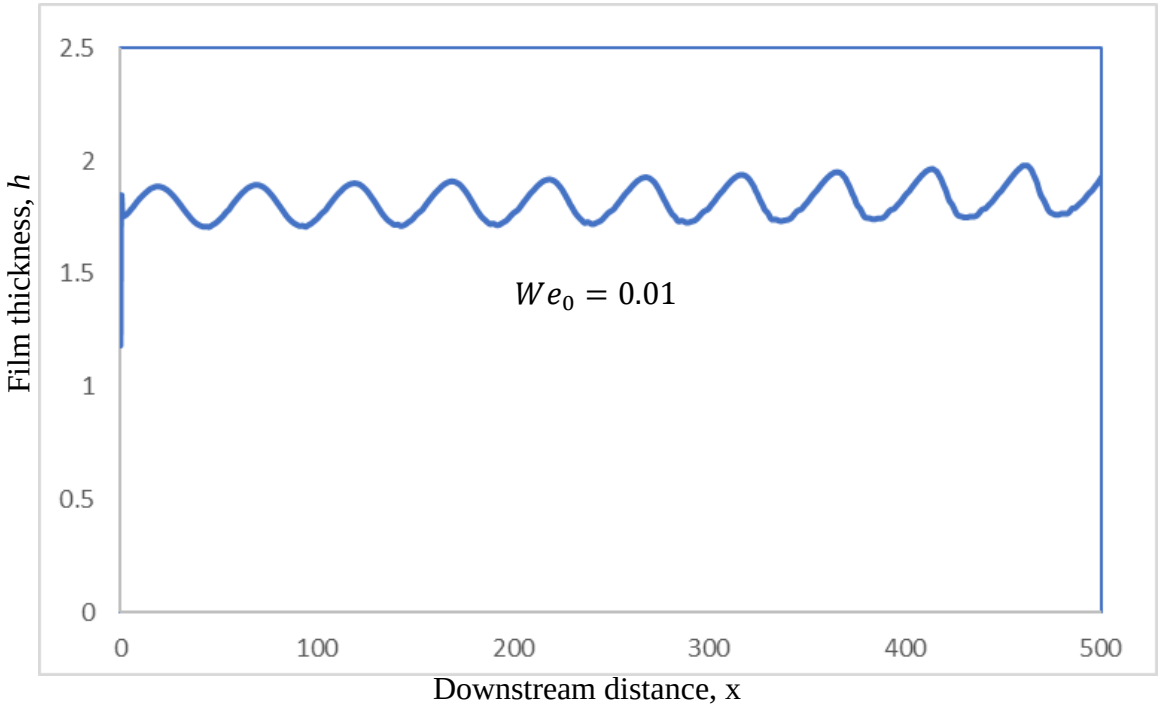

Figure 2.8 (a): Effects of Weber numbers $We_0 = 0.01$ on wave behavior for $Re_0 = 100,\ \varepsilon = 0.03, Da = 100, f = 0.02, b = 0.1$ and $Fry_0 = -0.5$

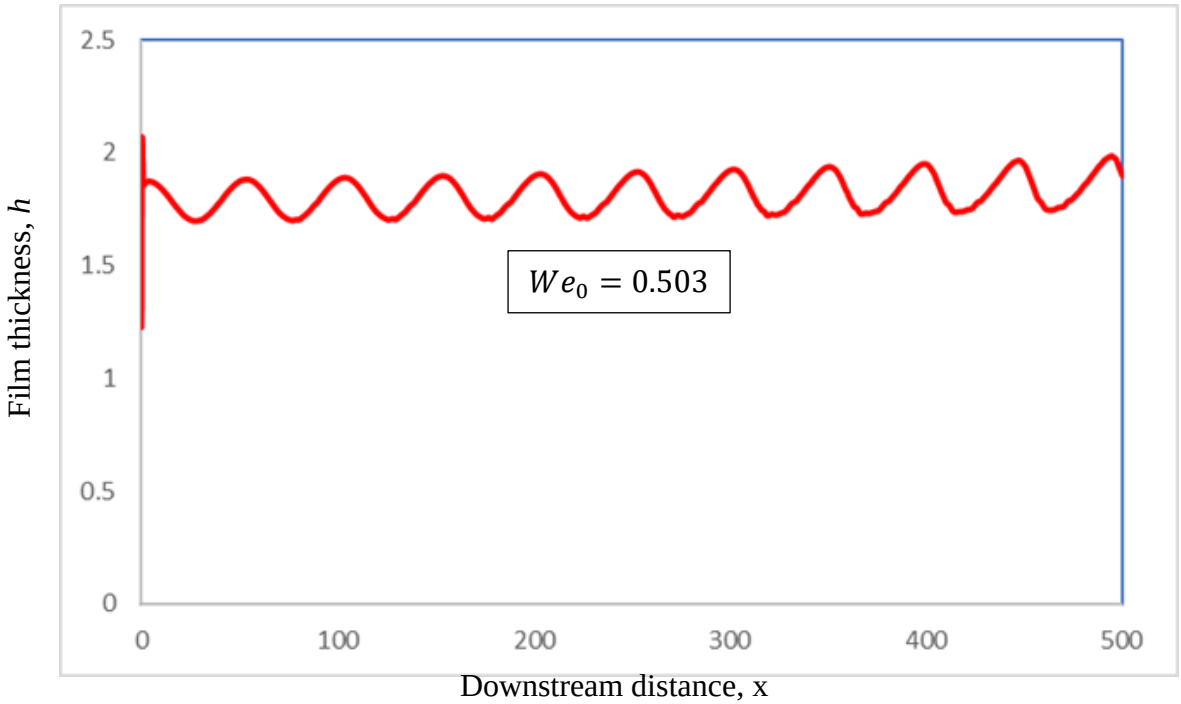

Figure 2.8 (b): Effects of Weber numbers $We_0 = 0.503$ on wave behavior for $Re_0 = 100,\ \varepsilon = 0.03, Da = 100, f = 0.02, b = 0.1$ and $Fry_0 = -0.5$

Effect of the Weber number We_0on the wave shape are shown in Figure 2.8(a) and 2.8(b). The Weber number is changed from 0.01 to 0.503, all the other parameters are constants. From these figures, it is clearly shown that starting wave peak height increases with an increase of the Weber number along the downstream.

2.5.6 Comparison the Film Thickness between Solid Substrate and Porous Wall

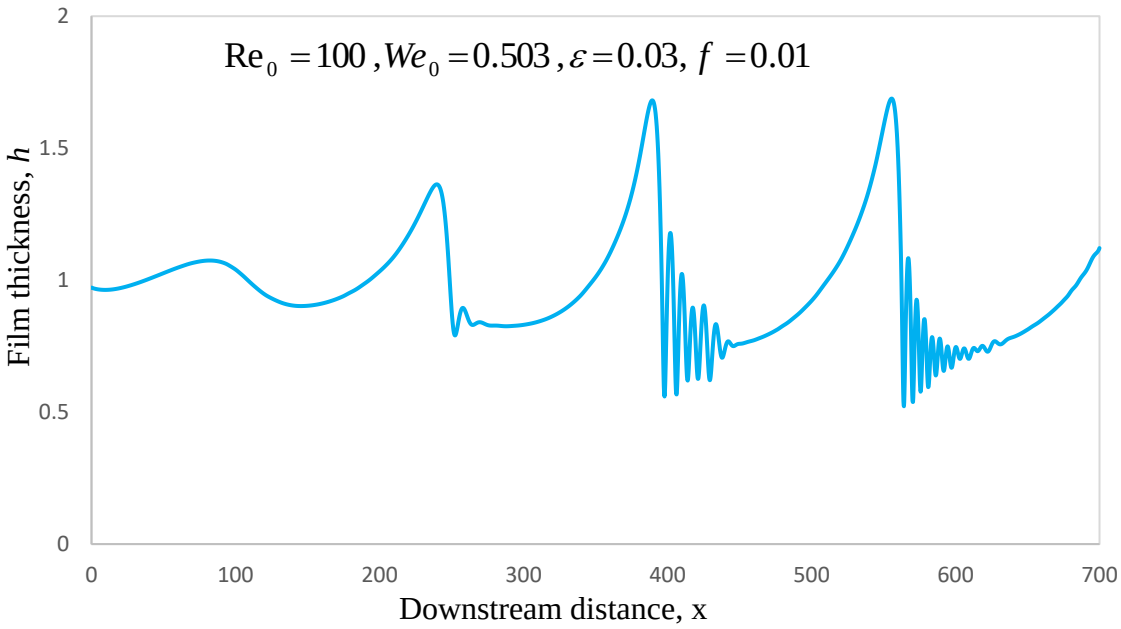

Figure 2.9 (a): Instantaneous film thickness for Solid substrate

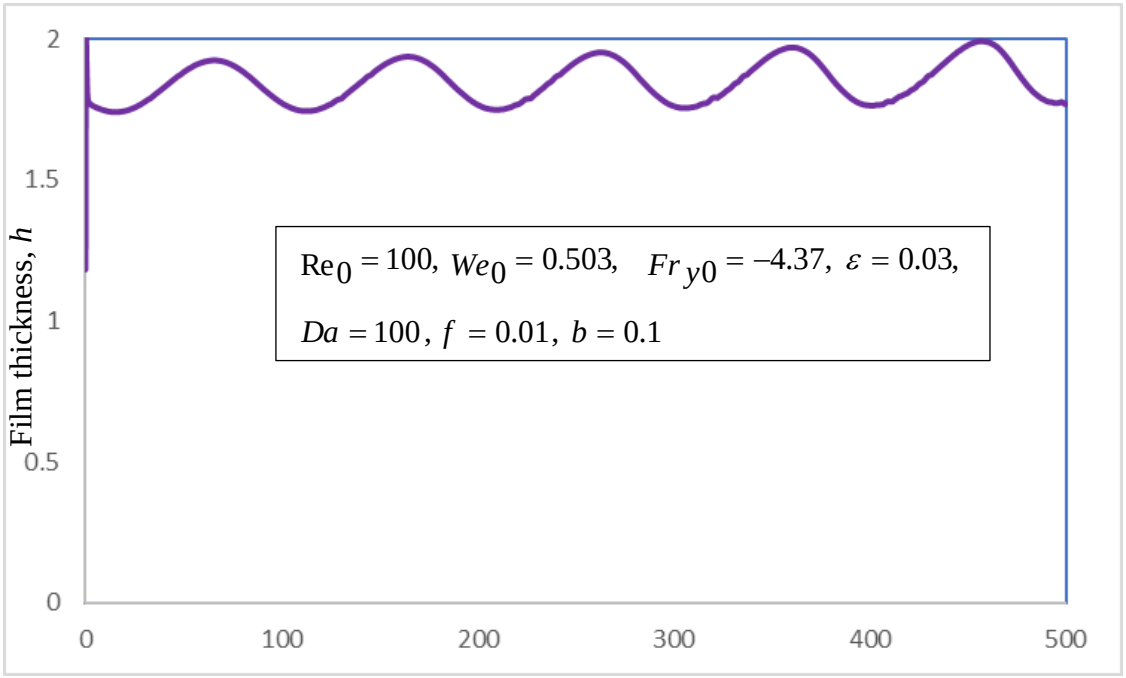

Figure 2.9 (b): Instantaneous film thickness for porous wall

Figure 2.9(a) showing the film thickness for the solid substrate and Figure 2.9(b) showing the film thickness for the porous wall. In the solid substrate, the capillary waves are observed. On the other hand, in porous wall, there is no capillary wave only the solitary waves are observed.

2.5.7 Compare the Velocity Profiles between Solid Substrate and Porous Wall

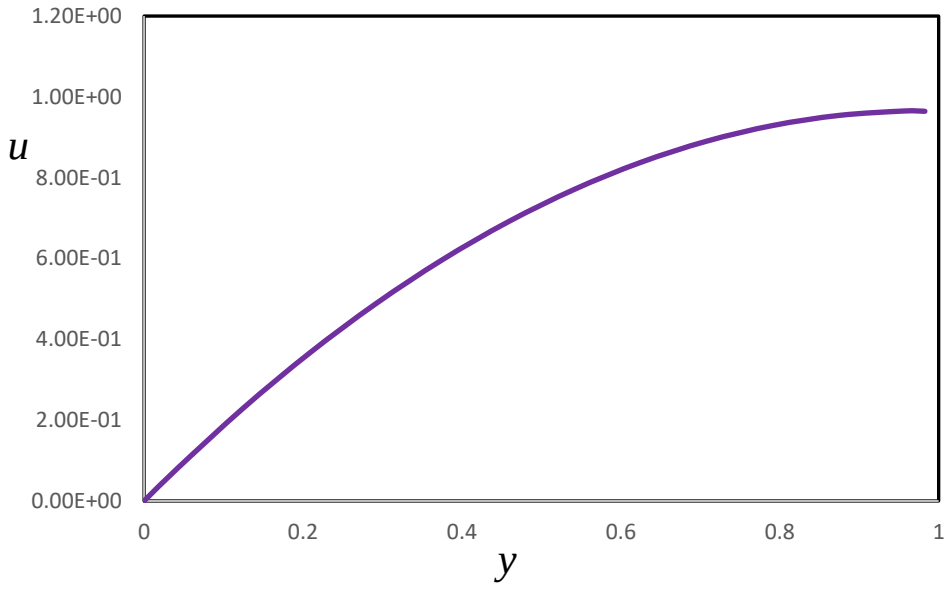

Figure 2.10 (a): Instantaneous velocity profile for solid substrate

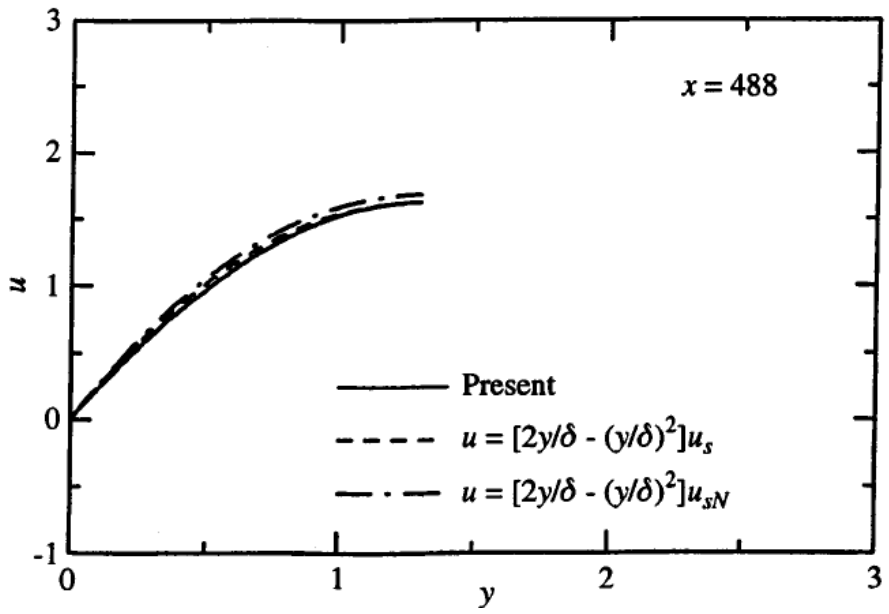

Figure 2.10 (b): Instantaneous velocity profile for Miyara's simulation

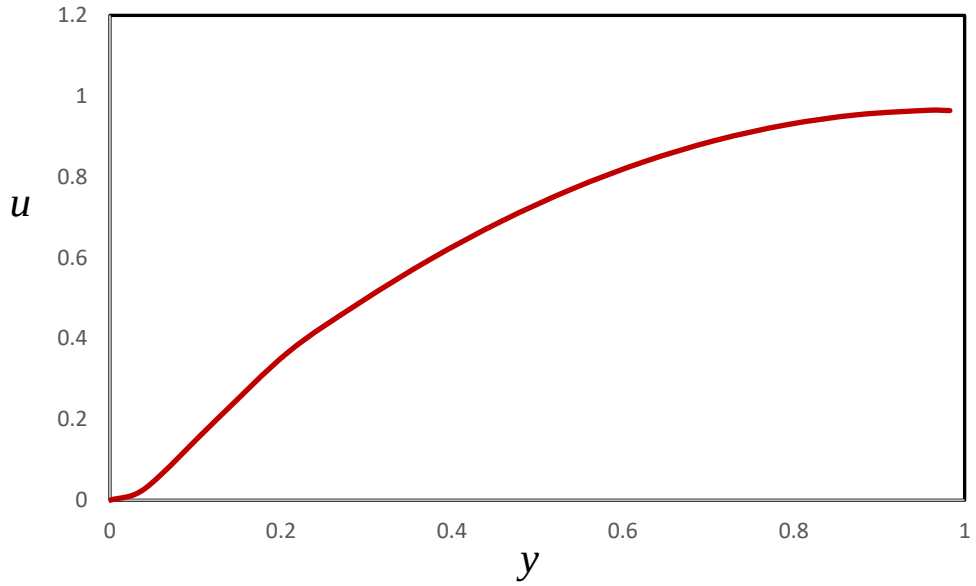

Figure 2.10 (c): Instantaneous velocity profile for porous wall

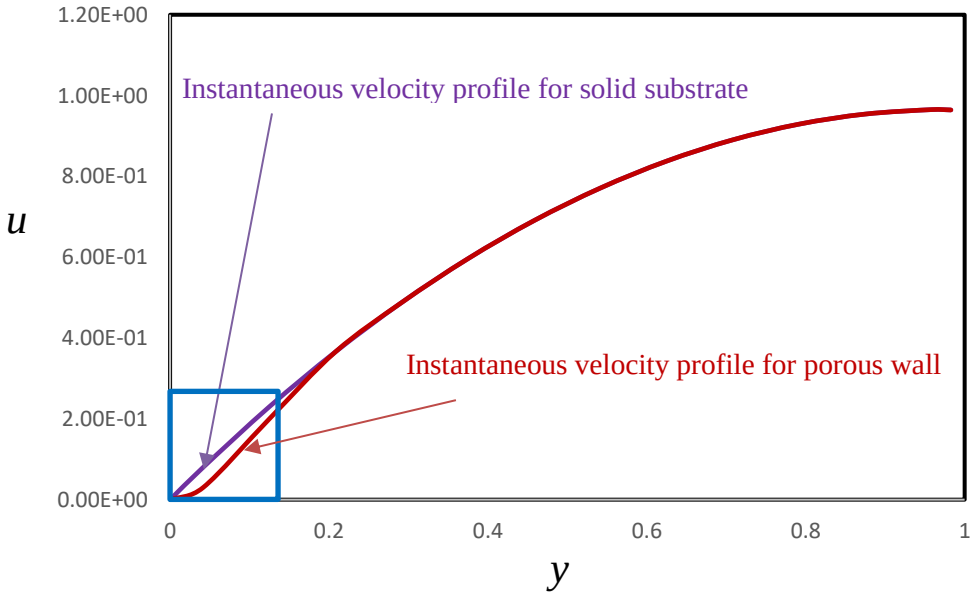

Figure 2.10 (d): Combine instantaneous velocity profile for solid substrate and porous wall

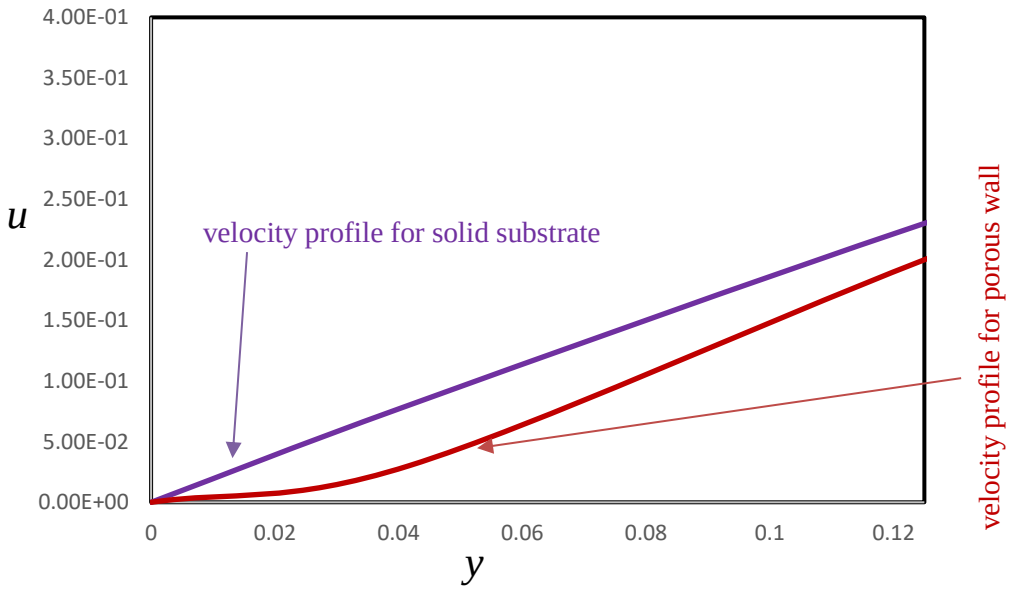

Figure 2.10 (e): Instantaneous velocity profile only for box

Figure 2.10(a) showing the velocity profiles for solid substrate which is almost similar to velocity profiles from Miyara's simulation in Figure 2.10(b). The parabolic velocity profiles with the calculated surface velocity u_s, the surface velocity calculated from the Nusselt theory as well as from the Miyara's simulation. Figure 2.10(c) showing the velocity profile for the porous wall from the present simulation. Also, Figure 2(d) showing the combine velocity profile for solid substrate and porous wall. It is clearly seen that in porous region the velocity is little be differing from the solid substrate. After the porosity the velocity profile is parabolic which is similar to solid substrate.The box portion is the porosity which is showing in Figure 2.10(e).

2.6 Conclusions

A two-dimensional numerical simulation of wavy liquid film flowing along an inclined porous wall has been performed. We investigated the effect of several parameters on the film thickness. In solid substrate, a small disturbance generated at the inflow grows to a solitary wave consisting of a big-amplitude roll wave and the small-amplitude short capillary waves, where as in porous wall only the solitary waves are observed and in low frequency, wave front is steeper than wave rear. Moreover, symmetrical waves are observed in the case of high frequency. For the low porosity the wave front is steeper than the wave rear. The principal effect of the porous substrate on the film flow is to displace the liquid-porous

interface to an effective liquid-solid interface located at the lower boundary of the upper momentum boundary layer in the porous medium.

References

[1] Alekseenko S.V., Nakoryakov V.E., Pokusaev B.G., 1994. Wave Flow of Liquid Films, Begell House, New York.

[2] H.-C. Chang, 1994. Wave evolution on a falling film, Annu. Rev. Fluid Mech. 26, 103.

[3] A. Oron, S. H. Davis, and S. G. Bankoff, 1997. Long-scale evolution of thin liquid films, Rev. Mod. Phys. 69, 931.

[4] D. J. Benney, 1966. Long waves on liquid films, J. Math. Phys. _Cambridge, Mass._ 45, 150.

[5] P. Rosenau, A. Oron, and J. Hyman, 1992. Bounded and unbounded patterns of the Benney equation, Phys. Fluids A 4, 1102.

[6] T. R. Salamon, R. C. Armstrong, and R. A. Brown, 1994. Traveling waves on vertical films: Numerical analysis using the finite element method," Phys.Fluids 6, 2202.

[7] A. Oron and O. Gottlieb, 2002. Nonlinear dynamics of temporally excited falling liquid films, Phys. Fluids 14, 2622.

[8] B. Scheid, C. Ruyer-Quil, U. Thiele, O. A. Kabov, J. C. Legros, and P. Colinet, 2005. Validity domain of the Benney equation including Marangoni effect for closed and open flows, J. Fluid Mech. 527, 303.

[9] G. S. Beavers and D. D. Joseph, 1967. Boundary conditions at a naturally permeable wall, J. Fluid Mech. 30, 197.

[10] P. G. Saffman, 1971. On the boundary condition at the surface of a porous medium, Stud. Appl. Math. 50, 93.

[11] G. S. Beavers, E. M. Sparrow, and R. A. Magnuson, 1970. Experiments on coupled parallel flows in a channel and a bounding porous medium, J. Basic Eng. 92, 843.

[12] J. T. Jeong, 1884. Slip boundary condition on an idealized porous wall, Phys. Fluids 13.

[13] D. F. James and A. M. J. Davis, 2001. Flow at the interface of a model fibrous porous medium, J. Fluid Mech. 426, 47.

[14] T. Levy, 1981. Loi de Darcy ou loi de Brinkman?" C. R. Acad. Sci. 292, 872.

[15] G. Neale and W. Nader, 1974. Practical significance of Brinkman's extension of Darcy's law: Coupled parallel flow within a channel and a bounding porous medium, Can. J. Chem. Eng. 52, 475.

[16] H. C. Brinkman, 1947. A calculation of the viscous force exerted by flowing fluid on a dense swarm of particles," Appl. Sci. Res. A1, 27.

[17] Benjamin T.B., 1957. Wave formation in laminar flow down an inclined plane, J. Fluid Mech. 2, 554–574.

[18] Yih C.-S., 1963. Stability of liquid flow down an inclined plane, Phys. Fluids 6 (3), 321–334.

[19] Bankoff S.G., 1971. Stability of liquid flow down a heated inclined plane, Int. J. Heat Mass Tran. 14, 377–385.

[20] Penev V., Krylov V.S., Boyadjiev CH., Vorotilin V.P., 1972. Wavy flow of thin liquid films, Int. J. Heat Mass Tran. 15, 1395–1406.

[21] Marschall E., Lee C.Y., 1973. Stability of condensate flow down a vertical wall, Int. J. Heat Mass Tran. 16, 41–48.

[22] Pierson F.W., Whitaker S., 1977. Some theoretical and experimental observations of the wave structure of falling liquid films, Ind. Engrg. Chem. Fundam. 16 (4), 401–408.

[23] Solorio F.J., Sen M., 1987. Linear stability of a cylindrical falling film, J. Fluid Mech. 183, 365–377.

[24] Benney D.J., 1966. Long waves on liquid films, J. Math. Phys. 45, 150–155.

[25] Lin S.P., 1969. Finite-amplitude stability of a parallel flow with a free surface, J. Fluid Mech. 36, 113–126.

[26] Gjevik B., 1970. Occurrence of finite-amplitude surface waves on falling liquid films, Phys. Fluids 13, 1918–1925.

[27] Nakaya C., Takaki R., 1967. Non-linear stability of liquid flow down an inclined plane, J. Phys. Soc. Japan 23 (3), 638–645.

[28] Nakaya C., 1975. Long waves on a thin fluid layer flowing down an inclined plane, Phys. Fluids 18, 1407–1412.

[29] Ünsal M., Thomas W.C., 1980. Nonlinear stability of film condensation, J. Heat

Tran. 102, 483–488.

[30] Pumir A., Manneville P., Pomeau Y., 1983. On solitary waves running down an inclined plane, J. Fluid Mech. 135, 27–50.

[31] Joo S.W., Davis S.H., Bankoff S.G., 1991. Long-wave instabilities of heated falling films: two-dimensional theory of uniform layers, J. Fluid Mech. 230, 117–146.

[32] Joo S.W., Davis S.H., 1992. Instabilities of three-dimensional viscous falling films, J. Fluid Mech. 242, 529–547.

[33] Chang H.-C., Cheng M., Demekhin E.A., Kopelevich D.I., 1994. Secondary and tertiary excitation of three-dimensional patterns on a falling film, J. Fluid Mech. 270, 251–275.

[34] J. P. Pascal, 1999. Linear stability of fluid flow down a porous inclined plane, J. Phys. D 32, 417.

[35] J. P. Pascal, 2006. Instability of power-law fluid flow down a porous incline, J. Non-Newtonian Fluid Mech. 133, 109.

[36] Nagasaki T., Hijikata K., 1989. A numerical study of interfacial waves on a falling liquid film, in: ANS Proceedings of the 1989 National Heat Transfer Conference, American Nuclear Society, Vol. 4, pp. 23–30.

[37] Kiyata M., Morioka I., Kiyoi M., 1994. Numerical analysis of waveform of falling films, Trans. JSME B 60 (580), 4177–4184.

[38] Stuhlträger E., Naridomi Y., Miyara A., Uehara H., 1993. Flow dynamics and heat transfer of a condensate film on a vertical wall—I. Numerical analysis and flow dynamics, Int. J. Heat Mass Tran. 36 (6), 1677–1686.

[39] Stuhlträger E., Miyara A., Uehara H., 1995. Flow dynamics and heat transfer of a condensate film on a vertical wall—II. Flow dynamics and heat transfer, Int. J. Heat Mass Tran. 38 (15) 2715–2722.

[40] Akio Miyara, 2000. Numerical simulation of wavy liquid film flowing down on a vertical wall and an inclined wall, Int. J. Therm. Sci. 39, 1015–1027.

[41] Shapiro M.A., O'Brien J.J., 1970. Boundary conditions for fine-mesh limited-area forecasts, J. Appl. Meteorology 9, 345–349.

[42] B. Goyeau, D. Lhuillier, D. Gobin, and M. G. Velarde, 2003. Momentum transport at a fluid-porous interface," Int. J. Heat Mass Transfer 46, 4071.

[43] S. Whitaker, 1996. The Forchheimer equation: A theoretical derivation of Darcy's law, Transp. Porous Media 25, 27.

[44] P. Bousquet-Melou, B. Goyeau, M. Quintard, F. Fichot, and D. Gobin, 2002. Average momentum equation for interdendritic flow in a solidifying columnar mushy zone, Int. J. Heat Mass Transfer 45, 3651.

[45] B. Goyeau, D. Lhuillier, D. Gobin, and M. G. Velarde, 2003. Momentum transport at a fluid-porous interface, Int. J. Heat Mass Transfer 46, 4071.

[46] S. Whitaker, 1996. The Forchheimer equation: A theoretical derivation of Darcy's law, Transp. Porous Media **25**, 27.

[47] P. Bousquet-Melou, B. Goyeau, M. Quintard, F. Fichot, and D. Gobin, 2002. Average momentum equation for interdendritic flow in a solidifying columnar mushy zone, Int. J. Heat Mass Transfer **45**, 3651.

[48] A. Miyara, 1999. Numerical analysis on flow dynamics and heat transfer of falling liquid films with interfacial waves, Heat and Mass Transfer, 35, 298-306.

CHAPTER THREE

Numerical Simulation of Wavy Liquid Film Flowing Along an Inclined Heated (Cooled) Porous Wall

3.1 Introduction

Liquid films on a vertical or inclined surface falling under the influence of gravity are important in numerous industrial applications, including absorbers, condensers, vertical tube evaporators, and falling film chemical reactors. In order to design these industrial equipment's reliably the transport rates of heat and mass must be accurately predicted. However, before the heat and mass transport properties can be evaluated, the momentum transfer and the hydrodynamic characteristics of the falling liquid film must be fully understood so that the film thickness and velocity distribution that govern this viscous flow system can be modeled and predicted. Falling films are inherently unstable and this instability leads to formation of waves on film surface. Instabilities in liquid flow have been studied extensively by numerous researchers since the pioneering experiments by Kapitza and Kapitza [1]. Instabilities of the interfacial waves have been studied intensively with linear, weak nonlinear and full nonlinear stability analyses. Interfacial waves can be developed by two ways: (i) disturbing the inlet flow rate or film thickness by periodic wave and (ii) by ambient noise (numeric random noise).

Through a long-wave approximation of the Navier–Stokes equations [2,3], liquid layers flowing on a solid wall and possessing a free surface can be described by a film thickness evolution equation obtained. Most works consider a smooth solid impervious substrate and therefore a no-slip and no-penetration boundary conditions for the fluid velocity at the fluid/substrate interface is adopted. In that case, past a critical Reynolds number the base flow is unstable to a long-wave instability which is explained by Benney [4]. However, Benney-type equations even with stabilizing surface tension have only a limited validity range since they lead to blow-up of solutions in finite time, which is not the case when solving the full Navier–Stokes equations [5-8]. On the other hand, it is observed that a liquid layer resting on a heated smooth horizontal plate past a critical Marangoni number is unstable to either a short or to a long-wave Marangoni-driven instability [9-14]. In the latter

case when the layer is really shallow film rupture and the emergence of dry spots is the result of instability if disjoining pressure and other molecular surface forces are not considered [15-19]. Joo et. al. [20] are studied long-wave instabilities of the uniform film by deriving an evolution equation for two-dimensional disturbances. Moreover, Thiele and Knobloch [18] explained that depending on the small inclination of the plate the final structures may exhibit small or large amplitude, e.g., surface waves or sliding drops, respectively.

Actually, solid substrates are rarely smooth, and they often are rather rough or even porous. Such situations are present in the bio-chemical, pharmaceutical, environmental, energy, and food industries. Beavers and Joseph [21] was performed a pioneering study involving flow at a fluid-porous interface. At the interface, Saffmann [22] was justified theoretically that the flows in the fluid and porous layers are described by the Stokes and Darcy equations, respectively, a semiempirical velocity slip boundary condition. Beavers et. al. [23] involved a dimensionless slip coefficient which depends on the local geometry of the interface. Neale and Nader [24] and Brinkman [25] explained that the geometry of the interface is generally unknown, and an alternative model consists in using the Darcy– Brinkman equation in the porous layer. In this case, partial differential equations for each region are of the same differential order and continuity of both velocity and shear stress can be satisfied at the fluid-porous interface. Solutions are found to be similar to the one obtained by Beavers and Joseph, with an unknown parameter being the effective viscosity coefficient of the Brinkman correction term.

A theoretical study has been performed in order to characterize the interface conditions for a thin film flow past a porous layer using Reynolds and Darcy equations in the film and the porous layer, respectively. Due to the nature of these equations, Bayada and. Chambat [26] explained that the coupling only provided a normal condition for the pressure at the interface. Previously, Pascal ([27], [28]) have been performed the two-stability analysis of fluid flow down an inclined isothermal porous surface. In both cases, Darcy's law was used for momentum transport in the porous layer and therefore viscous diffusion at the interface is not included. The results that depend on the slip coefficient values show the destabilizing effect of the permeability. Thiele et. al. [29] studied that the influence of a heated porous substrate on the stability of the liquid film flow. Their model is based on the Darcy–Brinkman equation in the porous substrate and a stress jump condition is imposed at the fluid-porous interface. The simulation code is developed by extending the previous work by Miyara [30] for hydrodynamics of wavy falling film.

In this chapter, a finite difference method is used, and the fixed grid is employed. The difficulties to apply the exact interfacial boundary conditions in the fixed grid have been overcome by using newly proposed techniques. The algorithm of the calculation is based on the HSMAC method and it is improved. The continuity, Navier-Stokes and energy equations are solved simultaneously. In this simulation, we got some non-dimensional numbers. We also tried to show the effect of these numbers on the film thickness.

3.2 Model and Governing Equations

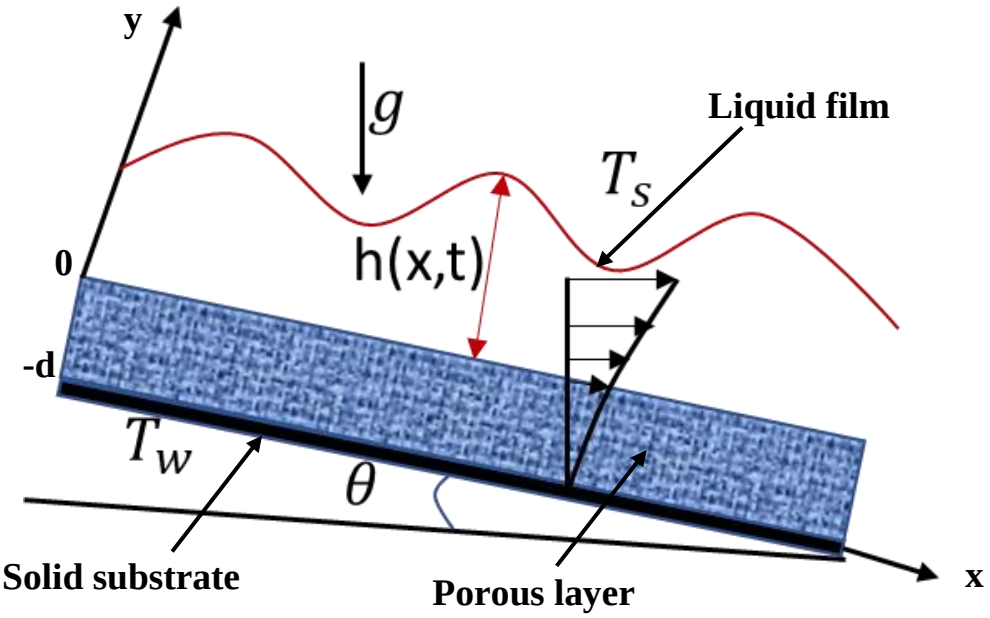

Figure 3.1: physical model and coordinates systems

We consider a two-dimensional incompressible Newtonian liquid fluid flowing over an inclined porous wall, saturated by the same liquid from the side of the substrate (Figure 3.1). Note that we consider a porous layer of a finite constant thickness *d* on a nonporous outer wall.

The hydrodynamics of falling can be expressed by following continuity equation and Navier-Stokes equations.

Continuity equation

$$\frac{\partial u'}{\partial x'} + \frac{\partial v'}{\partial y'} \tag{3.1}$$

Navier-Stokes equations

$$\rho\left(\frac{\partial u'}{\partial t'}+u'\frac{\partial u'}{\partial x'}+v'\frac{\partial u'}{\partial y'}\right)=-\frac{\partial p'}{\partial x'}+\mu\left(\frac{\partial^2 u'}{\partial x'^2}+\frac{\partial^2 u'}{\partial y'^2}\right)+\rho g\ sin\theta \tag{3.2}$$

$$\rho\left(\frac{\partial v'}{\partial t'}+u'\frac{\partial v'}{\partial x'}+v'\frac{\partial v'}{\partial y'}\right)=-\frac{\partial p'}{\partial y'}+\mu\left(\frac{\partial^2 v'}{\partial x'^2}+\frac{\partial^2 v'}{\partial y'^2}\right)-\rho g\ cos\theta \tag{3.3}$$

$$\frac{\partial T'}{\partial t'}+u'\frac{\partial T'}{\partial x'}+v'\frac{\partial T'}{\partial y'}=\alpha\left(\frac{\partial^2 T'}{\partial x'^2}+\frac{\partial^2 T'}{\partial y'^2}\right) \tag{3.4}$$

In the following, buoyancy will be neglected since we consider sufficiently thin films. The liquid film flow inside the porous substrate is described using the Darcy-Brinkman equation (Goyeau et al. [31], Whitaker, [32] and Bousquet et al. [33]).

$$\frac{\partial \tilde{u}'}{\partial x'}+\frac{\partial \tilde{v}'}{\partial y'}=0 \tag{3.5}$$

$$\frac{\rho}{b}\frac{\partial \tilde{u}'}{\partial t'}=-\frac{\partial \tilde{p}'}{\partial x'}+\mu_{eff}\left(\frac{\partial^2 \tilde{u}'}{\partial x'^2}+\frac{\partial^2 \tilde{u}'}{\partial y'^2}\right)-\frac{\mu}{K}\tilde{u}'+\rho g\ sin\theta \tag{3.6}$$

$$\frac{\rho}{b}\frac{\partial \tilde{v}'}{\partial t'}=-\frac{\partial \tilde{p}'}{\partial y'}+\mu_{eff}\left(\frac{\partial^2 \tilde{v}'}{\partial x'^2}+\frac{\partial^2 \tilde{v}'}{\partial y'^2}\right)-\frac{\mu}{K}\tilde{v}'-\rho g\ cos\theta \tag{3.7}$$

$$\frac{\partial \tilde{T}'}{\partial t'}+\tilde{u}\frac{\partial \tilde{T}'}{\partial x'}+\tilde{v}\frac{\partial \tilde{T}'}{\partial y'}=\alpha\left(\frac{\partial^2 \tilde{T}'}{\partial x'^2}+\frac{\partial^2 \tilde{T}'}{\partial y'^2}\right) \tag{3.8}$$

where $\tilde{u}'$ and $\tilde{v}'$ are the filtration velocities in the x and y-directions, *k* is the permeability, *b* is the porosity, ρ is the density, and μ_{eff} represents the effective viscosity. Following Whitaker [32], the reduced viscosity is given by $\frac{\mu}{\mu_{eff}}=\frac{1}{b}$. The flow in the porous wall is assumed to be slow enough to neglect inertial (Bousquet et al., [33]).

Definitions of dimensionless coordinates and variables are as follows:

$$x=\frac{x'}{\delta_0},\ \ y=\frac{y'}{\delta_0},\qquad t=\frac{\varepsilon u_0}{\delta_0}t' \tag{3.9}$$

$$u=\frac{u'}{u_0},\ \ \tilde{u}=\frac{\tilde{u}'}{u_0},\ \ v=\frac{v'}{u_0},\ \ \tilde{v}=\frac{\tilde{v}'}{u_0}\quad T=\frac{T'-T'_w}{T'_s-T'_w} \tag{3.10}$$

$$\tilde{T} = \frac{\tilde{T}' - T_w'}{T_s' - T_w'}, p = \frac{p'}{\rho u_0^2}, \qquad \tilde{p} = \frac{\tilde{p}'}{\rho u_0^2}, \quad h = \frac{h'}{\delta_0} \tag{3.11}$$

where δ_0 is the mean thickness of the film and ε is the ratio of the length scales $\frac{\delta_0}{L} \ll 1$, , L denotes the characteristic length scale for a surface deformation, $\delta = \frac{d}{\delta_0}$ is the dimensionless thickness of the porous substrate.

Above continuity equation and Navier-Stokes equations are converted into dimensionless by assuming constant physical properties.

Continuity equation

$$\frac{\partial u}{\partial x} + \frac{\partial v}{\partial y} = 0 \tag{3.12}$$

Navier-Stokes equations

$$\frac{\partial u}{\partial t} + u\frac{\partial u}{\partial x} + v\frac{\partial u}{\partial y} = -\frac{\partial p}{\partial x} + \frac{1}{Re_0}\left(\frac{\partial^2 u}{\partial x^2} + \frac{\partial^2 u}{\partial y^2}\right) + \frac{1}{Fr_{x0}} \tag{3.13}$$

$$\frac{\partial v}{\partial t} + u\frac{\partial v}{\partial x} + v\frac{\partial v}{\partial y} = -\frac{\partial p}{\partial y} + \frac{1}{Re_0}\left(\frac{\partial^2 v}{\partial x^2} + \frac{\partial^2 v}{\partial y^2}\right) + \frac{1}{Fr_{y0}} \tag{3.14}$$

$$\frac{\partial T}{\partial t} + u\frac{\partial T}{\partial x} + v\frac{\partial T}{\partial y} = \frac{1}{\mathrm{Pr}\, Re_0}\left(\frac{\partial^2 T}{\partial x^2} + \frac{\partial^2 T}{\partial y^2}\right) \tag{3.15}$$

While in the porous layer they take the form

Continuity equation

$$\frac{\partial \tilde{u}}{\partial x} + \frac{\partial \tilde{v}}{\partial y} = 0 \tag{3.16}$$

Navier-Stokes equations

$$\frac{1}{b}\frac{\partial \tilde{u}}{\partial t} = -\frac{\partial \tilde{p}}{\partial x} + \frac{1}{Re_0}\left(\frac{\partial^2 \tilde{u}}{\partial^2 x} + \frac{\partial^2 \tilde{u}}{\partial^2 y}\right) - \frac{1}{Da\, Re_0}\tilde{u} + \frac{1}{Fr_{x0}} \tag{3.17}$$

$$\frac{1}{b}\frac{\partial \tilde{v}}{\partial t} = -\frac{\partial \tilde{p}}{\partial y} + \frac{1}{Re_0}\left(\frac{\partial^2 \tilde{v}}{\partial^2 x} + \frac{\partial^2 \tilde{v}}{\partial^2 y}\right) - \frac{1}{Da\, Re_0}\tilde{v} + \frac{1}{Fr_{y0}} \tag{3.18}$$

$$\frac{\partial \tilde{T}}{\partial t} + u\frac{\partial \tilde{T}}{\partial x} + v\frac{\partial \tilde{T}}{\partial y} = \frac{1}{\mathrm{Pr}\, Re_0}\left(\frac{\partial^2 \tilde{T}}{\partial x^2} + \frac{\partial^2 \tilde{T}}{\partial y^2}\right) \tag{3.19}$$

where $\mathrm{Re}_0 = \frac{\rho u_0 \delta_0}{\mu}$ is the Reynolds number and $Da = \frac{k}{\bar{h}^2}$ is the number representing the dimensionless permeability. Hence, the porosity is not necessarily related to the Darcy number and its influence on the stability of the film will be studied independently of the dimensionless permeability.

The following relation between u_0 and δ_0 is given by:

$$u_0 = \frac{\rho \delta_0^2 \, sin\theta}{2\mu} \tag{3.20}$$

From this above equation, the dimensionless parameters are satisfied the following relations:

$$Fr_{x0} = \frac{1}{2} Re_0, \qquad Fr_{y0} = \frac{1}{2} Re_0 tan(\pi - \theta) \tag{3.21}$$

3.3 BOUNDARY CONDITIONS

3.3.1 Wall Surface:

Boundary conditions of the velocity at the wall surface are given as follows:

$$\tilde{u} = 0, \quad \tilde{v} = 0, \tilde{T} = 0 \text{ at } y = 0 \tag{3.22}$$

Pressure at the wall surface is obtained by substituting equation (3.22) into the Navier–Stokes equation of *y*-direction (3.18):

$$\frac{\partial \tilde{p}}{\partial y} = \frac{1}{Re_0} \frac{\partial^2 \tilde{v}}{\partial^2 y} + \frac{1}{Fr_{y0}} \tag{3.23}$$

3.3.2 Interface:

With the following kinematic boundary condition, the temporal variation of the film thickness is calculated:

$$\frac{\partial h}{\partial t} = \tilde{v} - \tilde{u} \frac{\partial h}{\partial x} \tag{3.24}$$

On the other hand, by integrating the continuity equation (3.16) between the limits *y*=0 *to y=h.*

$$\int_0^h \frac{\partial \tilde{u}}{\partial x} dh + \tilde{v}_{y=h} = 0 \tag{3.25}$$

From the differential and integral calculus,

$$\frac{\partial}{\partial x}\int_0^h \tilde{u}dy = \tilde{u}_{y=h}\frac{\partial h}{\partial x} + \int_0^h \frac{\partial \tilde{u}}{\partial x}dy \tag{3.26}$$

Consequently, from equations (3.24)– (3.26) we obtain the following equation:

$$\frac{\partial}{\partial x}\int_0^h \tilde{u}dy + \frac{\partial h}{\partial t} = 0 \tag{3.27}$$

Because calculated film thickness of new time step does not satisfy mass conservation due to truncation error, a correction of the new film thickness is required.

Including the effects of pressure, surface tension, and momentum, the force balance normal to the interface is obtained and the pressure at the interface is calculated with the following equations:

$$p = \frac{-\frac{\partial^2 h}{\partial x^2}}{We_0\left[1+\left(\frac{\partial h}{\partial x}\right)^2\right]^{\frac{3}{2}}} + \frac{2}{Re_0\left[1+\left(\frac{\partial h}{\partial x}\right)^2\right]}\left[\frac{\partial \tilde{u}}{\partial x}\left(\frac{\partial h}{\partial x}\right)^2 - \left(\frac{\partial \tilde{u}}{\partial y}+\frac{\partial \tilde{v}}{\partial x}\right)\frac{\partial h}{\partial x} + \frac{\partial \tilde{v}}{\partial y}\right] \tag{3.28}$$

where We_0 is the Weber number, defined as

$$We_0\frac{\rho u_0^2 \delta_0}{\sigma} \tag{3.29}$$

By using equation (3.20), We_0 can be rewritten as

$$We_0 = Re_0^{\frac{5}{3}}\left(\frac{1}{2}Ka\ sin\theta\right)^{\frac{1}{3}} \tag{3.30}$$

where Ka is the Kapitza number, defined as

$$Ka = \frac{g\mu^4}{\rho\sigma^3} \tag{3.31}$$

By neglecting the shear stress from the vapor phase, the force and momentum balance in the tangential direction becomes as follows:

$$\left(\frac{\partial \tilde{u}}{\partial y}+\frac{\partial \tilde{v}}{\partial x}\right)\left[1-\left(\frac{\partial h}{\partial x}\right)^2\right] - 2\frac{\partial h}{\partial x}\left(\frac{\partial \tilde{u}}{\partial x}-\frac{\partial \tilde{v}}{\partial y}\right) \tag{3.32}$$

3.3.3 Inflow Boundary:

At the inflow boundary, the film thickness is disturbed with the following equation.

$$h = 1 + H + F(t) \tag{3.33}$$

Two types of waves are modeled in this simulation: periodic force waves and natural waves. Periodic force waves are modeled by giving following periodic disturbance in the inflow boundary.

$$F(t) = \varepsilon \, sin(2\pi f t) \tag{3.34}$$

where ε is the disturbance amplitude and *f is* the dimensionless frequency, defined as

$$f = \frac{f' \delta_0}{u_0} \tag{3.35}$$

f' is the frequency with dimension Hz.

Nusselt solution is used to give an average film thickness and velocity profiles at inflow boundary. The amplitude of the disturbance wave is given as $\varepsilon = 0.5$. The magnitude of the amplitude affects wave growth rate while effects on the fully developed waves are small.

Natural waves are modeled by giving following random noise (white noise) in the inflow boundary in similar manner.

$$F(t) = \int_0^\infty \hat{F}(\omega) \, exp(-i\omega t) d\omega = \int_0^\infty \left|\hat{F}(\omega)\right| exp(i\alpha(\omega) - i\omega t) d\omega \tag{3.36}$$

where ω is angular frequency and $\alpha(\omega)$ is the phase of the complex amplitude $\hat{F}(\omega)$. Eq. (3.36) is approximated with *M* frequency units of width $\Delta\omega = \omega^* / M$. Where ω^* is some high frequency cutoff.

$$F(t) = \sum_{k=1}^{M} \left|\hat{F}(\omega)\right| exp(i\alpha(\omega_k) - ik \, \Delta\omega t) \Delta\omega \tag{3.37}$$

The phase $\alpha_k = \alpha(\omega_k)$ is taken from a random number generator from the range $\alpha_k \in [0, 2\pi]$ and $\left|\hat{F}(\omega)\right|$ can be arbitrarily specified.

3.3.4 Outflow Boundary

At outflow boundary, the following equations are employed for *x*-direction velocity $\tilde{u}$ and pressure $\tilde{p}$

$$\frac{\partial \tilde{u}}{\partial x} = 0, \qquad \frac{\partial \tilde{T}}{\partial x} = 0, \qquad \frac{\partial \tilde{p}}{\partial x} = 0 \tag{3.38}$$

From the above equations, the continuity equation, and the wall boundary condition, y-direction velocity $\tilde{v}$ becomes $\tilde{v} = 0$.

3.3.5 Initial Conditions

At t=0, the film thickness is one in the whole simulation region. Initial values of velocities and pressure are given from the Nusselt theory.

3.4 Simulation Results and Discussions

3.4.1 Effect of Wave Frequencies

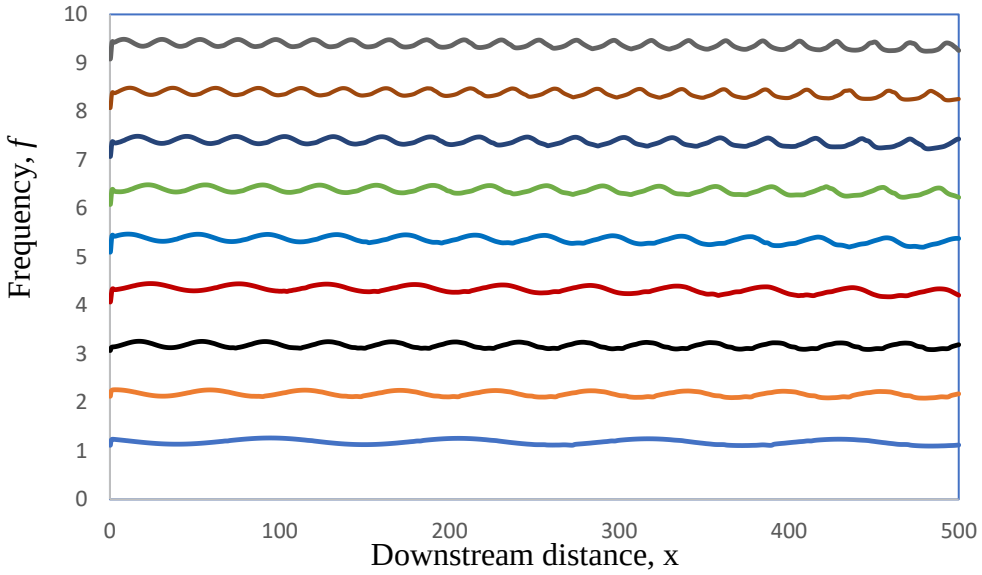

Figure 3.2: Developed waves generated by different inlet disturbance frequencies under the conditions of $Re_0 = 100, We_0 = 0.503, \varepsilon = 0.03, Da = 100, b = 0.01, Pr = 100$

Figure 3.2 shows wave shapes developed from different inlet disturbance frequencies. For all frequencies, the inlet disturbances quickly develop to saturated wave of which wave length and amplitude are almost constant along the downstream. Wave front is steeper than wave wear for the case of low frequency. In the case of high frequencies wave is almost symmetry.

3.4.2 Effect of Prandtl Numbers

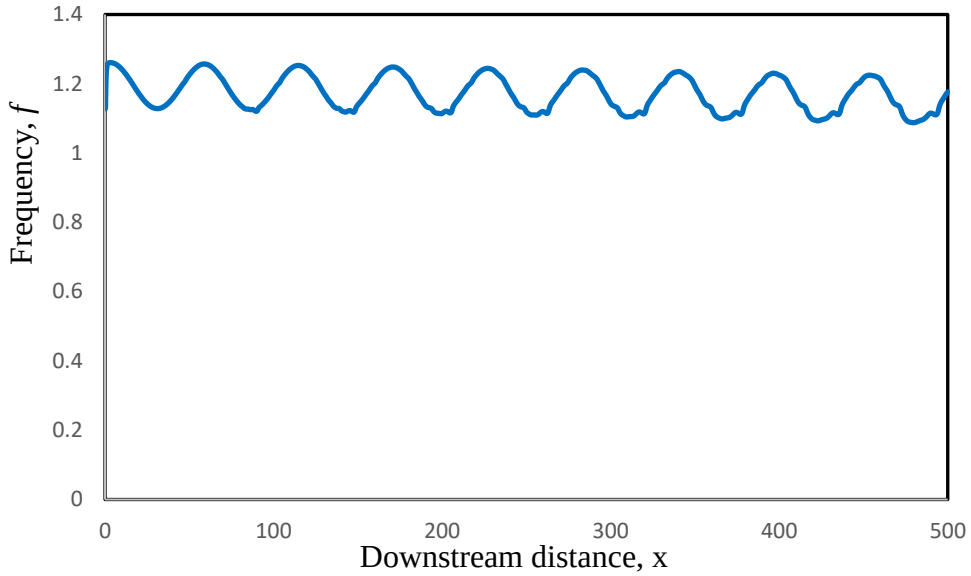

Figure 3.3 (a): Effects of Prandtl number Pr=10 on the wave behavior with the fixed values of $We_0 = 0.503, \varepsilon = 0.03, Re_0 = 100\,, Da = 100, f = 0.02$ and $b = 0.01$

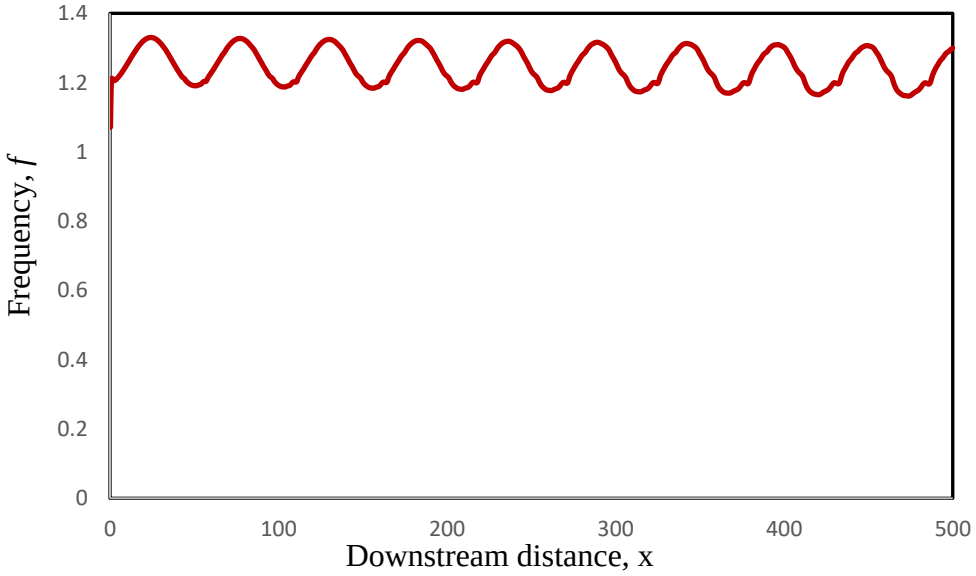

Figure 3.3 (b): Effects of Prandtl number Pr=100 on the wave behavior with the fixed values of $We_0 = 0.503, \varepsilon = 0.03, Re_0 = 100\,, Da = 100, f = 0.02$ and $b = 0.01$

Figure 3.3 (a) and (b) represented the effect of various Prandtl number on the wave behavior and all other parameters are constants. From these two figures show that with an increase the Prandtl number the wave peak height increases along the downstream.

3.4.3 Effect of Reynolds Numbers

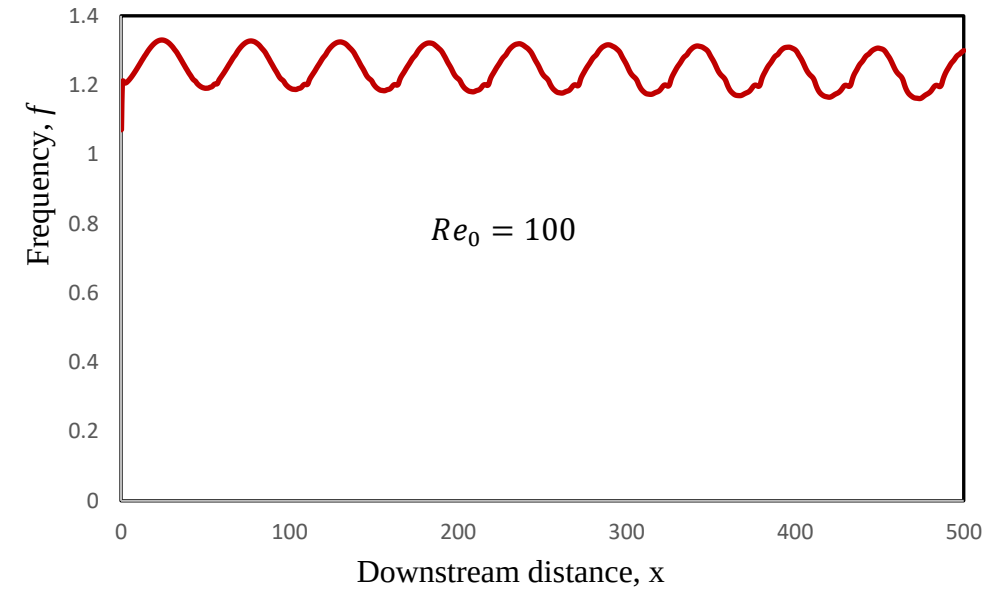

Figure 3.4 (a): Effects of Reynolds number $Re_0 = 100$ on the wave behavior with the fixed values of $We_0 = 0.503, \varepsilon = 0.03, Pr = 100$, $Da = 100, f = 0.02$ and $b = 0.01$

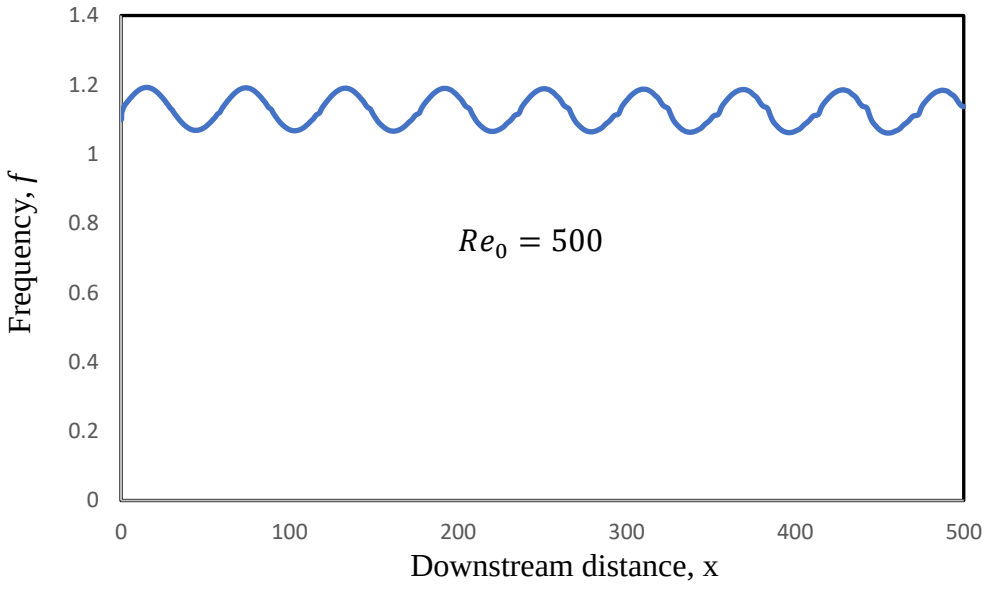

Figure 3.4 (b): Effects of Reynolds number $Re_0 = 500$ on the wave behavior with the fixed values of $We_0 = 0.503, \varepsilon = 0.03, Pr = 100$, $Da = 100, f = 0.02$ and $b = 0.01$

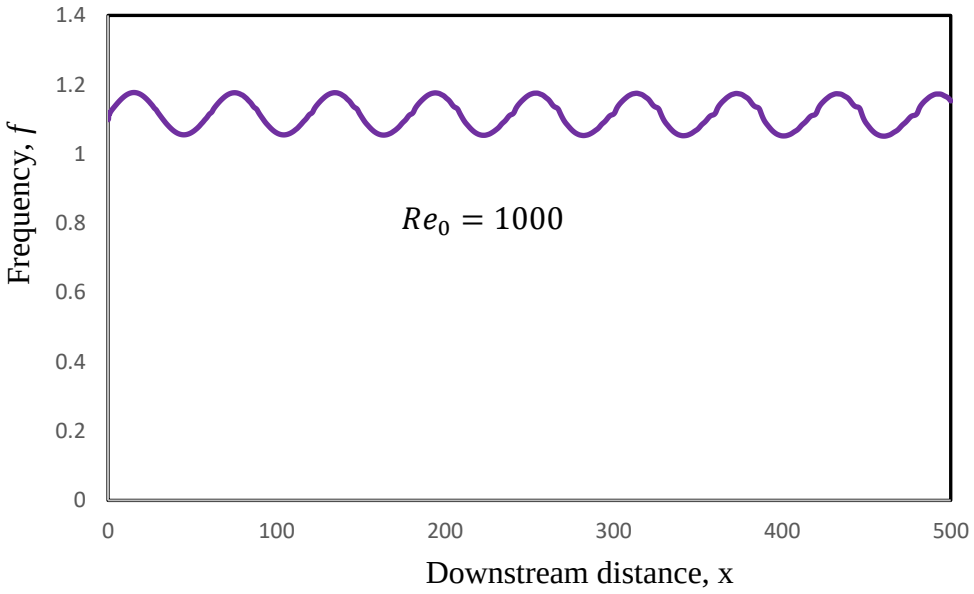

Figure 3.4 (c): Effects of Reynolds number $Re_0 = 500$ on the wave behavior with the fixed values of $We_0 = 0.503, \varepsilon = 0.03, Pr = 100$, $Da = 100, f = 0.02$ and $b = 0.01$

Figure 3.4 (a), (b) and (c) represent the effect of various Reynolds number on the wave behavior and all other parameters are constants. With an increase the Reynolds number the wave height decreases along the downstream.

3.4.4 Compare the Velocity Profiles between the Solid Substrate and the Porous Wall

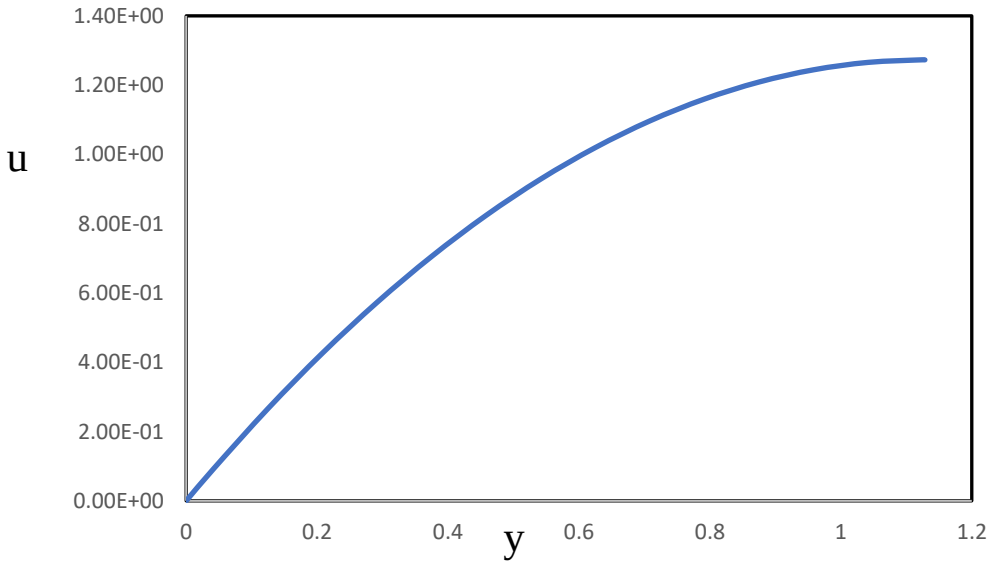

Figure 3.5 (a): Instantaneous velocity profile for solid substrate

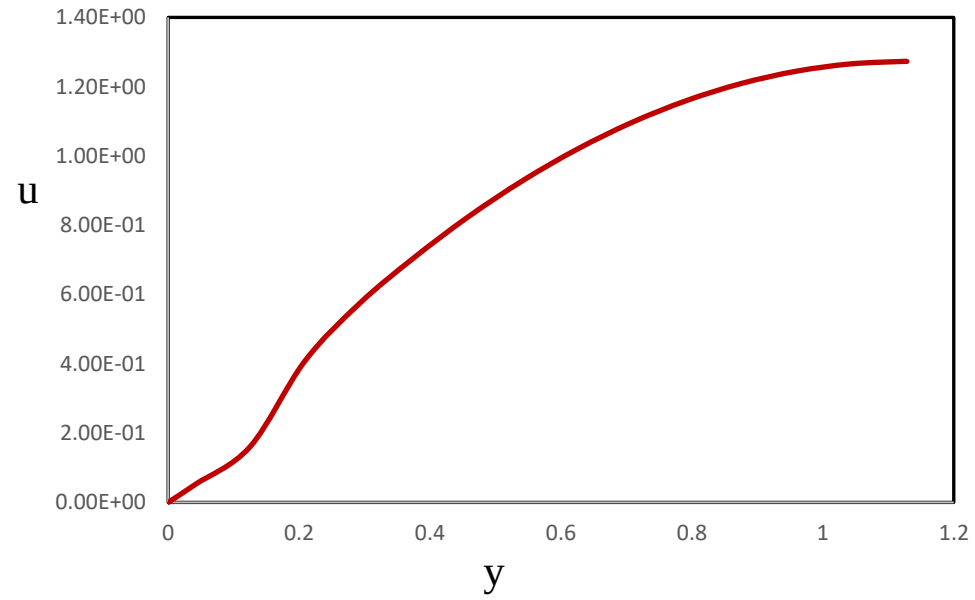

Figure 3.5 (b): Instantaneous velocity profile for porous wall

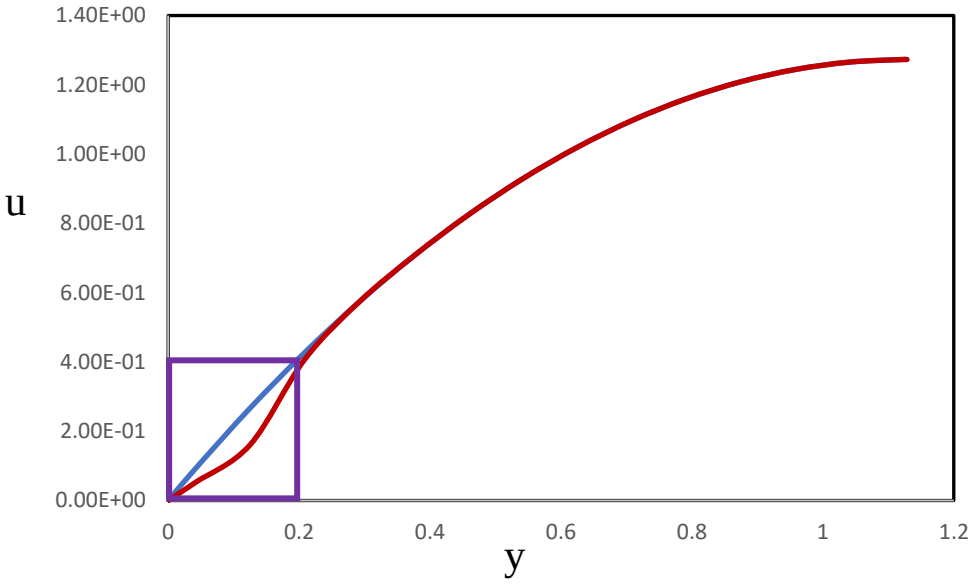

Figure 3.5 (c): Combine instantaneous velocity profile for solid substrate and porous wall

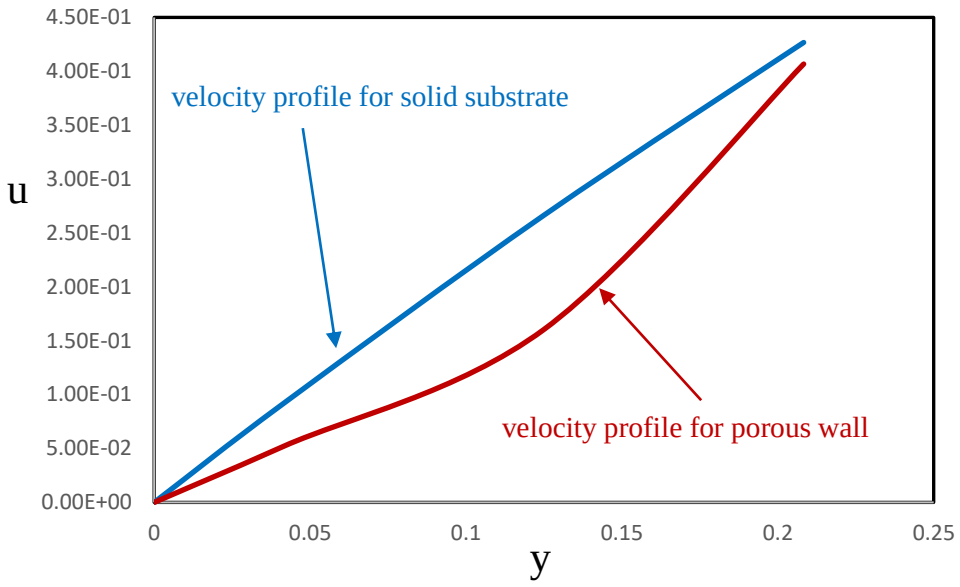

Figure 3.5 (d): Instantaneous velocity profile only for box

3.5 Conclusions

wave shapes developed from different inlet disturbance frequencies. For all frequencies, the inlet disturbances quickly develop to saturated wave of which wave length and amplitude are almost constant along the downstream. Wave front is steeper than wave wear for the case of low frequency. In the case of high frequencies wave is almost symmetry.

References

[1] Kapitza, P. L., Kapitza, S. P., 1949. Wave flow of thin fluid layers of liquid. Zh. Eksp. Teor. Fiz. 19, 105; also, in Collected Works of P. L. Kapitza, edited by D. Ter Haar Pergamon, Oxford, 1965.

[2] H.-C. Chang, "Wave evolution on a falling film, 1994. Annu. Rev. Fluid Mech. 26, 103.

[3] A. Oron, S. H. Davis, and S. G. Bankoff, 1997. Long-scale evolution of thin liquid films, Rev. Mod. Phys. 69, 931.

[4] D. J. Benney, 1966. Long waves on liquid films, J. Math. Phys. _Cambridge, Mass._ 45, 150.

[5] P. Rosenau, A. Oron, and J. Hyman, 1992. Bounded and unbounded patterns of the Benney equation, Phys. Fluids A 4, 1102.

[6] T. R. Salamon, R. C. Armstrong, and R. A. Brown, 1994. Traveling waves on vertical films: Numerical analysis using the finite element method, Phys. Fluids 6, 2202.

[7] A. Oron and O. Gottlieb, 2001. Nonlinear dynamics of temporally excited falling liquid films," Phys. Fluids 14, 2622.

[8] B. Scheid, C. Ruyer-Quil, U. Thiele, O. A. Kabov, J. C. Legros, and P. Colinet, 2005. Validity domain of the Benney equation including Marangoni effect for closed and open flows, J. Fluid Mech. 527, 303.

[9] J. P. Burelbach, S. G. Bankoff, and S. H. Davis, 1988. Nonlinear stability of evaporating/condensing liquid films, J. Fluid Mech. 195, 463.

[10] J. P. Burelbach, S. G. Bankoff, and S. H. Davis, 1990. Steady thermocapillary flows of thin liquid layers. II. Experiment, Phys. Fluids A 2, 322.

[11] A. A. Golovin, A. A. Nepomnyashchy, and L. M. Pismen, 1994. Interaction between short-scale Marangoni convection and long-scale deformational instability, Phys. Fluids 6, 34.

[12] S. J. VanHook, M. F. Schatz, W. D. McCormick, J. B. Swift, and H. L. Swinney, 1995. Long-wavelength instability in surface-tension-driven Bénard convection, Phys. Rev. Lett. **75**, 4397.

[13] S. J. VanHook, M. F. Schatz, J. B. Swift, W. D. McCormick, and H. L. Swinney, 1997. Long-wavelength surface-tension-driven Bénard convection: Experiment and theory, J. Fluid Mech. 345, 45.

[14] P. Colinet, J. C. Legros, and M. G. Velarde, 2001. *Surface-Tension-Driven Instabilities*, _Wiley-VCH, Berlin.

[15] A. Oron and P. Rosenau, 1992. Formation of patterns induced by thermocapillarity and gravity, J. Phys. II **2**, 131.

[16] A. Oron and S. G. Bankoff, 2001. Dynamics of a condensing liquid film under conjoining/disjoining pressures, Phys. Fluids 13, 1107.

[17] M. Bestehorn, A. Pototsky, and U. Thiele, 2003. 3D large scale Marangoni convection in liquid films," Eur. Phys. J. B 33, 457.

[18] U. Thiele and E. Knobloch, 2004. Thin liquid films on a slightly inclined heated plate," Physica D 190, 213.

[19] V. M. Starov, M. G. Velarde, and C. J. Radke, 2007. *Wetting and Spreading Dynamics* _Taylor & Francis, Boca Raton, FL.

[20] S. W. Joo, S. H. Davis, and S. G. Bankoff, 1991. Long-wave instabilities of heated falling films: Two-dimensional theory of uniform layers," J. Fluid Mech. 230, 117-146.

[21] G. S. Beavers and D. D. Joseph, 1967. Boundary conditions at a naturally permeable wall, J. Fluid Mech. 30, 197.

[22] P. G. Saffman, 1971. On the boundary condition at the surface of a porous medium, Stud. Appl. Math. 50, 93.

[23] G. S. Beavers, E. M. Sparrow, and R. A. Magnuson, 1970. Experiments on coupled parallel flows in a channel and a bounding porous medium, J. Basic Eng. 92, 843.

[24] G. Neale and W. Nader, 1974. Practical significance of Brinkman's extension of Darcy's law: Coupled parallel flow within a channel and a bounding porous medium, Can. J. Chem. Eng. 52, 475.

[25] H. C. Brinkman, 1947. A calculation of the viscous force exerted by flowing fluid on a dense swarm of particles, Appl. Sci. Res. A1, 27.

[26] G. Bayada and M. Chambat, 1995. On interface conditions for a thin film flow past a porous medium, SIAM J. Math. Anal. 26, 1113.

[27] J. P. Pascal, 1999. Linear stability of fluid flow down a porous inclined plane, J. Phys. D 32, 417.

[28] J. P. Pascal, 2006. Instability of power-law fluid flow down a porous incline," J.Non-Newtonian Fluid Mech. 133, 109.

[29] Uwe Thiele, Benoit Goyeau and Manuel G. Velarde, 2009. Stability analysis of thin film flow along a heated porous wall, PHYSICS OF FLUIDS 21, 014103

[30] Akio Miyara, 2000. Numerical simulation of wavy liquid film flowing down on a vertical wall and an inclined wall, Int. J. Therm. Sci. 39, 1015–1027.

[31] B. Goyeau, D. Lhuillier, D. Gobin, and M. G. Velarde, 2003. Momentum transport at a fluid-porous interface, Int. J. Heat Mass Transfer 46, 4071.

[32] S. Whitaker, 1996. The Forchheimer equation: A theoretical derivation of Darcy's law, Transp. Porous Media 25, 27.

[33] P. Bousquet-Melou, B. Goyeau, M. Quintard, F. Fichot, and D. Gobin, 2002. Average momentum equation for interdendritic flow in a solidifying columnar mushy zone," Int. J. Heat Mass Transfer 45, 3651.

CHAPTER FOUR

Similarity Solution of Heat and Mass transfer for Liquid Evaporation along a Vertical Plate Covered with a Thin Porous Layer

4.1 Introduction

Effective latent heat transfer mechanism widely utilized in industrial fields such as chemical distillation, air conditioning, cooling towers, drying, and desalination which is liquid film evaporation. With the liquid film exposed to a forced gas stream, the physical scheme consists of a thin liquid film flowing down along a heated plate. Because part of the liquid evaporates into the gas stream, liquid film evaporation possesses a high heat transfer coefficient, low feed rates and other inherent advantages. However, the transport phenomena involve the coupled heat and mass transfer at the liquid film–gas interface because the theoretical analysis of liquid film evaporation problem is inherently complicated.

The problem based on simplified 1-D and 2-D mathematical models are usually examined in previous research. [1-4] was used the 1-D model to develop the governing conservation of mass, mass species, momentum and energy by the conservation laws to the control volumes of the liquid film and moist air. The heat and mass transfer characteristics in a wet surface heat exchanger which are analyzed by MaClaine-Cross and Bank [1,2]. The experimental data are 20% smaller than their results. A 1-D design methodology for a counter-current falling film evaporative cooler which is illustrated by Wassel and Mills [3]. The narrow flow passages were found to be more effective than conventional designs for the thermal performance of the evaporative condenser. Perez-Blanco and Bird [4] was formulated a 1-D model of heat and mass transfer in the evaporative cooling process that takes place in a single-tube exchanger. In advance 2-D model composition focused on heat and mass transfer in the gas stream, with the liquid film considered to be at rest and with a very thin constant thickness. For the gas stream, the vaporizing liquid film is treated as the boundary condition (Gebhart and Pera [5], Chen and Yuh [6] and the temperature

distributions across the film are assumed to be linear (Shembharkar and Pai [7], Baumann [8]). There are many researches with more rigorous treatments of the equations governing the liquid film and liquid–gas interface have been published. The evaporative cooling of liquid film through interfacial heat and mass transfer in a vertical channel was studied by Yan and Lin [9]. The numerical solution for convective heat and mass transfer along an inclined heated plate with film evaporation which is presented by Yan and Soong [10]. The cooling characteristics of a wet surface heat exchanger with a liquid film evaporating into a countercurrent moist air flow which is numerically analyzed by Tsay [11]. Neglected inertia in the momentum equation and the normal convection term in the heat equation for liquid film flow, thus the liquid film flow is simplified to a 1-D momentum equation and 1-D (or 2-D) heat equation which are studied the above [9-11]. Recently Mezaache and Daguenet [12] was studied the complete two-dimensional boundary layer model for the evaporating liquid and gas flows along an inclined plate. Recently, J.-S. Leu et al. [14] studied the effect of the porous layer on heat and mass transfer. Their parametric analyses focused on features such as gas inlet conditions and the structural properties of the porous material on the performance of liquid film evaporation. The free convection boundary layer flow of a Darcy–Brinkman fluid induced by a horizontal surface embedded in a fluid-saturated porous layer which is explained by Rees and Vafai [15] for the studies of heat and mass transfer for liquid film flow in porous medium. The fluid flow and heat transfer interfacial conditions between a porous medium and a fluid layer which is detailed analyzed by Alazmi and Vafai [16]. The coupled heat and mass transfer in a stagnation point flow of air through a heated porous bed with thin liquid film evaporation studied by Zhao [17]. Also, Zhao [17] assumed the liquid layer was very thin and stationary, and the air stream was idealized as the stagnation point flow pattern to achieve the analytical solution. Khader and Megahed [18] are presented a numerical technique which is the implicit finite difference method to the search for the numerical solutions for the given equations. Their technique reduces the problem to a system of algebraic equations. Recently, M. Hasanuzzaman and A. Miyara[19] have been studied a possible similarity solution of unsteady natural convection laminar boundary layer flow of viscous incompressible fluid caused by a heated(or cooled) axi-symmetric slender body of finite axial length immersed vertically in a viscous incompressible fluid.

The purpose of the present study is, therefore, to find a possible similarity solution of heat and mass transfer for liquid evaporation along a vertical plate covered with a thin porous

layer. We are attempted to investigate the effects of several involved parameters on the velocity temperature and concentration fields. The numerical results including the velocity and temperature fields are to be presented graphically for different selected values of the established dimensionless parameters. The local skin friction, local Nusselt number and the local Sherwood numbers are computed numerically and graphically as well as analyzed.

4.2 Model and Governing Equations

Figure 4.1 shows the physical model and the coordinates.

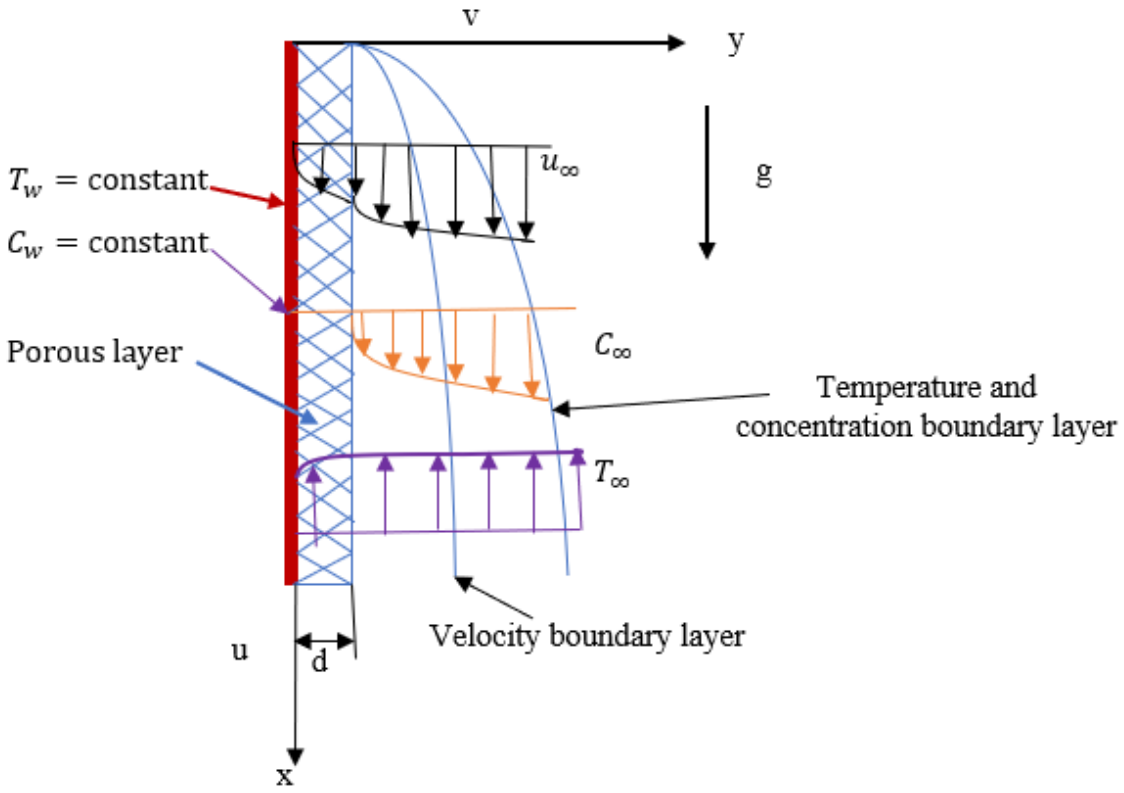

Figure 4.1: Physical model and coordinates system

4.2.1 Region of Liquid Film

The order of magnitude analysis showed that the inertia terms in the momentum equation can be neglected as compared with the diffusion term which is under the assumption of thin liquid film. The transverse direction is much greater than in the longitudinal gradients of velocity and temperature. The momentum and energy boundary layer equations by including the non-Darcian models of boundary viscous and inertia effects are as follows:

$$\frac{\partial u_l}{\partial x} + \frac{\partial v_l}{\partial y} = 0 \qquad (4.1)$$

$$0 = \rho_l g + \frac{\mu_l}{b}\frac{\partial^2 u_l}{\partial y^2} - \frac{\mu_l}{K}u_l - \frac{\rho_l C}{\sqrt{K}}u_l^2 \tag{4.2}$$

$$u_l \frac{\partial T_l}{\partial x} = \alpha_e \frac{\partial^2 T_l}{\partial y^2} \tag{4.3}$$

where the subscript "*l*" represents the variables of the liquid stream. *b* is the porosity, μ_l is the dynamic viscosity, *K* is the permeability of the porous medium, C is the flow inertia parameter [20], ρ_l is density and α_e is the effective thermal diffusivity.

4.2.2 Region of Gas Stream

The following two-dimensional laminar continuity, momentum, energy as well as concentration equations can be written as

$$\frac{\partial u_g}{\partial x} + \frac{\partial v_g}{\partial y} = 0 \tag{4.4}$$

$$u_g \frac{\partial u_g}{\partial x} + v_g \frac{\partial u_g}{\partial y} = \nu_g \frac{\partial^2 u_g}{\partial y^2} \tag{4.5}$$

$$u_g \frac{\partial T_g}{\partial x} + v_g \frac{\partial T_g}{\partial y} = \alpha_g \frac{\partial^2 T_g}{\partial y^2} \tag{4.6}$$

$$u_g \frac{\partial \omega}{\partial x} + v_g \frac{\partial \omega}{\partial y} = D \frac{\partial^2 \omega}{\partial y^2} \tag{4.7}$$

where the subscript "g" represents the variables of the gas stream. ω is the mass concentration, ρ is the density, ν is kinematic viscosity, α_g is the thermal diffusivity and *D* is the mass diffusivity of the gas.

4.3 Boundary Conditions

The appropriate boundary conditions for the present problem are:

at wall $y = 0$,

$$u_l = 0, T_l = T_w \tag{4.8}$$

at free stream $y = \infty$,

$$u_g = u_{g,\infty}, \quad T_g = T_{g,\infty}, \ \omega = \omega_\infty \tag{4.9}$$

at interface $y = d$,

$$u_i = u_{l,i} = u_{g,i}, \ T_i = T_{l,i} = T_{g,i} \tag{4.10}$$

$$v_{g,i} = -\frac{D}{1-\omega_i}\left(\frac{\partial \omega}{\partial y}\right)_i \tag{4.11}$$

$$\left(\mu_l \frac{\partial u}{\partial y}\right)_{l,i} = \left(\mu_g \frac{\partial u}{\partial y}\right)_{g,i} = \tau_i \tag{4.12}$$

$$\omega = \omega_i \tag{4.13}$$

$$q_t'' = -k_l \left(\frac{\partial T_l}{\partial y}\right)_i \text{ and } q_t'' = q_s'' + q_l'' = -k_g \left(\frac{\partial T_g}{\partial y}\right)_i + m_v'' h_{fg} \tag{4.14}$$

The continuity of shear stress and energy balance at the gas-liquid interface are expressed by eqs. (4.11) and (4.12). From the wall the total heat flux q_t'' can be transferred to two modes: one is the sensible heat flux via gas temperature gradient q_g'' , the other is the latent heat flux via the liquid film vaporization q_s''.

The interfacial evaporating mass flux during the calculated procedure is given by

$$m_v'' = \rho_g v_{g,i} = -\frac{\rho_g D}{1-\omega_i}\left(\frac{\partial \omega}{\partial y}\right)_i \tag{4.15}$$

And the mass concentration ω_i is expressed as

$$\omega_i = \frac{M_v}{M_g}\frac{p_{v,i}}{p_g} \tag{4.15}$$

where $p_{v,i}$ is the partial pressure of the saturated vapor at the gas-liquid interface. Bird et. al., [21] can be evaluated the inlet mass flow rate of the liquid film.

$$m_{l,in} = \frac{\rho_l g}{3\nu_l} d^3 b^3 \tag{4.16}$$

4.4 Similarity Transformations

The relation between stream functions and velocity components for the liquid film and the gas boundary layer which are defined, respectively, by

$$u_l = \frac{\partial \psi_l}{\partial y}, \quad v_l = -\frac{\partial \psi_l}{\partial x} \tag{4.17}$$

$$u_g = \frac{\partial \psi_g}{\partial y}, \quad v_g = -\frac{\partial \psi_g}{\partial x} \tag{4.18}$$

are introduced. Eq. (4.1) and (4.4) are automatically satisfied. We introduce the independent variables η_l and η_g, the dimensionless stream functions $F_l(\eta_l)$ and $F_g(\eta_g)$, the dimensionless temperatures $\theta_l(\eta_l)$ and $\theta_g(\eta_g)$, and the normalized concentration $\phi(\eta_g)$ as

$$\eta_l = y\left(\frac{u_{g\infty}}{\nu_l x}\right)^{\frac{1}{2}} \tag{4.19}$$

$$\eta_g = (y-d)\left(\frac{u_{g\infty}}{\nu_g x}\right)^{\frac{1}{2}} \tag{4.20}$$

$$F_l(\eta_l) = \frac{\psi_l}{\left(\nu_l u_{g\infty} x\right)^{\frac{1}{2}}} \tag{4.21}$$

$$F_g(\eta_g) = \frac{\psi_g}{\left(\nu_g u_{g\infty} x\right)^{\frac{1}{2}}} \tag{4.22}$$

$$\theta_l(\eta_l) = \frac{T_i - T_l}{T_i - T_w} \tag{4.23}$$

$$\theta_g(\eta_g) = \frac{T_{g\infty} - T_g}{T_{g\infty} - T_i} \tag{4.24}$$

$$\phi(\eta_g) = \frac{\omega - \omega_\infty}{\omega_i - \omega_\infty} \tag{4.25}$$

Now,

$$u_l = \frac{\partial \psi_l}{\partial y} = \frac{\partial}{\partial y}\left\{F_l(\eta_l)\left(\nu_l u_{g\infty} x\right)^{\frac{1}{2}}\right\}$$

$$= \left(\nu_l u_{g\infty} x\right)^{\frac{1}{2}} \frac{\partial}{\partial y}\{F_l(\eta_l)\}$$

$$= \left(\nu_l u_{g\infty} x\right)^{\frac{1}{2}} \frac{\partial}{\partial \eta_l}\{F_l(\eta_l)\}\frac{\partial \eta_l}{\partial y}$$

$$= \left(\nu_l u_{g\infty} x\right)^{\frac{1}{2}} F_l'(\eta_l)\left(\frac{u_{g\infty}}{\nu_l x}\right)^{\frac{1}{2}}$$

$$= u_{g\infty} F_l'(\eta_l) \tag{4.26}$$

$$v_l = -\frac{\partial \psi_l}{\partial x} = -\frac{\partial}{\partial x}\left\{F_l(\eta_l)\left(\nu_l u_{g\infty} x\right)^{\frac{1}{2}}\right\}$$

$$= -F_l(\eta_l)\left(\nu_l u_{g\infty}\right)^{\frac{1}{2}} \frac{\partial}{\partial x}\left\{(x)^{\frac{1}{2}}\right\} - \left(\nu_l u_{g\infty} x\right)^{\frac{1}{2}} \frac{\partial}{\partial x}\{F_l(\eta_l)\}$$

$$= -F_l(\eta_l)\left(\nu_l u_{g\infty}\right)^{\frac{1}{2}} \frac{1}{2} x^{-\frac{1}{2}} - \left(\nu_l u_{g\infty} x\right)^{\frac{1}{2}} \frac{\partial}{\partial \eta_l}\{F_l(\eta_l)\}\frac{\partial \eta_l}{\partial x}$$

$$= -\frac{1}{2} F_l(\eta_l)\left(\nu_l u_{g\infty}\right)^{\frac{1}{2}} x^{-\frac{1}{2}} - \left(\nu_l u_{g\infty} x\right)^{\frac{1}{2}} F_l'(\eta_l) F_l'(\eta_l) \frac{\partial}{\partial x}\left\{y\left(\frac{u_{g\infty}}{\nu_l x}\right)^{\frac{1}{2}}\right\}$$

$$= -\frac{1}{2} F_l(\eta_l)\left(\nu_l u_{g\infty}\right)^{\frac{1}{2}} x^{-\frac{1}{2}} - \left(\nu_l u_{g\infty} x\right)^{\frac{1}{2}} F_l'(\eta_l) y\left(\frac{u_{g\infty}}{\nu_l}\right)^{\frac{1}{2}}\left(-\frac{1}{2} x^{-\frac{3}{2}}\right)$$

$$= -\frac{1}{2}F_l(\eta_l)\left(\nu_l u_{g\infty}\right)^{\frac{1}{2}}x^{-\frac{1}{2}} + \frac{1}{2}\left(\nu_l u_{g\infty}x\right)^{\frac{1}{2}}F_l'(\eta_l)\eta_l\left(\frac{u_{g\infty}}{\nu_l x}\right)^{-\frac{1}{2}}\left(\frac{u_{g\infty}}{\nu_l}\right)^{\frac{1}{2}}\left(x^{-\frac{3}{2}}\right)$$

$$= -\frac{1}{2}F_l(\eta_l)\left(\nu_l u_{g\infty}\right)^{\frac{1}{2}}x^{-\frac{1}{2}} + \frac{1}{2}\left(\nu_l u_{g\infty}\right)^{\frac{1}{2}}F_l'(\eta_l)\eta_l x^{-\frac{1}{2}}$$

$$= \frac{1}{2}\left(\nu_l u_{g\infty}\right)^{\frac{1}{2}}x^{-\frac{1}{2}}[\eta_l F_l'(\eta_l) - F_l(\eta_l)] \qquad (4.27)$$

$$\frac{\partial u_l}{\partial x} = \frac{\partial}{\partial x}\{u_{g\infty}F_l'(\eta_l)\}$$

$$= u_{g\infty}\frac{\partial}{\partial \eta_l}\{F_l'(\eta_l)\}\frac{\partial \eta_l}{\partial x}$$

$$= u_{g\infty}F''_l(\eta_l)\frac{\partial}{\partial x}\left\{y\left(\frac{u_{g\infty}}{\nu_l x}\right)^{\frac{1}{2}}\right\}$$

$$= u_{g\infty}F''_l(\eta_l)y\left(\frac{u_{g\infty}}{\nu_l}\right)^{\frac{1}{2}}\left(-\frac{1}{2}x^{-\frac{3}{2}}\right)$$

$$= -\frac{1}{2}u_{g\infty}F''_l(\eta_l)\eta_l\left(\frac{u_{g\infty}}{\nu_l x}\right)^{-\frac{1}{2}}\left(\frac{u_{g\infty}}{\nu_l}\right)^{\frac{1}{2}}\left(x^{-\frac{3}{2}}\right)$$

$$= -\frac{1}{2}\frac{u_{g\infty}}{x}\eta_l F''_l(\eta_l) \qquad (4.28)$$

$$\frac{\partial v_l}{\partial y} = \frac{\partial}{\partial y}\left\{\frac{1}{2}\left(\nu_l u_{g\infty}\right)^{\frac{1}{2}}x^{-\frac{1}{2}}[\eta_l F_l'(\eta_l) - F_l(\eta_l)]\right\}$$

$$= \frac{1}{2}\left(\nu_l u_{g\infty}\right)^{\frac{1}{2}}x^{-\frac{1}{2}}\frac{\partial}{\partial y}[\eta_l F_l'(\eta_l) - F_l(\eta_l)]$$

$$= \frac{1}{2}\left(\nu_l u_{g\infty}\right)^{\frac{1}{2}}x^{-\frac{1}{2}}\frac{\partial}{\partial \eta_l}[\eta_l F_l'(\eta_l) - F_l(\eta_l)]\frac{\partial \eta_l}{\partial y}$$

$$= \frac{1}{2}\left(\nu_l u_{g\infty}\right)^{\frac{1}{2}}x^{-\frac{1}{2}}[\eta_l F_l''(\eta_l) + F_l'(\eta_l) - F_l'(\eta_l)]\left(\frac{u_{g\infty}}{\nu_l x}\right)^{\frac{1}{2}}$$

$$= \frac{1}{2}\frac{u_{g\infty}}{x}\eta_l F_l''(\eta_l) \qquad (4.29)$$

$$\frac{\partial u_l}{\partial y} = \frac{\partial}{\partial y}\{u_{g\infty}F_l'(\eta_l)\}$$

$$= u_{g\infty}\frac{\partial}{\partial \eta_l}\{F_l'(\eta_l)\}\frac{\partial \eta_l}{\partial y}$$

$$= u_{g\infty}\frac{\partial}{\partial \eta_l}\{F_l'(\eta_l)\}\left(\frac{u_{g\infty}}{\nu_l x}\right)^{\frac{1}{2}}$$

$$= \frac{u_{g\infty}^{\frac{3}{2}}}{(\nu_l x)^{\frac{1}{2}}}F_l''(\eta_l) \qquad (4.30)$$

$$\frac{\partial^2 u_l}{\partial y^2} = \frac{\partial}{\partial y}\left\{\frac{u_{g\infty}^{\frac{3}{2}}}{(\nu_l x)^{\frac{1}{2}}}F_l''(\eta_l)\right\}$$

$$= \frac{u_{g\infty}^{\frac{3}{2}}}{(\nu_l x)^{\frac{1}{2}}}\frac{\partial}{\partial \eta_l}\{F_l''(\eta_l)\}\frac{\partial \eta_l}{\partial y}$$

$$= \frac{u_{g\infty}^{\frac{3}{2}}}{(\nu_l x)^{\frac{1}{2}}}\frac{\partial}{\partial \eta_l}\{F_l''(\eta_l)\}\left(\frac{u_{g\infty}}{\nu_l x}\right)^{\frac{1}{2}}$$

$$= \frac{u_{g\infty}^{\frac{3}{2}}}{\nu_l x}F_l''(\eta_l) \qquad (4.31)$$

$$\frac{\partial T_l}{\partial x} = \frac{\partial}{\partial x}\{T_i + (T_w - T_i)\theta_l\}$$

$$= (T_w - T_i)\frac{\partial}{\partial x}\{\theta_l\}$$

$$= (T_w - T_i)\frac{\partial}{\partial \eta_l}\{\theta_l\}\frac{\partial \eta_l}{\partial x}$$

$$= (T_w - T_i)\theta_l'\frac{\partial}{\partial x}\left\{y\left(\frac{u_{g\infty}}{\nu_l x}\right)^{\frac{1}{2}}\right\}$$

$$= (T_w - T_i)\theta_l'\, y\left(\frac{u_{g\infty}}{\nu_l}\right)^{\frac{1}{2}}\left(-\frac{1}{2}x^{-\frac{3}{2}}\right)$$

$$= -\frac{1}{2}(T_w - T_i)\theta_l'\,\eta_l\left(\frac{u_{g\infty}}{\nu_l x}\right)^{-\frac{1}{2}}\left(\frac{u_{g\infty}}{\nu_l}\right)^{\frac{1}{2}}\left(x^{-\frac{3}{2}}\right)$$

$$= -\frac{1}{2}\frac{\eta_l}{x}(T_w - T_i)\theta_l' \qquad (4.32)$$

$$\frac{\partial T_l}{\partial y} = \frac{\partial}{\partial y}\{T_i + (T_w - T_i)\theta_l\}$$

$$= \frac{\partial}{\partial \eta_l}\{T_i + (T_w - T_i)\theta_l\}\frac{\partial \eta_l}{\partial y}$$

$$= (T_w - T_i)\theta_l'\left(\frac{u_{g\infty}}{\nu_l x}\right)^{\frac{1}{2}} \tag{4.33}$$

$$\frac{\partial^2 T_l}{\partial y^2} = \frac{\partial}{\partial y}\left\{(T_w - T_i)\theta_l'\left(\frac{u_{g\infty}}{\nu_l x}\right)^{\frac{1}{2}}\right\}$$

$$= \frac{\partial}{\partial \eta_l}\left\{(T_w - T_i)\theta_l'\left(\frac{u_{g\infty}}{\nu_l x}\right)^{\frac{1}{2}}\right\}\frac{\partial \eta_l}{\partial y}$$

$$= (T_w - T_i)\theta_l''\left(\frac{u_{g\infty}}{\nu_l x}\right)^{\frac{1}{2}}\left(\frac{u_{g\infty}}{\nu_l x}\right)^{\frac{1}{2}}$$

$$= \frac{u_{g\infty}}{\nu_l x}(T_w - T_i)\theta_l'' \tag{4.34}$$

Using Eqs. (4.26)- (4.43), the mathematical problems defined in liquid film region Eqs. (4.1) -(4.3) are then transferred into the following set of ordinary differential equations:

Now, Equ. (4.1) becomes

$$\frac{\partial u_l}{\partial x} + \frac{\partial v_l}{\partial y}$$

$$= -\frac{1}{2}\frac{u_{g\infty}}{x}\eta_l F_l''(\eta_l) + \frac{1}{2}\frac{u_{g\infty}}{x}\eta_l F_l''(\eta_l)$$

$$= 0$$

Hence the continuity equation in liquid film region is satisfied.

Again, Equ. (4.2) becomes

$$0 = \rho_l g + \frac{\mu_l}{b}\frac{\partial^2 u_l}{\partial y^2} - \frac{\mu_l}{K}u_l - \frac{\rho_l C}{\sqrt{K}}u_l^2$$

$$\Rightarrow 0 = \rho_l g + \frac{\mu_l}{b}\frac{u_{g\infty}^2}{\nu_l x}F_l'''(\eta_l) - \frac{\mu_l}{K}u_{g\infty}F_l'(\eta_l) - \frac{\rho_l C}{\sqrt{K}}u_{g\infty}^2 {F_l'}^2(\eta_l)$$

$$\Rightarrow 0 = \rho_l g\frac{\nu_l x}{\mu_l u_{g\infty}^2} + \frac{1}{b}F_l'''(\eta_l) - \frac{\mu_l}{K}\frac{\nu_l x}{\mu_l u_{g\infty}^2}u_{g\infty}F_l'(\eta_l) - \frac{\rho_l C}{\sqrt{K}}u_{g\infty}^2\frac{\nu_l x}{\mu_l u_{g\infty}^2}{F_l'}^2(\eta_l)$$

$$\Rightarrow 0 = \rho_l g\frac{\nu_l x}{\mu_l u_{g\infty}^2} + \frac{1}{b}F_l'''(\eta_l) - \frac{\mu_l}{K}\frac{\nu_l x}{\mu_l u_{g\infty}^2}u_{g\infty}F_l'(\eta_l) - \frac{\rho_l C}{\sqrt{K}}u_{g\infty}^2\frac{\nu_l x}{\mu_l u_{g\infty}^2}{F_l'}^2(\eta_l)$$

$$\Rightarrow 0 = \rho_l g\frac{\nu_l x}{\mu_l u_{g\infty}^2} + \frac{1}{b}F_l'''(\eta_l) - \frac{\mu_l}{K}\frac{\nu_l x}{\mu_l u_{g\infty}^2}u_{g\infty}F_l'(\eta_l) - \frac{\rho_l C}{\sqrt{K}}u_{g\infty}^2\frac{\nu_l x}{\mu_l u_{g\infty}^2}{F_l'}^2(\eta_l)$$

$$\Rightarrow 0 = \frac{gx}{u_{g\infty}^2} + \frac{1}{b}F_l'''(\eta_l) - \frac{\nu_l x}{K u_{g\infty}}F_l'(\eta_l) - \frac{xC}{\sqrt{K}}{F_l'}^2(\eta_l)$$

$$\Rightarrow 0 = \frac{gx}{u_{g\infty}^2} + \frac{1}{b}F_l'''(\eta_l) - \frac{\nu_l x}{K u_{g\infty}}F_l'(\eta_l) - \frac{\nu_l x}{K u_{g\infty}}\frac{C u_{g\infty}\sqrt{K}}{\nu_l}F_l'^2(\eta_l)$$

$$\Rightarrow 0 = \frac{1}{Fr^2} + \frac{1}{b}F_l'''(\eta_l) - \frac{1}{Da}F_l'(\eta_l) - \frac{\Gamma}{Da}F_l'^2(\eta_l) \quad (4.35)$$

And, Equ. (4.3) becomes

$$u_l\frac{\partial T_l}{\partial x} = \alpha_e\frac{\partial^2 T_l}{\partial y^2}$$

$$\Rightarrow -\frac{1}{2}u_{g\infty}F_l'(\eta_l)\frac{\eta_l}{x}(T_w - T_i)\theta_l' = \alpha_e\frac{u_{g\infty}}{\nu_l x}(T_w - T_i)\theta_l''$$

$$\Rightarrow -\frac{1}{2}\eta F_l'(\eta_l)\theta_l' = \frac{\alpha_e}{\nu_l}\theta_l''$$

$$\Rightarrow \frac{1}{Pr_l}\theta_l'' + \frac{1}{2}\eta F_l'(\eta_l)\theta_l' = 0 \quad (4.36)$$

$Fr = \frac{u_{g\infty}}{\sqrt{gx}}$ is the Froude number, $Da = \frac{u_{g\infty}}{\nu_l x}$ is the Darcy number, $\Gamma = \frac{C\sqrt{K}u_{g\infty}}{\nu_l}$ is the dimensionless inertia coefficient of non-Darcy flow and $Pr_l = \frac{\nu_l}{\alpha_e}$ is the Prandtl number in liquid film region.

Region of Gas Stream:

$$u_g = \frac{\partial \psi_g}{\partial y} = \frac{\partial}{\partial y}\left\{F_g(\eta_g)(\nu_g u_{g\infty}x)^{\frac{1}{2}}\right\}$$

$$= (\nu_g u_{g\infty}x)^{\frac{1}{2}}\frac{\partial}{\partial y}\{F_g(\eta_g)\}$$

$$= (\nu_g u_{g\infty}x)^{\frac{1}{2}}\frac{\partial}{\partial \eta_g}\{F_g(\eta_g)\}\frac{\partial \eta_g}{\partial y}$$

$$= (\nu_g u_{g\infty}x)^{\frac{1}{2}}F_g'(\eta_g)\left(\frac{u_{g\infty}}{\nu_g x}\right)^{\frac{1}{2}}$$

$$= u_{g\infty}F_g'(\eta_g) \quad (4.37)$$

$$v_g = -\frac{\partial \psi_l}{\partial x} = -\frac{\partial}{\partial x}\left\{F_g(\eta_g)(\nu_g u_{g\infty}x)^{\frac{1}{2}}\right\}$$

$$= -F_g(\eta_g)(\nu_g u_{g\infty})^{\frac{1}{2}}\frac{\partial}{\partial x}\left\{(x)^{\frac{1}{2}}\right\} - (\nu_g u_{g\infty}x)^{\frac{1}{2}}\frac{\partial}{\partial x}\{F_g(\eta_g)\}$$

$$= -F_g(\eta_g)(\nu_g u_{g\infty})^{\frac{1}{2}}\frac{1}{2}x^{-\frac{1}{2}} - (\nu_g u_{g\infty}x)^{\frac{1}{2}}\frac{\partial}{\partial \eta_g}\{F_g(\eta_g)\}\frac{\partial \eta_g}{\partial x}$$

$$= -\frac{1}{2}F_g(\eta_g)(\nu_g u_{g\infty})^{\frac{1}{2}}x^{-\frac{1}{2}} - (\nu_g u_{g\infty}x)^{\frac{1}{2}}F'_g(\eta_g)\frac{\partial}{\partial x}\left\{(y-d)\left(\frac{u_{g\infty}}{\nu_g x}\right)^{\frac{1}{2}}\right\}$$

$$= -\frac{1}{2}F_g(\eta_g)(\nu_g u_{g\infty})^{\frac{1}{2}}x^{-\frac{1}{2}} - (\nu_g u_{g\infty}x)^{\frac{1}{2}}F'_g(\eta_g)(y-d)\left(\frac{u_{g\infty}}{\nu_g}\right)^{\frac{1}{2}}\left(-\frac{1}{2}x^{-\frac{3}{2}}\right)$$

$$= -\frac{1}{2}F_g(\eta_g)(\nu_g u_{g\infty})^{\frac{1}{2}}x^{-\frac{1}{2}} + \frac{1}{2}(\nu_g u_{g\infty}x)^{\frac{1}{2}}F'_g(\eta_g)\eta_g\left(\frac{u_{g\infty}}{\nu_g x}\right)^{-\frac{1}{2}}\left(\frac{u_{g\infty}}{\nu_g}\right)^{\frac{1}{2}}\left(x^{-\frac{3}{2}}\right)$$

$$= -\frac{1}{2}F_g(\eta_g)(\nu_g u_{g\infty})^{\frac{1}{2}}x^{-\frac{1}{2}} + \frac{1}{2}(\nu_g u_{g\infty})^{\frac{1}{2}}F'_g(\eta_g)\eta_g x^{-\frac{1}{2}}$$

$$= \frac{1}{2}(\nu_g u_{g\infty})^{\frac{1}{2}}x^{-\frac{1}{2}}[\eta_g F'_g(\eta_g) - F_g(\eta_g)] \qquad (4.38)$$

$$\frac{\partial u_g}{\partial x} = \frac{\partial}{\partial x}\{u_{g\infty}F'_g(\eta_g)\}$$

$$= u_{g\infty}\frac{\partial}{\partial \eta_g}\{F'_g(\eta_g)\}\frac{\partial \eta_g}{\partial x}$$

$$= u_{g\infty}F''_g(\eta_g)\frac{\partial}{\partial x}\left\{(y-d)\left(\frac{u_{g\infty}}{\nu_g x}\right)^{\frac{1}{2}}\right\}$$

$$= u_{g\infty}F''_g(\eta_g)y\left(\frac{u_{g\infty}}{\nu_g}\right)^{\frac{1}{2}}\left(-\frac{1}{2}x^{-\frac{3}{2}}\right)$$

$$= -\frac{1}{2}u_{g\infty}F''_g(\eta_g)\eta_l\left(\frac{u_{g\infty}}{\nu_g x}\right)^{-\frac{1}{2}}\left(\frac{u_{g\infty}}{\nu_g}\right)^{\frac{1}{2}}\left(x^{-\frac{3}{2}}\right)$$

$$= -\frac{1}{2}\frac{u_{g\infty}}{x}\eta_g F'_g(\eta_g) \qquad (4.39)$$

$$\frac{\partial v_g}{\partial y} = \frac{\partial}{\partial y}\left\{\frac{1}{2}(\nu_g u_{g\infty})^{\frac{1}{2}}x^{-\frac{1}{2}}[\eta_g F'_g(\eta_g) - F_g(\eta_g)]\right\}$$

$$= \frac{1}{2}(\nu_g u_{g\infty})^{\frac{1}{2}}x^{-\frac{1}{2}}\frac{\partial}{\partial y}[\eta_g F'_g(\eta_g) - F_g(\eta_g)]$$

$$= \frac{1}{2}(\nu_g u_{g\infty})^{\frac{1}{2}}x^{-\frac{1}{2}}\frac{\partial}{\partial \eta_g}[\eta_g F'_g(\eta_g) - F_g(\eta_g)]\frac{\partial \eta_g}{\partial y}$$

$$= \frac{1}{2}(\nu_g u_{g\infty})^{\frac{1}{2}}x^{-\frac{1}{2}}[\eta_g F''_g(\eta_g) + F'_g(\eta_g) - F_g(\eta_g)]\left(\frac{u_{g\infty}}{\nu_g x}\right)^{\frac{1}{2}}$$

$$= \frac{1}{2}\frac{u_{g\infty}}{x}\eta_g F_g''(\eta_g) \tag{4.40}$$

$$\frac{\partial u_g}{\partial y} = \frac{\partial}{\partial y}\{u_{g\infty} F_g'(\eta_g)\}$$

$$= u_{g\infty}\frac{\partial}{\partial \eta_g}\{F_g'(\eta_g)\}\frac{\partial \eta_g}{\partial y}$$

$$= u_{g\infty}\frac{\partial}{\partial \eta_g}\{F_g'(\eta_g)\}\left(\frac{u_{g\infty}}{\nu_g x}\right)^{\frac{1}{2}}$$

$$= \frac{u_{g\infty}^{\frac{3}{2}}}{(\nu_g x)^{\frac{1}{2}}} F_g''(\eta_g) \tag{4.41}$$

$$\frac{\partial^2 u_g}{\partial y^2} = \frac{\partial}{\partial y}\left\{\frac{u_{g\infty}^{\frac{3}{2}}}{(\nu_g x)^{\frac{1}{2}}} F_g''(\eta_g)\right\}$$

$$= \frac{u_{g\infty}^{\frac{3}{2}}}{(\nu_g x)^{\frac{1}{2}}}\frac{\partial}{\partial \eta_g}\{F_g''(\eta_g)\}\frac{\partial \eta_g}{\partial y}$$

$$= \frac{u_{g\infty}^{\frac{3}{2}}}{(\nu_g x)^{\frac{1}{2}}}\frac{\partial}{\partial \eta_g}\{F_g''(\eta_g)\}\left(\frac{u_{g\infty}}{\nu_g x}\right)^{\frac{1}{2}}$$

$$= \frac{u_{g\infty}^2}{\nu_g x} F_g'''(\eta_g) \tag{4.42}$$

$$\frac{\partial T_g}{\partial x} = \frac{\partial}{\partial x}\{T_{g\infty} + (T_i - T_{g\infty})\theta_g\}$$

$$= (T_i - T_{g\infty})\frac{\partial}{\partial x}\{\theta_g\}$$

$$= (T_i - T_{g\infty})\frac{\partial}{\partial \eta_g}\{\theta_g\}\frac{\partial \eta_g}{\partial x}$$

$$= (T_i - T_{g\infty})\theta_g'\frac{\partial}{\partial x}\left\{(y-d)\left(\frac{u_{g\infty}}{\nu_g x}\right)^{\frac{1}{2}}\right\}$$

$$= (T_i - T_{g\infty})\theta_g'\,(y-d)\left(\frac{u_{g\infty}}{\nu_g}\right)^{\frac{1}{2}}\left(-\frac{1}{2}x^{-\frac{3}{2}}\right)$$

$$= -\frac{1}{2}(T_i - T_{g\infty})\theta_g' \, \eta_g \left(\frac{u_{g\infty}}{\nu_g x}\right)^{-\frac{1}{2}} \left(\frac{u_{g\infty}}{\nu_g}\right)^{\frac{1}{2}} \left(x^{-\frac{3}{2}}\right)$$

$$= -\frac{1}{2}\frac{\eta_g}{x}(T_i - T_{g\infty})\theta_g'$$

$$\frac{\partial T_g}{\partial y} = \frac{\partial}{\partial y}\{T_{g\infty} + (T_i - T_{g\infty})\theta_g\}$$

$$= \frac{\partial}{\partial \eta_g}\{T_{g\infty} + (T_i - T_{g\infty})\theta_g\}\frac{\partial \eta_g}{\partial y}$$

$$= (T_i - T_{g\infty})\theta_g' \left(\frac{u_{g\infty}}{\nu_g x}\right)^{\frac{1}{2}} \tag{4.43}$$

$$\frac{\partial^2 T_g}{\partial y^2} = \frac{\partial}{\partial y}\left\{(T_i - T_{g\infty})\theta_g' \left(\frac{u_{g\infty}}{\nu_g x}\right)^{\frac{1}{2}}\right\}$$

$$= \frac{\partial}{\partial \eta_g}\left\{(T_i - T_{g\infty})\theta_g' \left(\frac{u_{g\infty}}{\nu_g x}\right)^{\frac{1}{2}}\right\}\frac{\partial \eta_g}{\partial y}$$

$$= (T_i - T_{g\infty})\theta_g'' \left(\frac{u_{g\infty}}{\nu_g x}\right)^{\frac{1}{2}} \left(\frac{u_{g\infty}}{\nu_g x}\right)^{\frac{1}{2}}$$

$$= \frac{u_{g\infty}}{\nu_g x}(T_i - T_{g\infty})\theta_g'' \tag{4.44}$$

$$\frac{\partial \omega}{\partial x} = \frac{\partial}{\partial x}\{\omega_\infty + (\omega_i - \omega_\infty)\phi\}$$

$$= \frac{\partial}{\partial \eta_g}\{\omega_\infty + (\omega_i - \omega_\infty)\phi\}\frac{\partial \eta_g}{\partial x}$$

$$= (\omega_i - \omega_\infty)\phi' \frac{\partial}{\partial x}\left\{(y-d)\left(\frac{u_{g\infty}}{\nu_g x}\right)^{\frac{1}{2}}\right\}$$

$$= (\omega_i - \omega_\infty)\phi'(y-d)\left(\frac{u_{g\infty}}{\nu_g}\right)^{\frac{1}{2}}\left(-\frac{1}{2}x^{-\frac{3}{2}}\right)$$

$$= -\frac{1}{2}(\omega_i - \omega_\infty)\phi'\eta_g \left(\frac{u_{g\infty}}{\nu_g x}\right)^{-\frac{1}{2}} \left(\frac{u_{g\infty}}{\nu_g}\right)^{\frac{1}{2}} \left(x^{-\frac{3}{2}}\right)$$

$$= -\frac{1}{2}\frac{\eta_g}{x}(\omega_i - \omega_\infty)\phi' \tag{4.45}$$

$$\frac{\partial \omega}{\partial y} = \frac{\partial}{\partial y}\{\omega_\infty + (\omega_i - \omega_\infty)\phi\}$$
$$= \frac{\partial}{\partial \eta_g}\{\omega_\infty + (\omega_i - \omega_\infty)\phi\}\frac{\partial \eta_g}{\partial y}$$
$$= (\omega_i - \omega_\infty)\phi'\left(\frac{u_{g\infty}}{\nu_g x}\right)^{\frac{1}{2}} \tag{4.46}$$

$$\frac{\partial^2 \omega}{\partial y^2} = \frac{\partial}{\partial y}\left\{(\omega_i - \omega_\infty)\phi'\left(\frac{u_{g\infty}}{\nu_g x}\right)^{\frac{1}{2}}\right\}$$
$$= (\omega_i - \omega_\infty)\phi''\left(\frac{u_{g\infty}}{\nu_g x}\right)^{\frac{1}{2}}\left(\frac{u_{g\infty}}{\nu_g x}\right)^{\frac{1}{2}}$$
$$= (\omega_i - \omega_\infty)\phi''\left(\frac{u_{g\infty}}{\nu_g x}\right) \tag{4.47}$$

Again, using Eqs. (4.37)- (4.47), the mathematical problems defined in liquid film region Equs. (4.4) -(4.7) are then transferred into the following set of ordinary differential equations:

Now, Equ. (4.4) becomes

$$\frac{\partial u_g}{\partial x} + \frac{\partial v_g}{\partial y}$$
$$= -\frac{1}{2}\frac{u_{g\infty}}{x}\eta_g F'_g(\eta_g) + \frac{1}{2}\frac{u_{g\infty}}{x}\eta_g F'_g(\eta_g)$$
$$= 0$$

Hence the continuity equation in gas stream region is satisfied.

Again, Equ. (4.5) becomes

$$u_g\frac{\partial u_g}{\partial x} + v_g\frac{\partial u_g}{\partial y} = \nu_g\frac{\partial^2 u_g}{\partial y^2}$$

$$\Rightarrow u_{g\infty}F_g'(\eta_g)\left\{-\frac{1}{2}\frac{u_{g\infty}}{x}\eta_g F'_g(\eta_g)\right\}$$

$$+\frac{1}{2}(\nu_g u_{g\infty})^{\frac{1}{2}}x^{-\frac{1}{2}}[\eta_g F_g'(\eta_g)-F_g(\eta_g)]\times\frac{u_{g\infty}^{\frac{3}{2}}}{(\nu_g x)^{\frac{1}{2}}}F_g''(\eta_g)$$

$$=\nu_g\ \frac{u_{g\infty}^2}{\nu_g x}F_g'''(\eta_g)$$

$$\Rightarrow -\frac{1}{2}\frac{u_{g\infty}^2}{x}\eta_g F'_g(\eta_g)F_g'(\eta_g)+\frac{1}{2}\frac{u_{g\infty}^2}{x}\eta_g F'_g(\eta_g)F_g'(\eta_g)-\frac{1}{2}\frac{u_{g\infty}^2}{x}F_g(\eta_g)F_g''(\eta_g)$$

$$=\ \frac{u_{g\infty}^2}{x}F_g'''(\eta_g)$$

$$\Rightarrow -\frac{1}{2}\frac{u_{g\infty}^2}{x}F_g(\eta_g)F_g''(\eta_g)=\ \frac{u_{g\infty}^2}{x}F_g'''(\eta_g)$$

$$\Rightarrow -\frac{1}{2}F_g(\eta_g)F_g''(\eta_g)=\ F_g'''(\eta_g)$$

$$\Rightarrow F_g'''(\eta_g)+\frac{1}{2}F_g(\eta_g)F_g''(\eta_g)=\ 0 \qquad (4.48)$$

and, Equ. (4.6) becomes

$$u_g\frac{\partial T_g}{\partial x}+v_g\frac{\partial T_g}{\partial y}=\alpha_g\frac{\partial^2 T_g}{\partial y^2}$$

$$\Rightarrow u_{g\infty}F_g'(\eta_g)\left\{-\frac{1}{2}\frac{\eta_g}{x}(T_i-T_{g\infty})\theta_g'\right\}$$

$$+\frac{1}{2}(\nu_g u_{g\infty})^{\frac{1}{2}}x^{-\frac{1}{2}}[\eta_g F_g'(\eta_g)-F_g(\eta_g)]\times(T_i-T_{g\infty})\theta_g'\left(\frac{u_{g\infty}}{\nu_g x}\right)^{\frac{1}{2}}$$

$$=\alpha_g\frac{u_{g\infty}}{\nu_g x}(T_i-T_{g\infty})\theta_g''$$

$$\Rightarrow -\frac{1}{2}\frac{\eta_g}{x}(T_i-T_{g\infty})u_{g\infty}F_g'(\eta_g)\theta_g'+\frac{1}{2}\frac{\eta_g}{x}(T_i-T_{g\infty})u_{g\infty}F_g'(\eta_g)\theta_g'$$

$$-\frac{1}{2x}(T_i-T_{g\infty})u_{g\infty}F_g(\eta_g)\theta_g'=\alpha_g\frac{u_{g\infty}}{\nu_g x}(T_i-T_{g\infty})\theta_g''$$

$$\Rightarrow -\frac{1}{2x}(T_i-T_{g\infty})u_{g\infty}F_g(\eta_g)\theta_g'=\alpha_g\frac{u_{g\infty}}{\nu_g x}(T_i-T_{g\infty})\theta_g''$$

$$\Rightarrow -\frac{1}{2}F_g(\eta_g)\theta_g'=\frac{\alpha_g}{\nu_g}\theta_g''$$

$$\Rightarrow -\frac{1}{2}F_g(\eta_g)\theta_g'=\frac{\alpha_g}{\nu_g}\theta_g''$$

$$\Rightarrow \frac{1}{2}\theta_g'' + \frac{1}{2}F_g\theta_g' = 0$$

$$\Rightarrow \theta_g'' + \frac{1}{2}Pr_gF_g\theta_g' = 0 \qquad (4.49)$$

Then Equ. (4.7) becomes,

$$u_g\frac{\partial\omega}{\partial x} + v_g\frac{\partial\omega}{\partial y} = D\frac{\partial^2\omega}{\partial y^2}$$

$$\Rightarrow u_{g\infty}F_g'(\eta_g)\left\{-\frac{1}{2}\frac{\eta_g}{x}(\omega_i - \omega_\infty)\phi'\right\}$$

$$+\frac{1}{2}(\nu_g u_{g\infty})^{\frac{1}{2}}x^{-\frac{1}{2}}[\eta_g F_g'(\eta_g) - F_g(\eta_g)](\omega_i - \omega_\infty)\phi'\left(\frac{u_{g\infty}}{\nu_g x}\right)^{\frac{1}{2}}$$

$$= D(\omega_i - \omega_\infty)\phi''\left(\frac{u_{g\infty}}{\nu_g x}\right)$$

$$\Rightarrow -\frac{1}{2}\frac{\eta_g u_{g\infty}}{x}F_g'(\eta_g)\phi' + \frac{1}{2}\frac{\eta_g u_{g\infty}}{x}F_g'(\eta_g)\phi' - \frac{1}{2}\frac{u_{g\infty}}{x}F_g(\eta_g)\phi' = D\frac{u_{g\infty}}{\nu_g x}\phi''$$

$$\Rightarrow -\frac{1}{2}F_g(\eta_g)\phi' = \frac{1}{Le}\phi''$$

$$\Rightarrow \phi'' + -\frac{1}{2}LeF_g(\eta_g)\phi' = 0 \qquad (4.50)$$

Subject to the boundary conditions:

$F_l' = 0, \quad F_l = 0, \quad \theta_l = 1 \quad$ at $\eta_l = 0$ (4.51)

$F_g' = 1, \quad \theta_g = 0, \quad \phi = 0 \quad$ at $\eta_g \to \infty$ (4.52)

The liquid film thickness *d* corresponds to η_{li} which must be a constant for enabling the similarity transformation. Consequently, the compatibility conditions (4.10)- (4.14) are transferred as

at $\eta_l = \eta_{li}$, or $\eta_g = 0$:

$$(F_l')_i = \left(F_g'\right)_i \qquad (4.53)$$

$$(\theta_l)_i = 0 \qquad (4.54)$$

$$\left(\theta_g\right)_i = 1 \qquad (4.55)$$

$$\left(F_g\right)_i = \frac{2}{Pr_gLe}\frac{\omega_i - \omega_\infty}{1 - \omega_i}\phi_i' \qquad (4.56)$$

$$\left(F_g''\right)_i = R(F_l'')_i \qquad (4.57)$$

$$\phi = 1 \tag{4.58}$$

$$(\theta_l')_i = \frac{Pr_l}{Pr_g}\left(\frac{\nu_g}{\nu_l}\right)^{\frac{1}{2}}\left[\frac{T_i - T_{g\infty}}{T_\omega - T_i}\left(\theta_g'\right)_i + \frac{H}{Le}\frac{\omega_i - \omega_\infty}{(1-\omega_i)(T_\omega - T_i)}(\phi')_i\right] \tag{4.59}$$

where $Pr_g = \frac{\nu_g}{\alpha_g}$ is the Prandtl number in gas stream region, $R = \left(\frac{\rho_l \mu_l}{\rho_g \mu_g}\right)^{\frac{1}{2}}$, $Le = \frac{\nu_g}{D}$ is the Lewis's number.

4.5 Flow Parameters

The physical quantities of interest are the local Nusselt number Nu_x and local Sherwood number Sh_x which are given by:

$$Nu_x = -\frac{x}{T_w - T_i}\frac{\partial T_l}{\partial y}\Big|_{y=0}$$

$$= -\frac{x}{T_w - T_i}(T_w - T_i)\left(\frac{u_{g\infty}}{\nu_l x}\right)^{\frac{1}{2}}\ \theta_l'(0)$$

$$= \left(\frac{u_{g\infty} x}{\nu_l}\right)^{\frac{1}{2}}\ \theta_l'(0)$$

$$= \frac{1}{Re_x^{\frac{1}{2}}}\theta_l'(0) \tag{4.60}$$

And

$$Sh_x = -\frac{x}{\omega_i - \omega_\infty}\frac{\partial \omega}{\partial y}\Big|_{y=d}$$

$$= -\frac{x}{\omega_i - \omega_\infty}(\omega_i - \omega_\infty)\phi'\left(\frac{u_{g\infty}}{\nu_g x}\right)^{\frac{1}{2}}$$

$$= -\left(\frac{u_{g\infty} x}{\nu_g}\right)^{\frac{1}{2}}\ \phi'(0)$$

$$= -\frac{1}{Re_x^{\frac{1}{2}}}\phi'(0) \tag{4.61}$$

where $Re_x = \frac{\nu_l}{x\, u_{g\infty}}$ is the local Reynolds number.

4.6 Numerical Simulations and Discussions

By using the shooting technique in MATLAB, the set of ordinary differential equations (4.35)- (4.36) and (4.48)- (4.50) with the boundary conditions (4.51)- (4.59) are solved numerically. Here the velocity, temperature and concentration are determined as a function of coordinate η. To get the solution of differential equations 4.35)- (4.36) and (4.48)- (4.50) with the boundary conditions (4.51)- (4.59), we have adopted a numerical technique based on MATLAB. In this simulation, we got some non-dimensional numbers such as the Darcy number *Da*, Froude number *Fr*, Prandtl number *Pr* and Lewis number *Le*. We tried to show the effect of these above parameters on velocity, temperature and concentration are plotted in the figures 4.2-4.8. To observe the effect of Darcy number *Da*, the other parameters are constants. Similarly, we observed the effect of the parameters *Fr*, *Pr*, *Le* by taking the rest parameters are constants, respectively.

4.6.1 Effect of Froude Number *Fr* on Velocity and Temperature Profiles

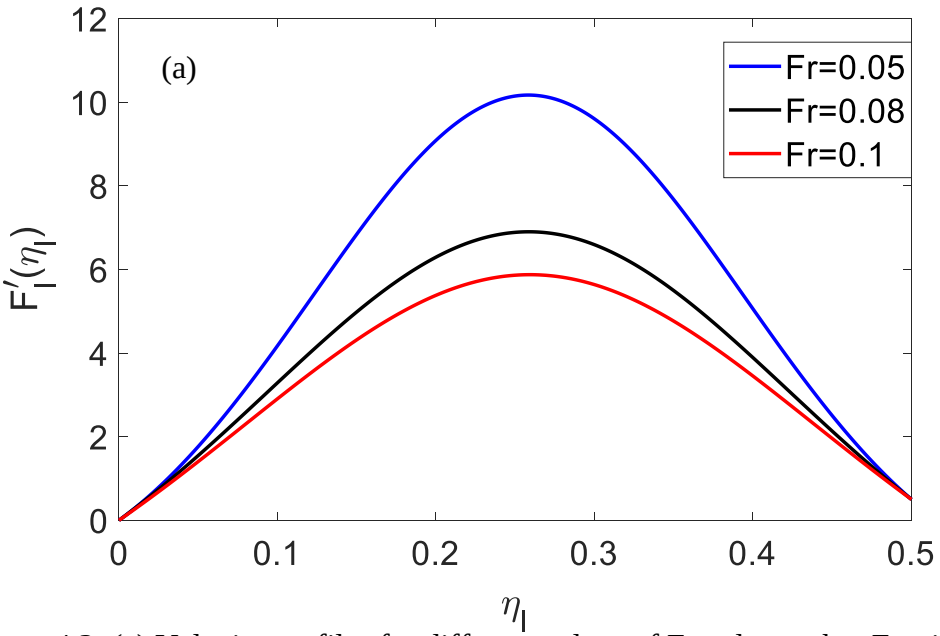

Figure 4.2: (a) Velocity profiles for different values of Froude number Fr with fixed values $Pr_l = 10, Da = 0.05, b = 0.8, \Gamma = 0.5$

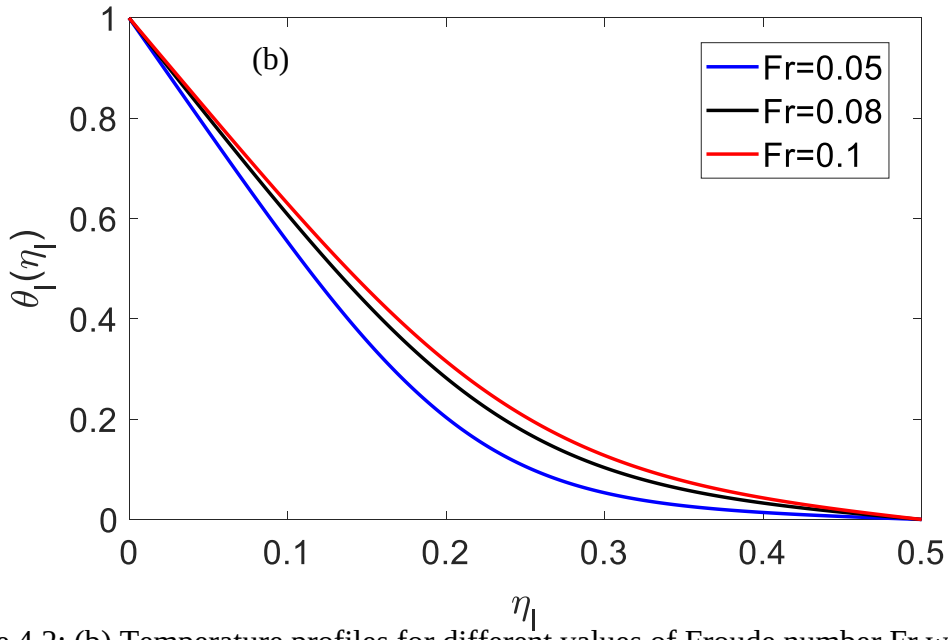

Figure 4.2: (b) Temperature profiles for different values of Froude number Fr with fixed values $Pr_l = 10, Da = 0.05, b = 0.8, \Gamma = 0.5$

Figure 4.2(a) and (b) demonstrates the effect of the Froude number *Fr* on the velocity and temperature profiles. It is stated from Fig. 4.2(a) that the velocity decreases as the Froude number increases along the similarity variable η_l. Also, with an increase the Froude number the temperature decreases which are shown in Fig. 4.2(b). Due to gravitational effect, with an increase of the gravitational force the velocity decrease and enhancing the temperature.

4.6.2 Effect of porosity b on Velocity and Temperature Profiles

From Fig. 4.3(a) and 4.3(b), illustrate the effect of the porosity b on the velocity and temperature profiles, respectively. From Fig. 4.3(a), the results show that the velocity decreases along the surface within an increase of the porosity. Also, as the porosity increase the temperature increase which are shown in Fig. 4.3(b). This is due to fact that porosity produce a resistive type of force which causes a reduction in the fluid velocity as well as enhancing the temperature.

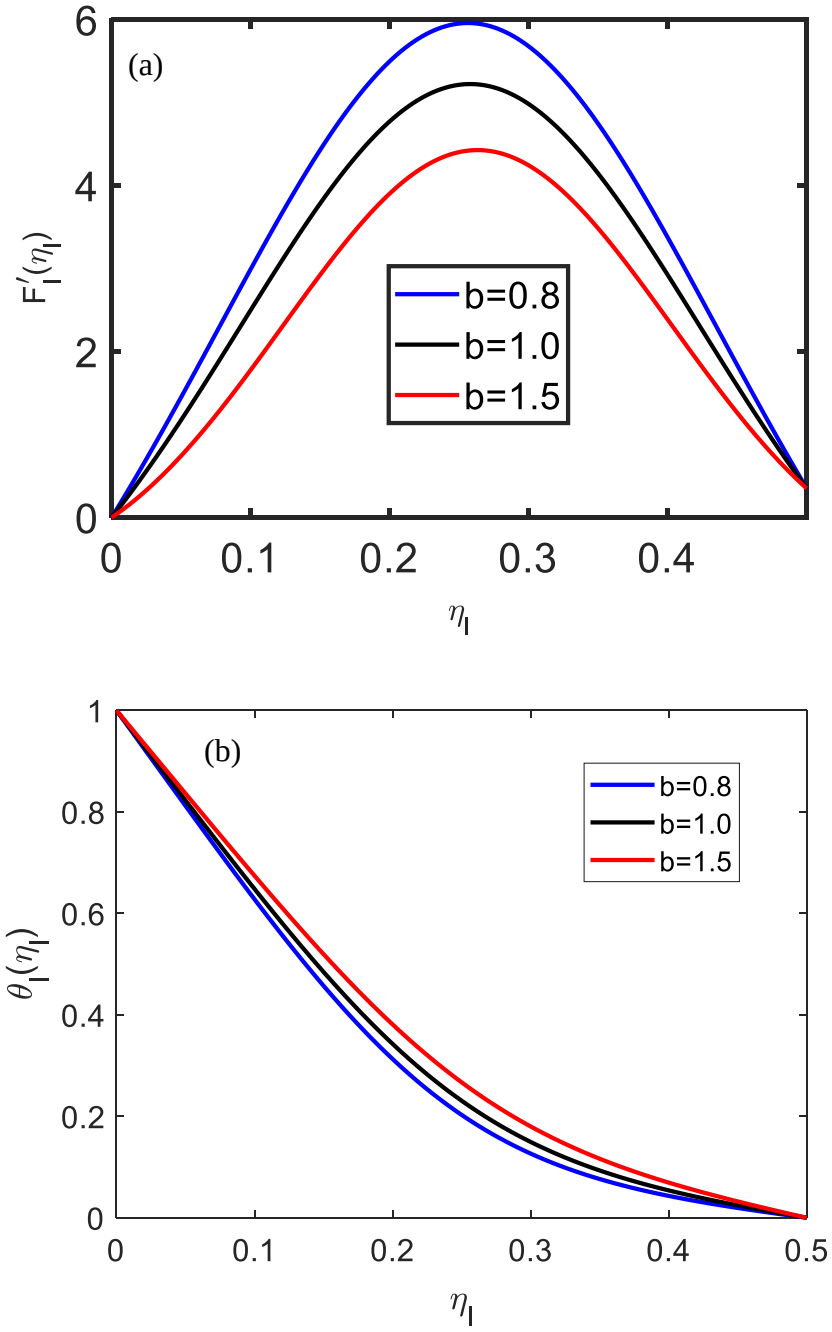

Figure 4.3: (a) Velocity profiles, and (b) Temperature profiles for different values of porosity , b with fixed values $Pr_l = 10, Da = 0.05, Fr = 0.1, \Gamma = 0.5$

4.6.3 Effect of Dimensionless Inertia Coefficient of Porous Medium Γ on Velocity and Temperature Profiles

The effect of dimensionless inertia coefficient of porous medium Γ on the velocity and dimensionless temperature are shown in Fig. 4.4(a) and 4.4(b), respectively. From Fig. 4.4(a), it is observed that the velocity decreases with the increase of dimensionless inertia

coefficient of porous medium Γ. The temperature is reduced for the increasing value of dimensionless inertia coefficient of porous medium Γ is shown in Fig. 4.4(b).

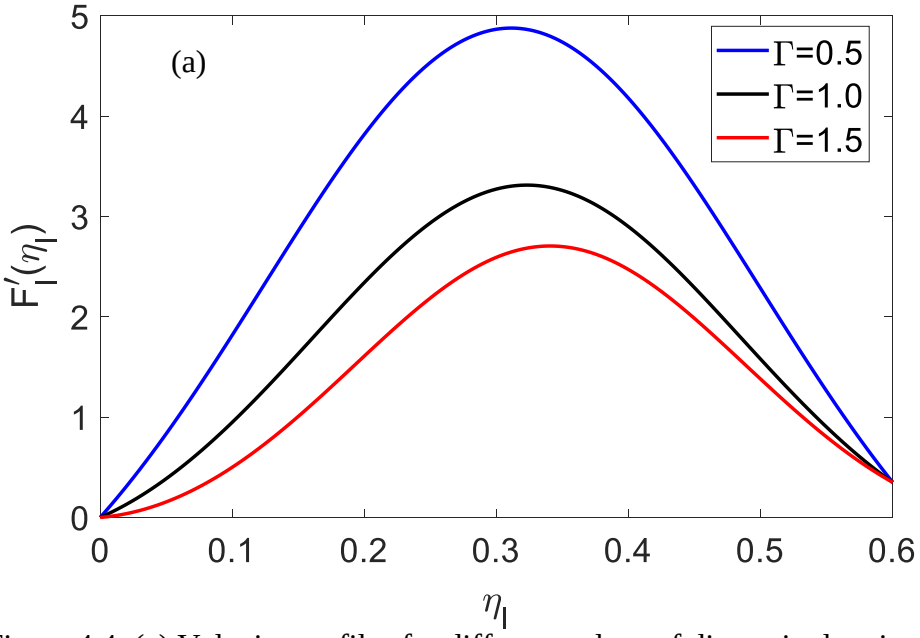

Figure 4.4: (a) Velocity profiles for different values of dimensionless inertia coefficient of porous medium Γ with fixed values $Pr_l = 10, Da = 0.05, Fr = 0.1, b = 0.8$

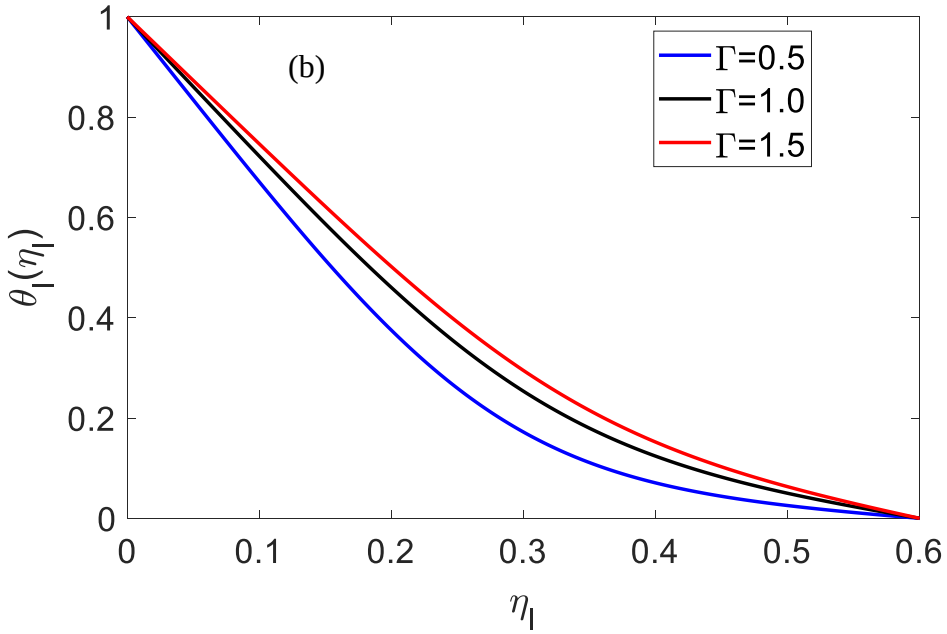

Figure 4.4: (b) Temperature profiles for different values of dimensionless inertia coefficient of porous medium Γ with fixed values $Pr_l = 10, Da = 0.05, Fr = 0.1, b = 0.8$

4.6.4 Effect of Darcy Number *Da* on Velocity and Temperature Profiles

The effect of the Darcy number *Da* against η_l on the velocity field and temperature field are shown in Figure 4.5(a) and (b), respectively. From Fig. 4.5(a), it is revealed that the velocity increases as the Darcy parameter increase. With an increase the Darcy number the temperature decreases along η_l which shown in Fig. 4.5(b).

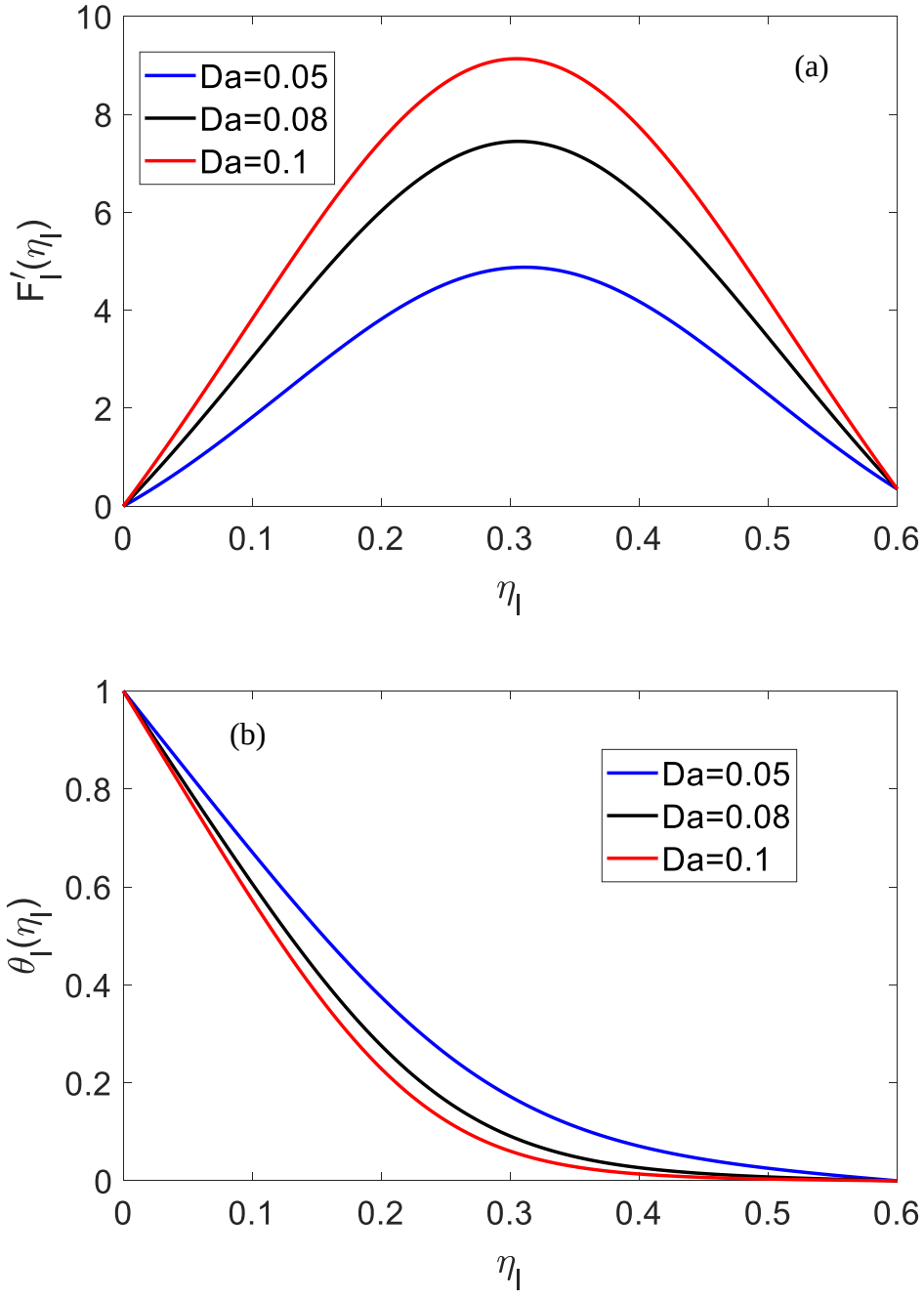

Figure 4.5: (a) Velocity profiles and (b) Temperature profiles for different values of Darcy number *Da* with fixed values $Pr_l = 0.1, Fr = 0.1, b = 0.8, \Gamma = 0.5$

4.6.5 Effect of Prandtl Number Pr_l (for Liquid Film) on Temperature Profiles

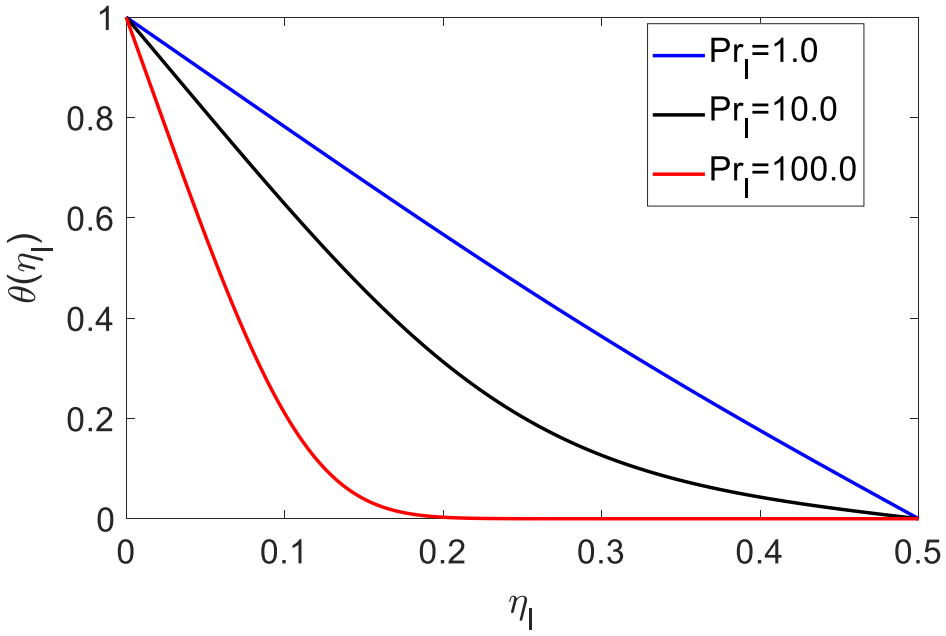

Figure 4.6: Temperature profiles for different values of Prandtl number Pr_l with fixed values $Da = 0.05, Fr = 0.1, b = 0.8, \Gamma = 0.5$

The variation of the dimensionless temperature against η_l for various values of the Prandtl number Pr_l are displayed in Fig.4.6. Fig. 4.6 shown that the temperature decreases with the increase of the Prandtl number Pr_l . This is because in gas stream region a fluid with large Prandtl number possesses large heat capacity and hence augments the heat transfer.

4.6.6 Effect of Prandtl Number Pr_g (for Gas Region) on Temperature Profiles

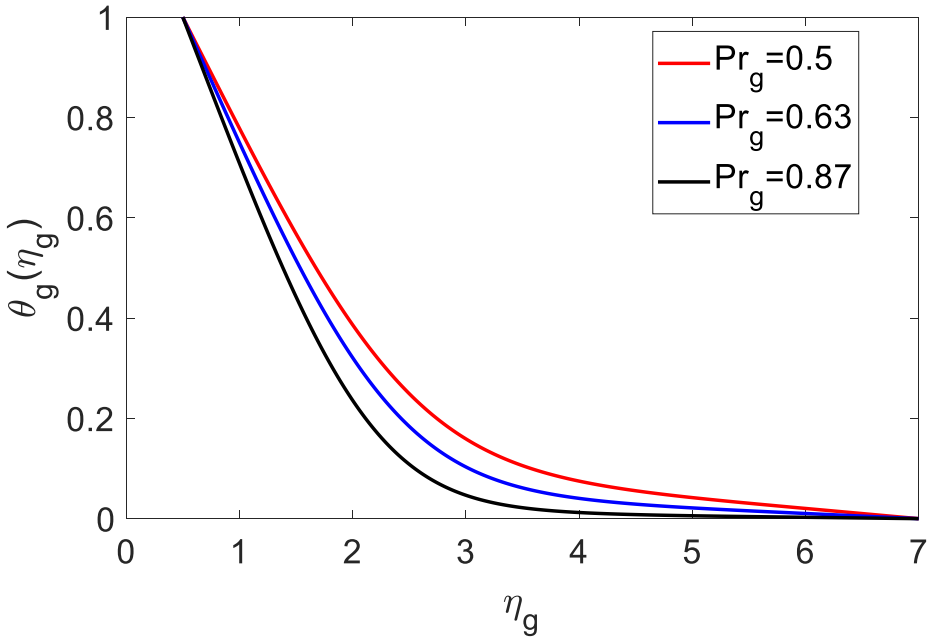

Figure 4.7: Temperature profiles for different values of Prandtl number Pr_g

For the gas stream region, Fig. 4.7 demonstrates the effect of the Prandtl number Pr_g on the dimensionless temperature against η_g. It is observed that the temperature decreases with the increase of the Prandtl number Pr_g. This is because in gas stream region a fluid with large Prandtl number possesses large heat capacity and hence augments the heat transfer.

4.6.7 Effect of Lewis *Le* on Concentration Profiles

The variation of the dimensionless temperature against η_g for various values of the Lewis number *Le* are displayed in Fig. 4.8. It is observed that the concentration decreases with the increase of the Lewis number *Le*. This is because that with decreases the mass diffusivity the concentration decreases along η_g.

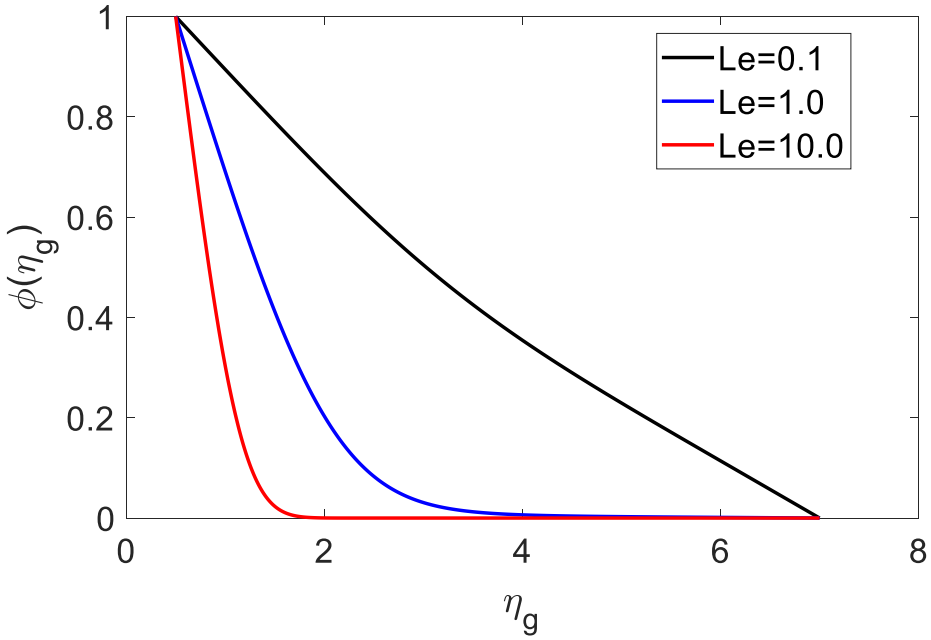

Figure 4.8: Concentration profiles for different values of Lewis number *Le*

4.6.8 Variation of Flow Parameters

Figure 4.9 illustrates the effect of Prandtl number Pr_l on the local Nusselt number Nu_x along the local Reynolds number Re_x. The Prandtl number $Pr_l = \frac{\nu_l}{\alpha_e}$ represents the relative extent of the temperature field. The local Nusselt number increase with an increase the Prandtl number along the local Reynold number. This due to fact that for increasing the Prandtl numbers larger heat transfer rate is achieved. The Lewis number $Le = \frac{\alpha_g}{D}$, is a dimensionless number defined as the ratio of thermal diffusivity to mass diffusivity. With an increase the Lewis number the local Sherwood number decrease along the local Reynolds number. This is because that for increasing the Lewis number smaller mass flow rate is achieved which is shown in Fig. 4.10.

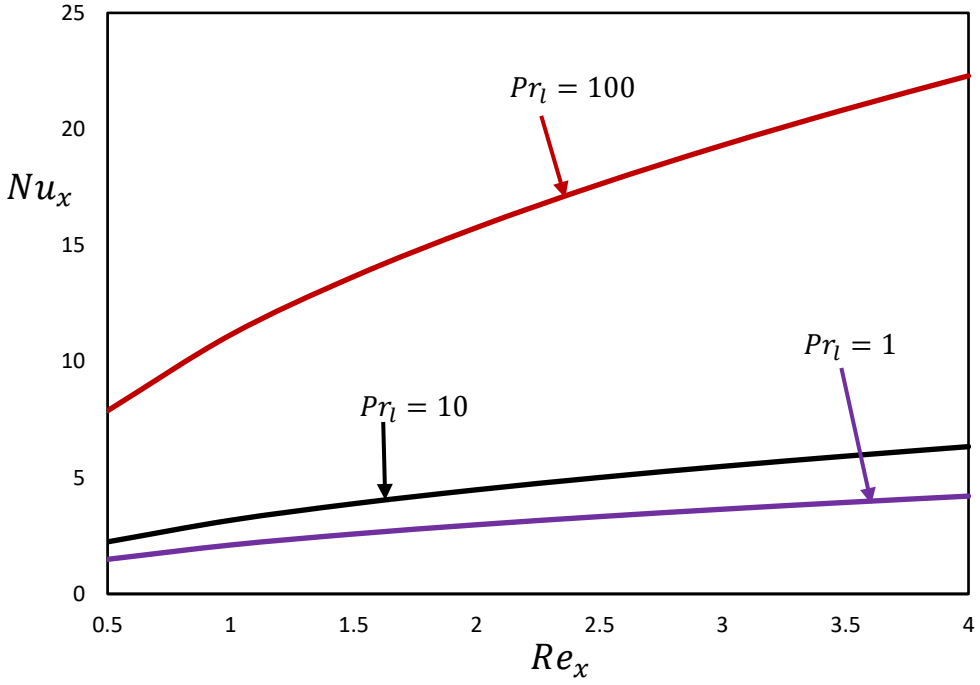

Figure 4.9: Variation of local Nusselt number Nu_x with Re_x for various Prandtl number Pr_l

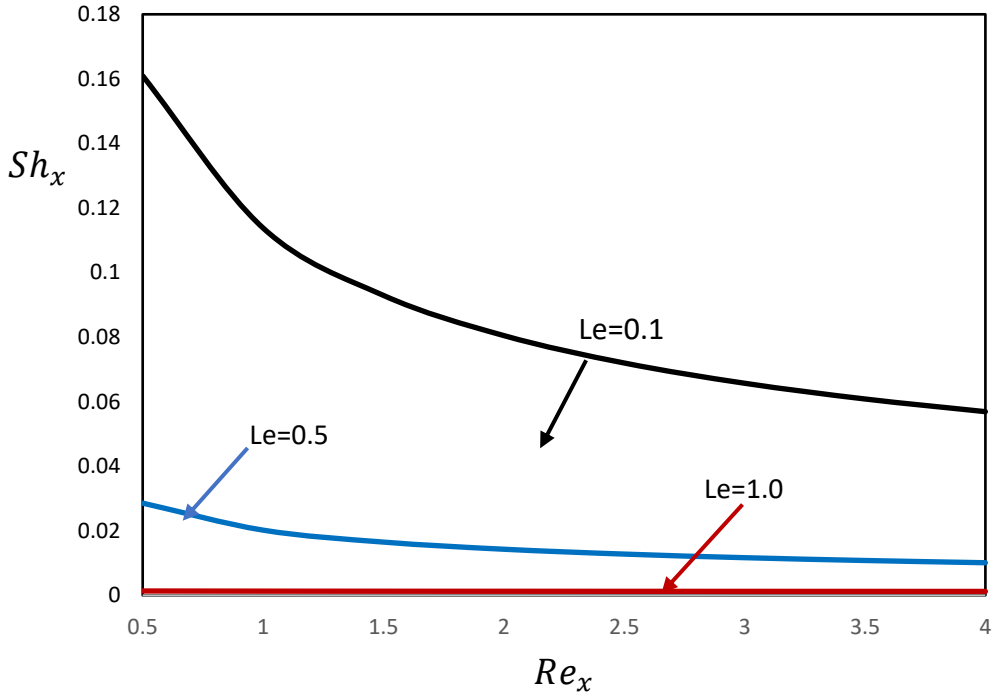

Figure 4.10: Variation of local Sherwood number Sh_x with Re_x for various Lewis number Le

4.7 Conclusions

In this research, the analytical and numerical solutions of the considered problems which have been obtained by using similarity solution technique in MATLAB. Similarity transformations were used to convert the partial differential equations describing the problem into a system of ordinary differential equations. In liquid film region, with an increase of the gravitational force the velocity decrease and enhancing the temperature. Also, a fluid with large Prandtl number possesses small heat capacity, and hence reduce the heat transfer. The velocity decreases with an increase of the porosity. This is due to fact that the porous medium produces a resistive type of force which causes a reduction in the fluid velocity. Where as in gas stream region, large Prandtl fluids possess lower thermal diffusivity and smaller Prandtl fluids have higher thermal diffusivity. The concentration decreases with an increase of the Lewis number. This is because with decrease diffusivity the concentration decrease. Moreover, the Prandtl number in liquid region increase the larger heat transfer rate is achieved and the Lewis number increase the smaller mass transfer rate is achieved.

References

[1] I.L. Maclaine-Cross, P.J. Banks, 1972. Coupled heat and mass transfer in regenerators-prediction using an analogy with heat transfer, J. Heat Mass Transfer 15 (1972) 1225–1242.

[2] I.L. Maclaine-Cross, P.J. Banks, 1981. A general theory of wet surface heat exchangers and its application to regenerative evaporative cooling, ASME J. Heat Transfer 103, 579–585.

[3] A.T. Wassel, A.F. Mills, 1987. Design methodology for a counter-current falling film evaporative condenser, ASME J. Heat Transfer 109 784–787.

[4] H. Peres-Blanco, W.A. Bird, 1984. Study of heat and mass transfer in a vertical-tube evaporative cooler, ASME J. Heat Transfer 106, 210–215.

[5] B. Gebhart, L. Pera, 1971. The nature of vertical natural convection flows resulting from the combined buoyancy effects of thermal and mass diffusion, Int. J. Heat Mass Transfer 14, 2028–2050.

[6] T.S. Chen, C.F. Yuh, 1979. Combined heat and mass transfer in natural convection on inclined surfaces, Numer. Heat Transfer 2, 233– 250.

[7] T.R. Shembharkar, B.R. Pai, 1986. Prediction of film cooling with a liquid coolant, Int. J. Heat Mass Transfer 29, 899–908.

[8] W.W. Baumann, F. Thiele, 1990. Heat and mass transfer in evaporating two-component liquid film flow, Int. J. Heat Mass Transfer 33, 267–273.

[9] W.M. Yan, T.F. Lin, 1991. Evaporative cooling of liquid film through interfacial heat and mass transfer in a vertical channel—II. Numerical study, Int. J. Heat Mass Transfer 34, 1113–1124.

[10] W.M. Yan, C.Y. Soong, 1995. Convection heat and mass transfer along an inclined heated plate with film evaporation, Int. J. Heat Mass Transfer 38, 1261–1269.

[11] Y.L. Tsay, 1995. Heat transfer enhancement through liquid film evaporation into countercurrent moist air flow in a vertical plate channel, Heat Mass Transfer 30, 473–480.

[12] E. Mezaache, M. Daguenet, 2005. Effects of inlet conditions on film evaporation along an inclined plate, Solar Energy 78, 535–542.

[13] J.C. Han, L.R. Glicksman, W.M. Rohsenow, 1978. An investigation of heat transfer and friction for rib-roughened surfaces, Int. J. Heat Mass Transfer 21 1143–1156

[14] Jin-Sheng Leu, Jiin-Yuh Jang and Yin Chou, 2006. Heat and mass transfer for liquid film evaporation along a vertical plate covered with a thin porous layer, Int. J. Heat and Mass ,49(11), 1937-1945.

[15] D.A.S. Rees, K. Vafai, 1999. Darcy–Brinkman free convection from a heated horizontal surface, Numer. Heat Transfer, Pt A 35, 191–204.

[16] B. Alazmi, K. Vafai, 2001. Analysis of fluid and heat transfer interfacial conditions between a porous medium and a fluid layer, Int. J. Heat Mass Transfer 44 ,1735–1749.

[17] T.S. Zhao, 1999. Coupled heat and mass transfer of a stagnation point flow in a heated porous bed with liquid film evaporation, Int. J. Heat Mass Transfer 42 (1999) 861–872.

[18] Khader M. M., Megahed Ahmed M., 2013. Numerical simulation using the finite difference method for the flow and heat transfer in a thin liquid film over

an unsteady stretching sheet in a saturated porous medium in the presence of thermal radiation, Journal of King Saud University – Engineering Sciences 25, 29 – 34.

[19] Md. Hasanuzzaman and Akio Miyara, 2017. Similarity solution of natural convective boundary layer flow around a vertical slender body with suction and blowing, J. Mech. Cont. & Math. Sci., 11, 8-22.

[20] S. Ergyn, Fluid flow through packed columns, Chem. Eng. Progr. 48 (1952) 89–94.

[21] R.B. Bird, W.E. Stewant, E.N. Lightfoot, 1960. Transport Phenomena, John Wiley and sons, New York, (Chapter 2).

CHAPTER FIVE

Similarity Solution of Heat and Mass Transfer for the Falling Film Flow on a Porous Medium in Presence of Heat Generation or Absorption

5.1 Introduction

There are many applications in heat pumps, chillers and air-conditioners which is the gas absorption process taking place on a falling liquid film has received much attention. In these absorption machines, the refrigerant vapor from evaporator is absorbed by a falling film of an absorbent solution in an absorber, and then the absorbent solution is regenerated by releasing the refrigerant vapor in a regenerator (boiler). Since these absorption machines are driven mainly by low-grade energy, heat, Jones and Hawkins [1], rather than by high-grade energy, electricity, their application is especially interesting in areas where the electric power supply is limited. The performance of the absorption machine is controlled by the heat and mass transfer rates of the absorption process. Therefore, it is important to study the means of enhancing the heat and mass transfer rates of an absorption process. The absorption process for an absorption process taking place on a falling film flow in a porous medium which is considered by Yang and Jou [2]. The application of porous media in a falling film absorption process is mainly to enhance the wetting conditions which is also discussed by Yang and Jou [3].

Gebhart and Pera [4] and Chen and Yuh [5] treated the vaporizing liquid film as the boundary condition for the gas stream and Shembharkar and Pai [6] and Baumann and Thiele [7] assumed the temperature distribution across the film to be linear. Recently, researches with more rigorous treatments of the equations governing the liquid film and liquid–gas interface have been published. Yan and Lin [8] studied the evaporative cooling of liquid film through interfacial heat and mass transfer in a vertical channel. A. Miyara [9] investigated the flow dynamics and heat transfer characteristics of wavy liquid films. Leu et al. [10] analyzed the liquid film evaporation flow along a vertical isothermal plate covered with a thin liquid-saturated porous layer.

Khader and Megahed [11] are presented a numerical technique which is the implicit finite difference method to the search for the numerical solutions for the given equations. Their technique reduces the problem to a system of algebraic equations. Recently, M. Hasanuzzaman and A. Miyara [12] have been studied a possible similarity solution of unsteady natural convection laminar boundary layer flow of viscous incompressible fluid caused by a heated (or cooled) axi-symmetric slender body of finite axial length immersed vertically in a viscous incompressible fluid.

The basic theme of the present study is to investigate the effect of heat generation or absorption, thermal radiation and chemical reaction on the velocity, temperature and concentration fields in the thin liquid film on a porous medium. Mathematical modelling is developed under the considerations of heat generation or absorption, thermal radiation and chemical reaction stratification effects. The effects of various emerging parameters on velocity, temperature as well as concentration fields are presented graphically. The local Nusselt number and the local Sherwood numbers are computed and analyzed both numerically and graphically.

5.2 Model and Governing Equations

The physical model and coordinate system are shown in Figure 5.1. Two-dimensional wavy film on a vertical wall is considered. With the usual boundary layer approximations, the gas flow is assumed as laminar and steady.

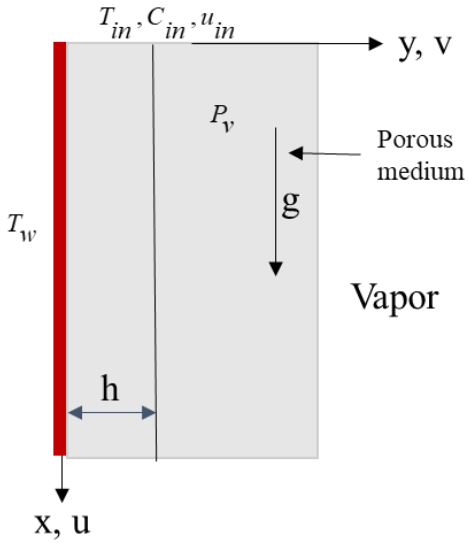

Fig.5.1: Physical model and coordinates system

The two-dimensional laminar continuity equation, momentum equation, energy equation and mass balance equations are the governing equations:

$$\frac{\partial u}{\partial x}+\frac{\partial v}{\partial y}=0 \tag{5.1}$$

$$u\frac{\partial u}{\partial x}+v\frac{\partial u}{\partial y}=\nu\frac{\partial^2 u}{\partial y^2}-\frac{\nu}{K}u+g \tag{5.2}$$

$$u\frac{\partial T}{\partial x}+v\frac{\partial T}{\partial y}=\alpha\frac{\partial^2 T}{\partial y^2}+\frac{Q_0}{\rho C_p}(T-T_s)-\frac{1}{\rho C_p}\frac{\partial q_r}{\partial y} \tag{5.3}$$

$$u\frac{\partial C}{\partial x}+v\frac{\partial C}{\partial y}=D\frac{\partial^2 C}{\partial y^2}-Kr'C \tag{5.4}$$

where u and v are the velocity components along the x and y directions, respectively. ρ is the fluid density, T is the temperature and C is the concentration of the fluid, ν is the kinematic viscosity, h is the thickness of porous medium, K is the permeability of the porous medium, g is the gravitational acceleration, α is the thermal diffusivity, $Q_0(T-T_S)$ are heat generated or absorbed per unit volume ($Q_0$is constant), q_r is the radiation heat flux, D is the mass diffusivity and Kr' is the chemical reaction rate of species concentration.

5.3 Boundary Conditions

Subject to the following boundary conditions are:

$$u=0,\quad v=0,\quad T=T_w(x) \text{ and } \frac{\partial \mathrm{C}}{\partial \mathrm{y}} \quad \text{at } y=0 \tag{5.5}$$

$$\frac{\partial u}{\partial y}=0,\qquad T=T_S \text{ and } \quad C=C_S \text{ at } y\to h \tag{5.6}$$

where T_w is the wall temperature, T_S and C_S are the surface temperature concentration, respectively.

According to Rosseland approximation (Raptis, [13]), the radiation heat flux q_r is given by

$$q_r = -\frac{4\sigma^*}{3k^*}\frac{\partial T^4}{\partial y} \tag{5.7}$$

where σ^* is termed as Stafan-Boltzman constant and k^* is as the mean absorption coefficient, Following Raptis [13]**,** we assume that the temperature difference within the flow is small such that may be expressed as a linear function of the temperature. Expanding T^4 in a Taylor series about T_0 and neglecting higher order terms, we have:

$$T^4 \cong 4T_0^3 T - 3T_0^4 \tag{5.8}$$

We also used the relation between the velocity components as well as the stream functions which are given by:

$$u = \frac{\partial \psi(x,y)}{\partial y}, \qquad v = -\frac{\partial \psi(x,y)}{\partial x} \tag{5.9}$$

5.4 Similarity Transforms

The similarity transformations which are given by:

$$\eta = \frac{y}{h},\ \ \psi = \sqrt{\nu}\, x f(\eta),\ \ \theta = \frac{T - T_S}{T_w - T_S}, \qquad \phi = C - C_\infty \tag{5.10}$$

Using the equations (5.5) -(5.10), the problems defined in equations (5.1) -(5.4) are then transformed into the following set of ordinary differential equations:

$$f'''(\eta) + \gamma\{f(\eta)f''(\eta) - f'^2(\eta) - Daf'(\eta) + Fr\} = 0 \tag{5.11}$$

$$\theta''(\eta) + \frac{Pr}{1+N_R}[f(\eta)\theta'(\eta) + \Delta\,\theta(\eta) - f'(\eta)\theta(\eta)] = 0 \tag{5.12}$$

$$\phi''(\eta) + Sc\big[f(\eta)\phi'(\eta) - f'(\eta)\phi(\eta) - Kr_x\big(Nc + \phi(\eta)\big)\big] = 0 \tag{5.13}$$

with the boundary conditions

$$f(0) = 0,\ \ f'(0) = 0, \theta(0) = 1,\ \ \phi'(0) = 0 \tag{5.14}$$

$$f''(1) = 0,\ \ \theta(1) = 0, \qquad \phi(1) = 0 \tag{5.15}$$

where primes denote differentiation with respect to η, $Da = \frac{\nu}{K}$ is the Darcy number, $\gamma = \frac{h}{\sqrt{\nu}}$ is the dimensionless film thickness, $Fr = \frac{g\rho^2 h^3}{\mu^2}$is the Froude number, $Pr = \frac{\nu}{\alpha}$ is the Prandtl number, $N_R = \frac{16\sigma^* T_0^3}{k^* k}$ is the radiation parameter, $\Delta = \frac{Q_0}{\rho C_P}$ is heat generation/absorption coefficients, $Sc = \frac{\nu}{D}$ is the Schmidt number, $Kr_x = \frac{Kr'}{a}$ is the local chemical reaction .

5.5 Flow Parameters

The physical quantities of interest the local Nusselt number Nu_x and the local Sherwood number Sh_x which are given by

$$Nu_x = \frac{1}{h}\theta'(0), \qquad Sh_x = \frac{1}{h}\phi'(0) \tag{5.16}$$

5.6 Numerical Results and Discussions

By using the similarity solution technique in MATLAB, the set of ordinary differential equations (5.11)- (5.13) with the boundary conditions (5.14)- (5.15) are solved numerically. Here the velocity, temperature and concentration are determined as a function of coordinate η. We have adopted a numerical procedure based on MATLAB for getting the solution of the differential equations (5.11) -(5.13) with the boundary conditions (5.14) -(5.15). The fundamental parameters that governed the flow are the dimensionless film thickness, Froude number, Darcy number, Prandtl number, thermal radiation parameter, heat generation/absorption parameter, Schmidt number and chemical reaction parameter. According to study their effects, a MATLAB program is written to enumerate and produce the graphs for the velocity, temperature and concentration for different values of these parameters. Few delegate results are given in Figures 5.2-5.9.

5.6.1 Effect of the Froude Number Fr on the Velocity, Temperature and Concentration Profiles

Figure 5.2(a), (b) and (c) are shown the effect of the Froude number Fr on the velocity, temperature and concentration profiles. From Fig. 5.2(a), it is observed that in all cases the velocity is started at 0(zero) and then the velocity increase with the increase of η. After η=0.5 again the velocity decrease with the increase in the similarity variable η. Also, the velocity increases with the increase of the Froude number Fr along the similarity variable η. The dimensionless temperature profiles shown as in Figure 5.2(b) for different values of Froude number *Fr*. It is clearly seen that the temperature at any point decreases with the increase in Fr. The concentration increases with increase in Froude number *Fr* along the similarity variable η which as shown in Fig. 5.2(c). This is due to fact that influence of the gravitation force enhancing the velocity and concentration as well as reduce the temperature of the fluid.

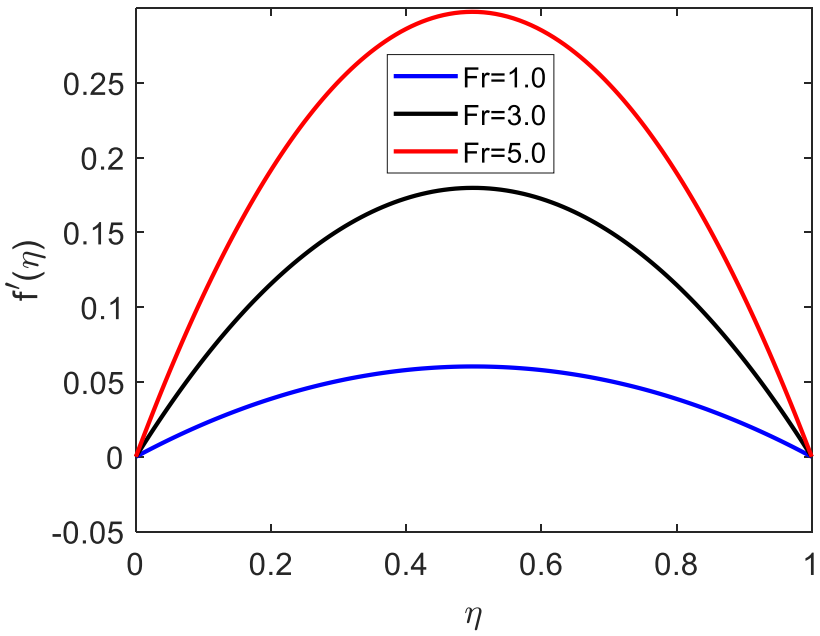

Figure 5.2: (a) Velocity profiles for different values of *Fr* with fixed values of Pr=10, N_R=1, Da=0.6, Sc=50, γ=0.5 and Kr_x=0.5

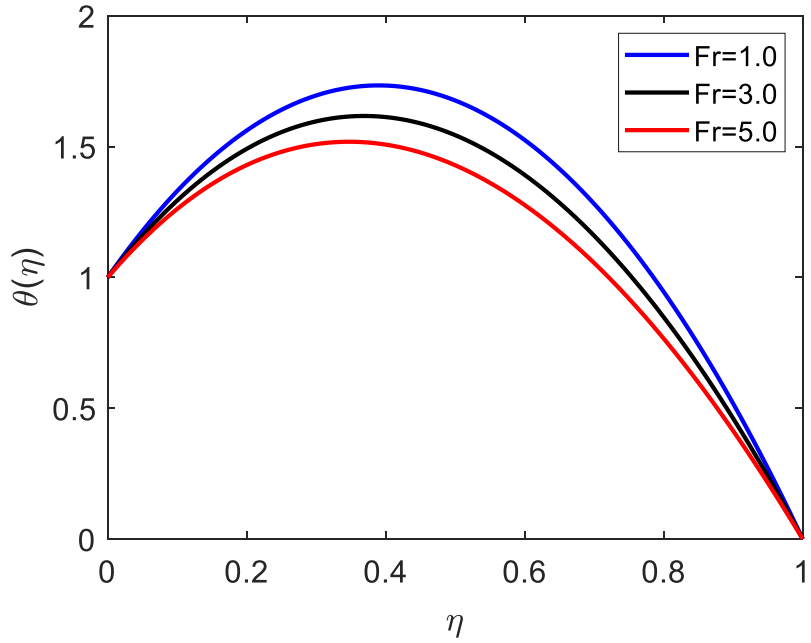

Figure 5.2: (b) Temperature profiles for different values of *Fr* with fixed values of Pr=10, N_R=1, Da=0.6, Sc=50, γ=0.5 and Kr_x=0.5

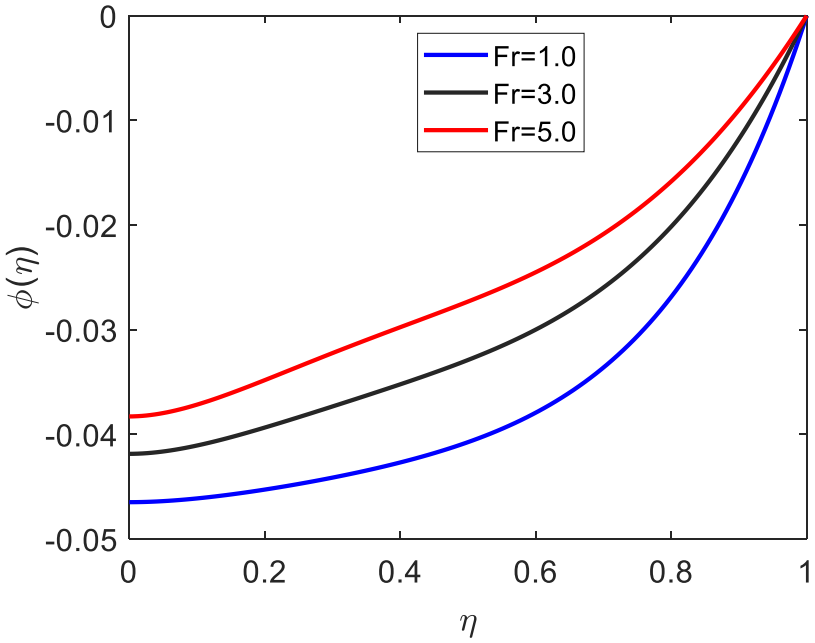

Figure 5.2: (c) Concentration profiles for different values of *Fr* with fixed values of Pr=10, N_R=1, Da=0.6, Sc=50, γ=0.5 and Kr_x=0.5

5.6.2 Effect of the Dimensionless Film Thickness γ on the Velocity, Temperature and Concentration Profiles

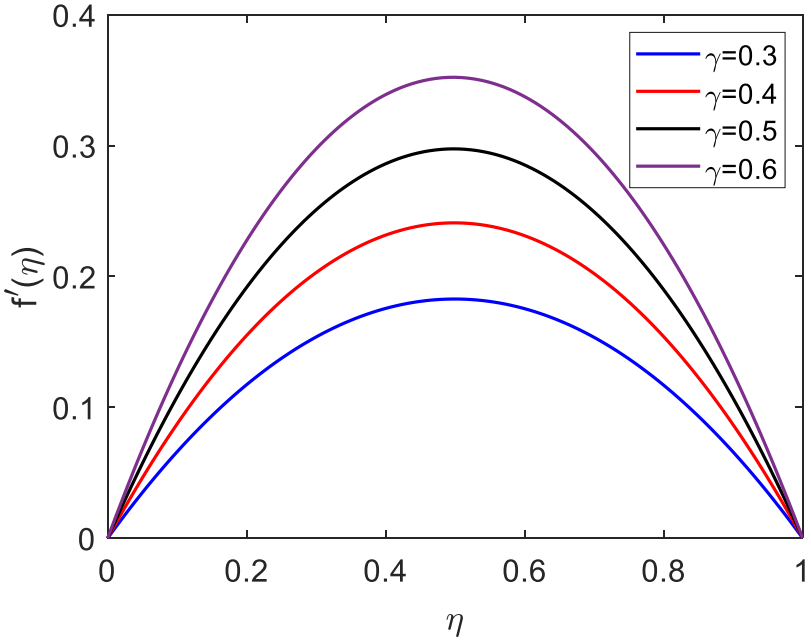

Figure 5.3: (a) Velocity profiles for different values of γ with fixed values of Pr=10, N_R=1, Da=0.6, Sc=50, Fr =0.5 and Kr_x=0.5

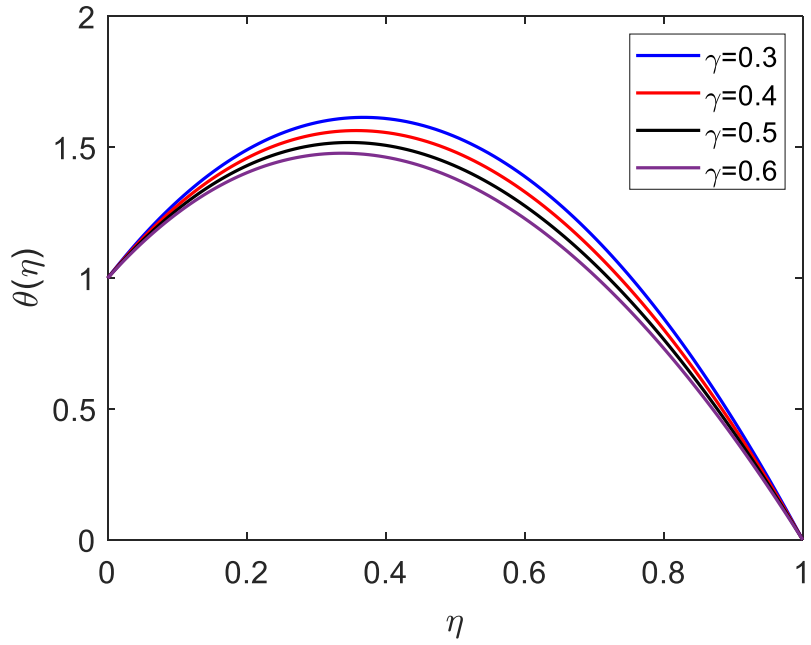

Figure 5.3: (b) Temperature profiles for different values of γ with fixed values of Pr=10, N_R=1, Da=0.6, Sc=50, Fr =0.5 and Kr_x=0.5

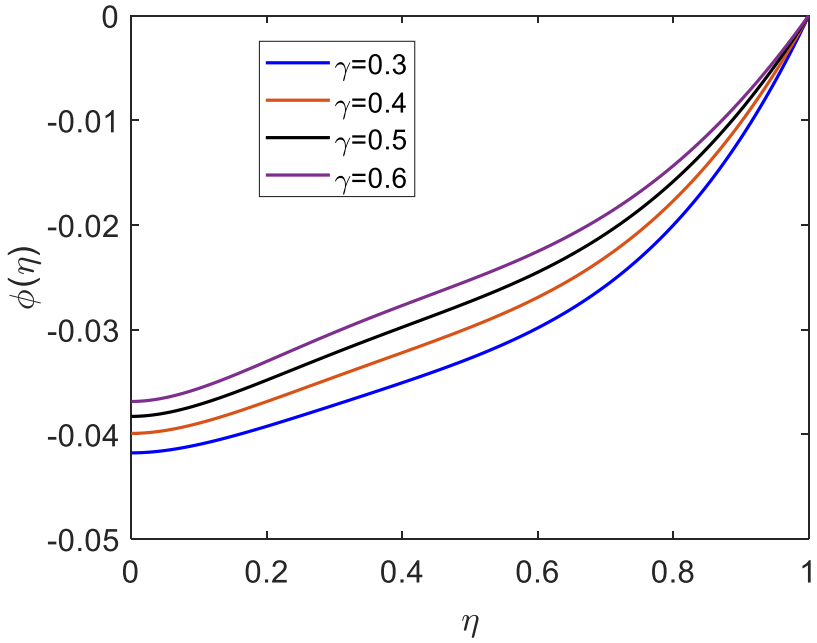

Figure 5.3: (c) Concentration profiles for different values of γ with fixed values of Pr=10, N_R=1, Da=0.6, Sc=50, Fr =0.5 and Kr_x=0.5

Figures 5.3(a), (b) and (c) demonstrates the effect of the dimensionless film thickness $\boldsymbol{\gamma}$ on the velocity, temperature and concentration profiles, respectively. It is clearly observed from Fig. 5.3(a) that the fluid increases with the increase in dimensionless film thickness $\boldsymbol{\gamma}$ along the similarity variable η. Temperature of the fluid decreases with the increase in $\boldsymbol{\gamma}$ along the similarity variable η which is shown in Fig. 5.3(b). Also, the concentration behavior is opposite for increasing dimensionless film thickness $\boldsymbol{\gamma}$. With an increase of dimensionless film thickness $\boldsymbol{\gamma}$ the concentration increases along the similarity variable η which is shown in Fig. 5.3(c).

5.6.3 Influence of the Darcy Number *Da* on the Velocity Profiles

The influence of the Darcy number *Da* on the velocity profile is shown in Fig. 5.4. The results show that the velocity decreases as the Darcy parameter increases. This is because that the porous medium produces a resistive type of force which causes a reduction in the fluid velocity.

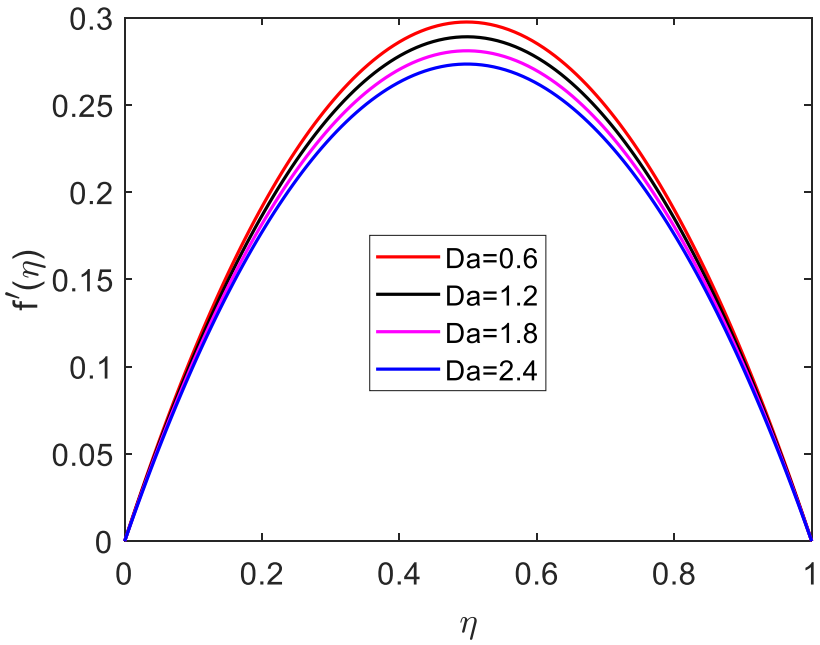

Figure 5.4: Velocity profiles for different values of Darcy number *Da* with fixed values of Pr=10, N_R=1, γ =0.5, Sc=50, *Fr* =0.5 and Kr_x=0.5

5.6.4 Effect of the Prandtl Number *Pr* on the Temperature Profiles

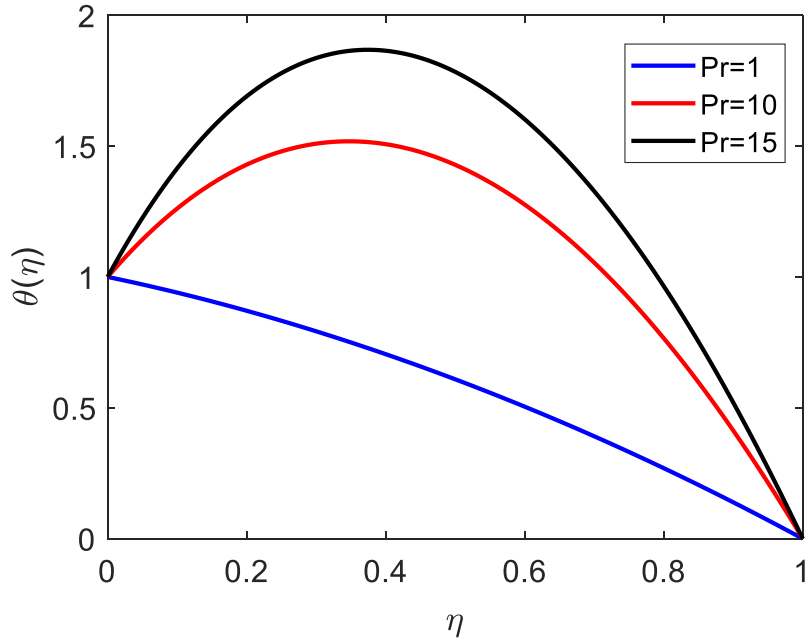

Figure 5.5: Temperature profiles for different values of Prandtl number *Pr* with fixed values of *Da*=10, N_R=1, γ =0.5, *Sc*=50, *Fr* =0.5 and Kr_x=0.5

Figure 5.5 illustrate the effect of the Prandtl number *Pr* on the temperature profiles. It is observed that the temperature increases with the increase of the Prandtl number. This is due to fact that a fluid with large Prandtl number possesses large heat capacity, and hence augments the heat transfer.

5.6.5 Effect of the Radiation Parameter N_R on the Dimensionless Temperature Profiles

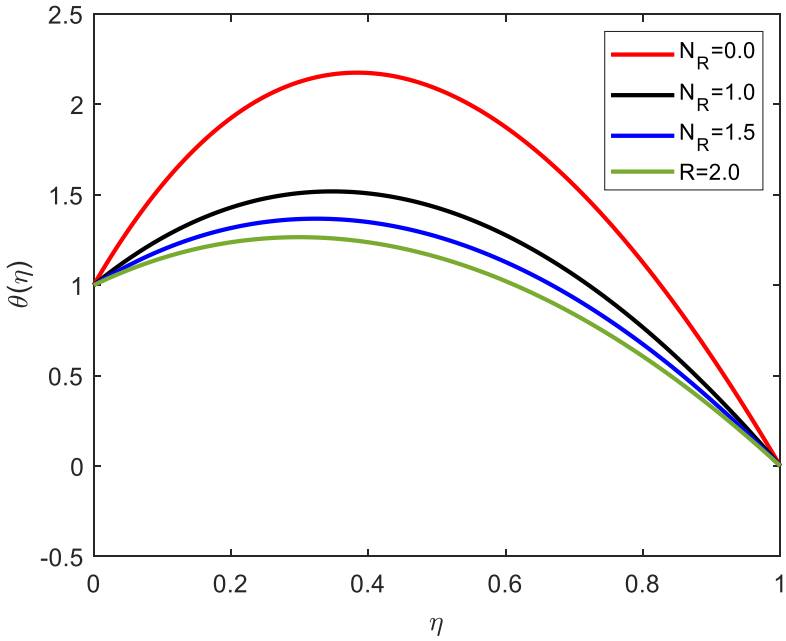

Figure 5.6: Temperature profiles for different values of radiation parameter N_R with fixed values of *Da*=10, *Pr*=10, γ =0.5, *Sc*=50, *Fr* =0.5 and Kr_x=0.5

The effect of the radiation parameter $\boldsymbol{N_R}$ on the dimensionless temperature is shown in Fig. 5.6. It is observed that with an increase in the radiation parameter the temperature decreases along the similarity variable η. This is because the increase in the radiation parameter implies higher surface heat flux and there-by decreasing the temperature of the fluid.

5.6.6 Effect of Heat Generation ($\Delta > 0$) and Heat Absorption ($\Delta < 0$) on the Temperature Profiles

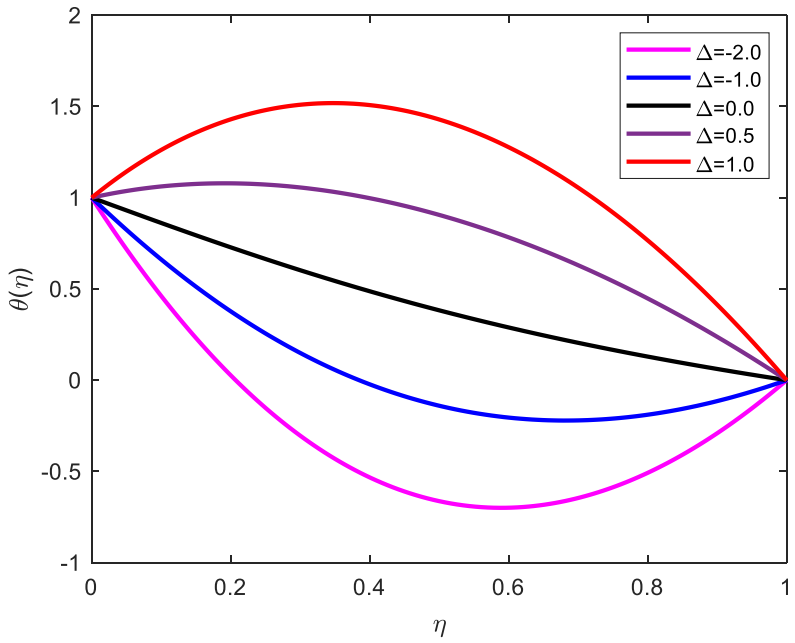

Figure 5.7: Temperature profiles for different values of heat generation and absorption with fixed values of Da=10, N_R=1, γ =0.5, Sc=50, Fr =0.5 and Kr_x=0.5

Figure: 5.7 represents the effect of heat generation ($\Delta > \mathbf{0}$) and a heat absorption generation ($\Delta < \mathbf{0}$) on the temperature profile. It is clearly observed that with an increase the heat generation the temperature increases. This increase in the fluid temperature causes more induced flow towards the plate through the thermal buoyancy effect. For the case of absorption, the temperature decreases with an increase the absorption.

5.6.7 Effect of Schmidt Number *Sc* on Concentration Profiles

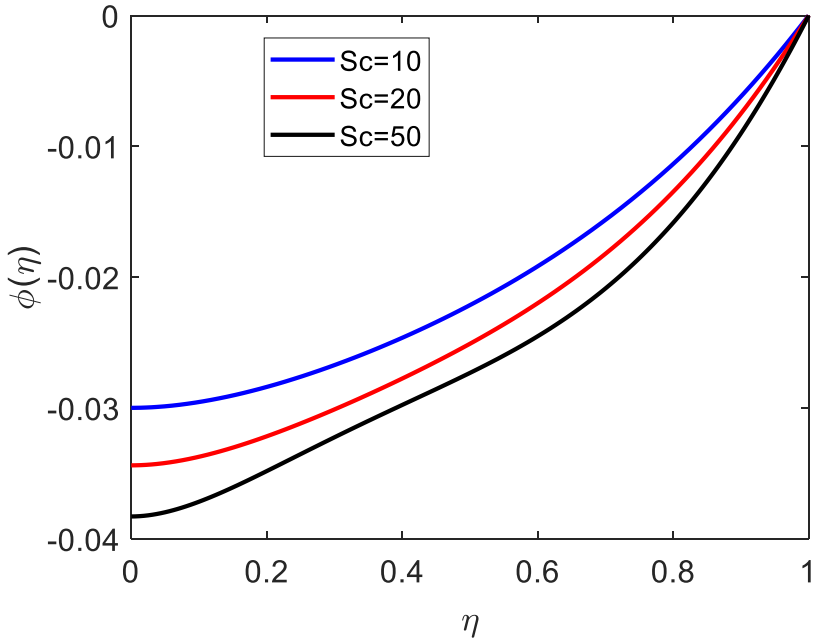

Figure 5.8: Concentration profiles for different values of Schmidt number *Sc* with fixed values of Pr=10, N_R=1, Da=0.6, γ =0.5, *Fr* =0.5 and Kr_x=0.5

The variation of the dimensionless concentration against the similarity variable η for various values of the Schmidt number *Sc* are displayed in Fig. 5.8. It is seen that the increase of the Schmidt number leads to decrease in the concentration. Schmidt number is inversely proportional to the diffusion coefficient. Hence with an increase in Schmidt number corresponding to a smaller diffusion coefficient. Such smaller diffusion coefficient creates a reduction in the concentration.

5.6.8 Influence of the Chemical Reaction Rate Constant Kr_x on the Concentration Profiles

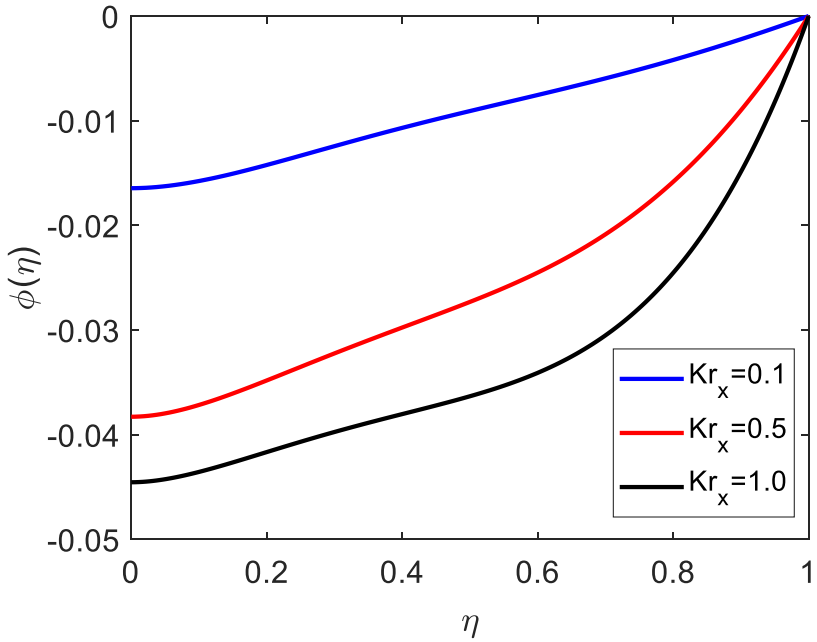

Figure 5.9: Concentration profiles for different values of chemical reaction parameter Kr_x with fixed values of Pr=10, N_R=1, Da=0.6, γ =0.5, *Fr* =0.5 and *Sc*

The influence of the chemical reaction rate constant Kr_x on the concentration profile within the boundary layer is given in Fig. 5.9. An increase in the chemical reaction effects increases the concentration within the thermal boundary layer region. This is because increasing the chemical reaction rate causes a thickening of the mass transfer boundary layer.

5.6.9 Variation of Flow Parameters

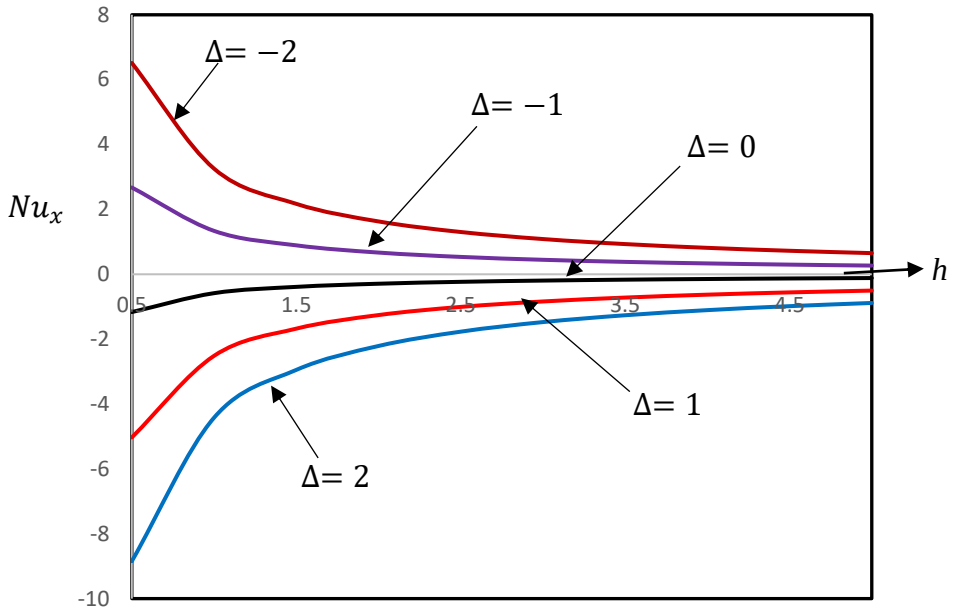

Figure 5.10: Variation of local Nussult number Nu_x with h for various heat generation and absorption parameter Δ

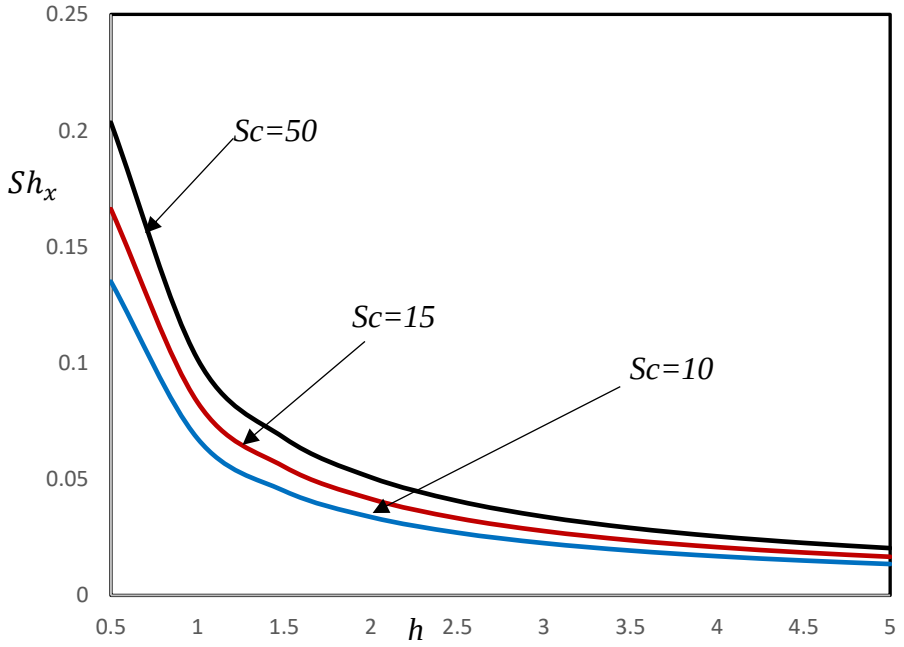

Figure 5.11: Variation of local Sherwood number Sh_x with h for various Schmidt number Sc

Figure 5.10 is shown the variation of local Nusselt number $\boldsymbol{Nu_x}$ versus thickness of porous medium *h* for selected values of heat generation and absorption Δ. With an increase the heat generation parameter the local Nusselt number decrease within the boundary along *h*. Also, increases the absorption the local Nusselt number increase along *h*. The Schmidt number $Sc = \upsilon/D$ indicates the relative extent of the concentration field. The local Sherwood number Sh_x increases with the increase the Schmidt number *Sc* along *h*. This is because, for increasing Schmidt number, larger mass flow rate is achieved which is shown in Fig. 5.11.

5.7 Conclusions

Influence of triple stratification in the falling film flow on a porous medium with heat generation and absorption, thermal radiation and chemical reaction are examined. The velocity and concentration increase as well as temperature decreases with an increase in Froude number. This is due to fact that influence of the gravitation force enhancing the velocity and concentration as well as reduce the temperature of the fluid. With an increase the heat generation the temperature increases. This increase in the fluid temperature causes more induced flow towards the plate through the thermal buoyancy effect. For the case of absorption, the temperature decreases with an increase the absorption. The increase in the radiation parameter implies higher surface heat flux and there-by decreasing the temperature of the fluid. An increase in the chemical reaction effects increases the concentration within the thermal boundary layer region. This is because increasing the chemical reaction rate causes a thickening of the mass transfer boundary layer. In addition, for the absorption and Schmidt number increase, larger heat transfer rate and mass flow rate are achieved.

References

[1] Jones, J. B., Hawkins, G. A. 1986. Engineering Thermodynamics, Wiley, New York: 646.

[2] Yang, R., Jou, D. M., 1993. Heat and mass transfer on the wavy film absorption process, Can. J. Chem. Engn 9(71), 533 538.

[3] Yang, R. U., Jou D., 1995. Heat and mass transfer of absorption process for the falling film flow inside a porous médium, lnt. J. Heat Mass Transfer, 38(6), 1121-1126.

[4] Gebhart, B., Pera, L. 1971. The nature of vertical natural convection flows resulting from the combined buoyancy effects of thermal and mass diffusion, Int. J. Heat Mass Transfer 14, 2028–2050.

[5] Chen, T. S., Yuh, C. F., 1979. Combined heat and mass transfer in natural convection on inclined surfaces, Numer. Heat Transfer 2, 233– 250.

[6] Shembharkar, T. R., Pai, B. R., 1986. Prediction of film cooling with a liquid coolant, Int. J. Heat Mass Transfer 29, 899–908.

[7] Baumann, W.W., Thiele, F., 1990. Heat and mass transfer in evaporating two-component liquid film flow, Int. J. Heat Mass Transfer 33, 267–273.

[8] Yan, W. M., Lin, T. F., 1991. Evaporative cooling of liquid film through interfacial heat and mass transfer in a vertical channel—II. Numerical study, Int. J. Heat Mass Transfer 34, 1113–1124.

[9] Miyara, A., 2000. Numerical Analysis on Heat Transfer Enhancement by Waves on Falling Liquid Film, J. of Thermal Science, 9(3), 236-242.

[10] Leu, J. S., Jang, J. Y., Chou, Y. 2006. Heat and mass transfer for liquid film evaporation along a vertical plate covered with a thin porous layer, lnt. J. Heat Mass Transfer, 49, 1937-1945.

[11] Khader, M.M., Megahed, A. M., 2013. Numerical simulation using the finite difference method for the flow and heat transfer in a thin liquid film over an unsteady stretching sheet in a saturated porous medium in the presence of thermal radiation, Journal of King Saud University – Engineering Sciences, 25, 29–34.

[12] Md. Hasanuzzaman and Akio Miyara, Similarity solution of natural convective boundary layer flow around a vertical slender body with suction and blowing, J. Mech. Cont. & Math. Sci., 11(2017), 8-22.

[13] Raptis, A., 1998. Flow of a micropolar fluid past a continuously moving plate by the presence of radiation. Int. J. Heat Mass Transfer 41, 2865–2866.

[14] Yang, R., Yan, W. J., 1992. Simulation study for an opencycle absorption solar cooling system operated in a humid area, Energy 17(7), 649-655.

CHAPTER SIX

Effect of Thermal Radiation and Rhemical Reaction on Heat and Mass Transfer Flow over a Moving Porous Sheet with Suction and Blowing

6.1 Introduction

Flow of an incompressible viscous fluid and heat transfer phenomena over a stretching sheet have received great attention during the past decades owing to the abundance of practical applications in chemical and manufacturing process, such as polymer extrusion, drawing of copper wires, and continuous casting of metals, wire drawing and glass blowing. The prime aim in almost every extrusion is to maintain the surface quality of the extrudate. The problem of extrusion of thin surface layers needs special attention to gain some knowledge for controlling the coating efficiently. Crane [1] was studied the pioneering work of the flow of Newtonian fluid over a linearly stretching surface. Many researchers [2-8] are extended the pioneering works of Crane [1] to explore various aspects of the flow and heat transfer occurring in an infinite domain of the fluid surrounding the stretching sheet. After all, these studies treated with a steady flow only. In some cases, the flow field and heat transfer can be unsteady due to a sudden stretching of the flat sheet or by a steep change of the temperature of the sheet.

Hossain et al. [9] explained the effect of radiation on natural convection flow of an optically thick viscous incompressible flow past a heated vertical porous plate with a uniform surface temperature and a uniform rate of suction where radiation is included by assuming the Rosseland discussion approximation. A similarity transformation the flow of a thin liquid film of a power-law fluid by unsteady stretching of a surface which is investigated by Andersson et al. [10]. Later, Andersson et al. [11] analyzed the momentum and heat transfer in a laminar liquid film on a horizontal stretching sheet governed by time-dependent boundary layer equations.

Similarity solutions of the boundary layer equations, which describe the unsteady flow and heat transfer over an unsteady stretching sheet which is presented by Elbashbeshy and Bazid [15]. Thermal radiation plays a very significant role in controlling heat transfer in polymer processing industry. The quality of the final product depends to a great extent on the heat

controlling factors, and the knowledge of radiative heat transfer in the system can perhaps lead to a desired product with sought qualities. Dandapat et al. [2] explored how the hydrodynamics and heat transfer in a liquid film on unsteady stretching surface are affected by thermo-capillarity. Tsai et al. [13] studied the non-uniform heat source/sink effect on the flow and heat transfer from an unsteady stretching sheet through a quiescent fluid medium extending to infinity.

In this chapter, we investigated the effect of thermal radiation and chemical reaction on heat and mass transfer flow over a moving porous sheet with suction and blowing. Under the consideration of thermal and chemical reaction stratification effects the Mathematical modelling is developed. The effects of various emerging parameters on the velocity, temperature and concentration fields are presented through graphically and tables. The local skin friction, the local Nusselt number and the local Sherwood numbers are computed numerically and analyzed.

6.2 Model and Governing Equations

In this present study on effect of thermal radiation and chemical reaction, we assumed the flow to be laminar flow of a viscous, incompressible fluid past a stretching sheet. In order to give way for possible wall fluid suction/injection, the stretching sheet is assumed to be permeable. Figure 6.1 shows the physical model and the coordinate system.

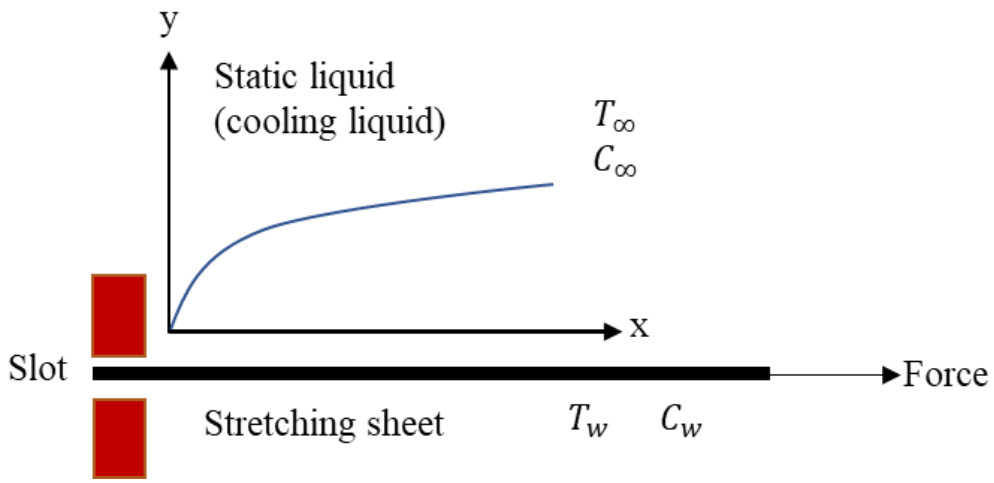

Figure 6.1: Physical model and coordinates system

The governing equations for the continuity equation, momentum equation, energy equation and mass balance equations are given by

$$\frac{\partial u}{\partial x}+\frac{\partial v}{\partial y}=0 \tag{6.1}$$

$$u\frac{\partial u}{\partial x}+v\frac{\partial u}{\partial y}=\nu\frac{\partial^2 u}{\partial y^2}-\frac{\mu}{\rho K}u+g\beta_T(T-T_\infty)+g\beta_C(C-C_\infty) \tag{6.2}$$

$$u\frac{\partial T}{\partial x}+v\frac{\partial T}{\partial y}=\alpha\frac{\partial^2 T}{\partial y^2}+\frac{Q_0}{\rho C_p}(T-T_\infty)+\frac{\beta^* u}{\rho C_p}(T_\infty-T)+\frac{16\sigma^*}{3\rho C_p k^*}T_\infty^3\frac{\partial^2 T}{\partial y^2} \tag{6.3}$$

$$u\frac{\partial C}{\partial x}+v\frac{\partial C}{\partial y}=D\frac{\partial^2 C}{\partial y^2}-Kr'C \tag{6.4}$$

Subject to the following boundary conditions are:

$$u=ax,\quad v=v_w,\quad T=T_w(x)=T_\infty+Ax,\quad C=C_w(x)=C_\infty+Bx\quad \text{at } y=0 \tag{6.5}$$

$$u\to 0,\qquad T\to T_\infty,\qquad C\to C_\infty\quad \text{at } y\to\infty \tag{6.6}$$

where u, v, T and C are the velocity, temperature and concentration components in x and y-directions, respectively, g is the acceleration due to gravity, T_w and C_w are as the wall temperature and concentration, respectively, a is the stretching rate which is constant, v_w is the wall suction when$(v_w<0)$ and injection $(v_w>0)$. Also, C_p is the specific heat at constant pressure, ν is the kinematic viscosity, K is the permeability, β_T is the thermal expansion coefficient, β_C is the solutal expansion coefficient, α is the thermal diffusivity of the fluid, D is the mass diffusivity, ρ is the density, $\beta^*(T_\infty-T)$ and $Q_0(T-T_\infty)$ are heat generated or absorbed per unit volume (β^* and Q_0 are constants), σ^* is termed as Stafan-Boltzman constant and k^* is as the mean absorption coefficient and Kr' is the chemical reaction rate of species concentration.

In this chapter, we used the relation between the velocity components as well as the stream functions which are given by:

$$u=\frac{\partial\psi(x,y)}{\partial y},\qquad v=-\frac{\partial\psi(x,y)}{\partial x} \tag{6.7}$$

6.3 Similarity Transforms

Also, using the similarity transformations which are given by:

$$\eta = y\sqrt{\frac{a}{\nu}},\ \ \psi = \sqrt{\nu a}\, xf(\eta), \qquad \theta(\eta) = \frac{T - T_\infty}{T_w - T_\infty}, \qquad \phi(\eta) = \frac{C - C_\infty}{C_w - C_\infty} \tag{6.8}$$

Now,

$$u = \frac{\partial \psi(x,y)}{\partial y}$$

$$= \frac{\partial}{\partial y}\{\sqrt{\nu a}\, xf(\eta)\}$$

$$= \sqrt{\nu a} x \frac{\partial}{\partial y}\{f(\eta)\}$$

$$= \sqrt{\nu a} x \frac{\partial}{\partial \eta}\{f(\eta)\}\frac{\partial \eta}{\partial y}$$

$$= \sqrt{\nu a} x f'(\eta)\sqrt{\frac{a}{\nu}}$$

$$= axf'(\eta) \tag{6.9}$$

$$v = -\frac{\partial \psi(x,y)}{\partial x}$$

$$= -\frac{\partial}{\partial x}\{\sqrt{\nu a}\, xf(\eta)\}$$

$$= -\sqrt{\nu a}\left[x\frac{\partial}{\partial x}\{f(\eta)\} + f(\eta)\right]$$

$$= -\sqrt{\nu a}\left[x\frac{\partial}{\partial \eta}\{f(\eta)\}\frac{\partial \eta}{\partial x} + f(\eta)\right]$$

$$= -\sqrt{\nu a} f(\eta) \tag{6.10}$$

$$\frac{\partial u}{\partial x} = \frac{\partial}{\partial x}\{axf'(\eta)\}$$

$$= af'(\eta) \tag{6.11}$$

$$\frac{\partial v}{\partial y} = \frac{\partial}{\partial y}\{-\sqrt{\nu a} f(\eta)\}$$

$$= -\sqrt{\nu a}\frac{\partial}{\partial \eta}\{f(\eta)\}\frac{\partial \eta}{\partial y}$$

$$= -\sqrt{\nu a} f'(\eta)\sqrt{\frac{a}{\nu}}$$

$$= -a f'(\eta) \qquad (6.12)$$

Hence the equation of continuity (6.1) becomes

$$\frac{\partial u}{\partial x} + \frac{\partial v}{\partial y} = a f'(\eta) - a f'(\eta) = 0 \qquad (6.13)$$

So, the equation of continuity is satisfied.

$$\frac{\partial u}{\partial y} = \frac{\partial}{\partial y}\{a x f'(\eta)\}$$

$$= a x \frac{\partial}{\partial \eta}\{f'(\eta)\}\frac{\partial \eta}{\partial y}$$

$$= a x \frac{\partial}{\partial \eta}\{f'(\eta)\}\sqrt{\frac{a}{\nu}}$$

$$= \frac{a^{\frac{3}{2}}}{\sqrt{\nu}} x f''(\eta) \qquad (6.14)$$

$$\frac{\partial^2 u}{\partial y^2} = \frac{\partial}{\partial y}\left\{\frac{\partial u}{\partial y}\right\}$$

$$= \frac{\partial}{\partial y}\left\{\frac{a^{\frac{3}{2}}}{\sqrt{\nu}} x f''(\eta)\right\}$$

$$= \frac{\partial}{\partial \eta}\left\{\frac{a^{\frac{3}{2}}}{\sqrt{\nu}} x f''(\eta)\right\}\frac{\partial \eta}{\partial y}$$

$$= \frac{a^{\frac{3}{2}}}{\sqrt{\nu}} x f'''(\eta)\sqrt{\frac{a}{\nu}}$$

$$= \frac{a^2}{\nu} x f'''(\eta) \tag{6.15}$$

$$\frac{\partial T}{\partial x} = \frac{\partial}{\partial x}\{T_\infty + (T_w - T_\infty)\theta\}$$

$$= (T_w - T_\infty)\frac{\partial}{\partial \eta}\{\theta(\eta)\}\frac{\partial \eta}{\partial x}$$

$$= 0 \tag{6.16}$$

$$\frac{\partial T}{\partial y} = \frac{\partial}{\partial y}\{T_\infty + (T_w - T_\infty)\theta(\eta)\}$$

$$= \frac{\partial}{\partial \eta}\{T_\infty + (T_w - T_\infty)\theta(\eta)\}\frac{\partial \eta}{\partial y}$$

$$= (T_w - T_\infty)\theta'(\eta)\sqrt{\frac{a}{\nu}} \tag{6.17}$$

$$\frac{\partial^2 T}{\partial y^2} = \frac{\partial}{\partial y}\left\{\frac{\partial T}{\partial y}\right\}$$

$$= \frac{\partial}{\partial y}\left\{(T_w - T_\infty)\theta'(\eta)\sqrt{\frac{a}{\nu}}\ \right\}$$

$$= \frac{\partial}{\partial \eta}\left\{(T_w - T_\infty)\theta'(\eta)\sqrt{\frac{a}{\nu}}\ \right\}\frac{\partial \eta}{\partial y}$$

$$= (T_w - T_\infty)\theta''(\eta)\sqrt{\frac{a}{\nu}}\sqrt{\frac{a}{\nu}}$$

$$= (T_w - T_\infty)\theta''(\eta)\frac{a}{\nu} \tag{6.18}$$

$$\frac{\partial C}{\partial x} = \frac{\partial}{\partial x}\{C_\infty + (C_w - C_\infty)\phi(\eta)\}$$

$$= (C_w - C_\infty)\frac{\partial}{\partial \eta}\{\phi(\eta)\}\frac{\partial \eta}{\partial x}$$

$$= 0 \tag{6.19}$$

$$\frac{\partial C}{\partial y} = \frac{\partial}{\partial y}\{C_\infty + (C_w - C_\infty)\phi(\eta)\}$$

$$= \frac{\partial}{\partial \eta}\{C_\infty + (C_w - C_\infty)\phi(\eta)\}\frac{\partial \eta}{\partial y}$$

$$= (C_w - C_\infty)\phi'(\eta)\sqrt{\frac{a}{\nu}} \tag{6.20}$$

$$\frac{\partial^2 C}{\partial y^2} = \frac{\partial}{\partial y}\left\{\frac{\partial C}{\partial y}\right\}$$

$$= \frac{\partial}{\partial y}\left\{(C_w - C_\infty)\phi'(\eta)\sqrt{\frac{a}{\nu}}\right\}$$

$$= \frac{\partial}{\partial \eta}\left\{(C_w - C_\infty)\phi'(\eta)\sqrt{\frac{a}{\nu}}\right\}\frac{\partial \eta}{\partial y}$$

$$= (C_w - C_\infty)\phi''(\eta)\sqrt{\frac{a}{\nu}}\sqrt{\frac{a}{\nu}}$$

$$= (C_w - C_\infty)\phi''(\eta)\frac{a}{\nu} \tag{6.21}$$

Using the equations (6.5) -(6.21), the problems defined in equations (6.2) -(6.4) are then transformed into the following set of ordinary differential equations:

Equation (6.2) becomes:

$$u\frac{\partial u}{\partial x} + v\frac{\partial u}{\partial y} = \nu\frac{\partial^2 u}{\partial y^2} - \frac{\mu}{\rho K}u + g\beta_T(T - T_\infty) + g\beta_C(C - C_\infty)$$

$$\Rightarrow axf'(\eta) \times af'(\eta) - \sqrt{\nu a}f(\eta) \times \frac{a^{\frac{3}{2}}}{\sqrt{\nu}}xf''(\eta)$$

$$= \nu\frac{a^2}{\nu}xf'''(\eta) - \frac{\mu}{\rho K}axf'(\eta) + g\beta_T(T_w - T_\infty)\theta + g\beta_C(C_w - C_\infty)\phi$$

$$\Rightarrow a^2 xf'^2(\eta) - a^2 xf(\eta)f''(\eta)$$

$$= a^2 xf'''(\eta) - -\frac{\mu}{\rho K}axf'(\eta) + g\beta_T(T_w - T_\infty)\theta + g\beta_C(C_w - C_\infty)\phi$$

$$\Rightarrow f'^2(\eta) - f(\eta)f''(\eta) = f'''(\eta) - \frac{\nu}{aK}f'(\eta) + \frac{g\beta_T}{a^2 x}(T_w - T_\infty)\theta + \frac{g\beta_C}{a^2 x}(C_w - C_\infty)\phi$$

$$\Rightarrow f'^2(\eta) - f(\eta)f''(\eta) = f'''(\eta) - \frac{1}{Da}f'(\eta) + Gr_T\theta + Gr_C\phi$$

$$\Rightarrow f'''(\eta) - f'^2(\eta) + f(\eta)f''(\eta) - \frac{1}{Da}f'(\eta) + Gr_T\theta + Gr_C\phi = 0 \qquad (6.22)$$

Also, equation (6.3) implies that

$$u\frac{\partial T}{\partial x} + v\frac{\partial T}{\partial y} = \alpha\frac{\partial^2 T}{\partial y^2} + \frac{Q_0}{\rho C_p}(T - T_\infty) + \frac{\beta^* u}{\rho C_p}(T_\infty - T) + \frac{16\sigma^*}{3\rho C_p k^*}T_\infty^3\frac{\partial^2 T}{\partial y^2}$$

$$\Rightarrow axf'(\eta) \times 0 - \sqrt{va}f(\eta) \times (T_w - T_\infty)\theta'(\eta)\sqrt{\frac{a}{\nu}} = \alpha(T_w - T_\infty)\theta''(\eta)\frac{a}{\nu}$$

$$+\frac{Q_0}{\rho C_p}(T_w - T_\infty)\theta(\eta) - \frac{\beta^* u}{\rho C_p}axf'(\eta) \times (T_w - T_\infty)\theta(\eta) + \frac{16\sigma^*}{3\rho C_p k^*}T_\infty^3(T_w - T_\infty)\theta''(\eta)\frac{a}{\nu}$$

$$\Rightarrow -a(T_w - T_\infty)f(\eta)\theta'(\eta) = \alpha(T_w - T_\infty)\theta''(\eta)\frac{a}{\nu} + \frac{Q_0}{\rho C_p}(T_w - T_\infty)\theta(\eta)$$

$$-\frac{\beta^* u}{\rho C_p}axf'(\eta) \times (T_w - T_\infty)\theta(\eta) + \frac{16\sigma^*}{3\rho C_p k^*}T_\infty^3(T_w - T_\infty)\theta''(\eta)\frac{a}{\nu}$$

$$\Rightarrow -f(\eta)\theta'(\eta) = \frac{\alpha}{\nu}\theta''(\eta) + \frac{Q_0}{\rho a C_p}\theta(\eta) - \frac{\beta^* x}{\rho C_p}f'(\eta)\theta(\eta) + \frac{16\sigma^*}{3\rho C_p k^*}\theta''(\eta)\frac{1}{\nu}$$

$$\Rightarrow -f(\eta)\theta'(\eta) = \frac{1}{Pr}\theta''(\eta) + \Delta\theta(\eta) - \delta_x f'(\eta)\theta(\eta) + \frac{N_R}{Pr}\theta''(\eta)$$

$$\Rightarrow \frac{1 + N_R}{Pr}\theta''(\eta) + \Delta\theta(\eta) - \delta_x f'(\eta)\theta(\eta) + f(\eta)\theta'(\eta) = 0$$

$$\Rightarrow \theta''(\eta) + \frac{Pr}{1+N_R}[f(\eta)\theta'(\eta) + \Delta\,\theta(\eta) - \delta_x f'(\eta)\theta(\eta)] = 0 \qquad (6.23)$$

Again, equation (6.4) becomes

$$u\frac{\partial C}{\partial x} + v\frac{\partial C}{\partial y} = D\frac{\partial^2 C}{\partial y^2} - Kr'C$$

$$\Rightarrow axf'(\eta) \times 0 - \sqrt{va}f(\eta) \times (C_w - C_\infty)\phi'(\eta)\sqrt{\frac{a}{\nu}}$$

$$= D(C_w - C_\infty)\phi''(\eta)\frac{a}{\nu} - Kr'\,(C_w - C_\infty)\phi(\eta)$$

$$\Rightarrow -af(\eta)\phi'(\eta) = D\frac{a}{\nu}\phi''(\eta) - Kr'\,\phi(\eta)$$

$$\Rightarrow \frac{D}{\nu}\phi''(\eta) - \frac{Kr'}{a}\,\phi(\eta) + f(\eta)\phi'(\eta) = 0$$

$$\Rightarrow \frac{1}{Sc}\phi''(\eta) - Kr_x\,\phi(\eta) + f(\eta)\phi'(\eta) = 0$$

$$\Rightarrow \phi''(\eta) + Sc[f(\eta)\phi'(\eta) - Kr_x\phi(\eta)] = 0 \qquad (6.24)$$

with the boundary conditions

$$f(0) = F_W, \quad f'(0) = 1, \quad \theta(0) = 1, \quad \phi(0) = 1 \qquad (6.25)$$

$$f(\infty) = 0, \quad \theta(\infty) = 0, \quad \phi(\infty) = 0 \qquad (6.26)$$

where primes denote differentiation with respect to η , $F_W = \frac{v_w}{\sqrt{va}}$ is the dimensionless suction/ blowing velocity, $Da = \frac{aK}{\nu}$ is the Darcy number, $Gr_T = g\beta_T \frac{(T_w - T_\infty)}{a^2 x}$ is the Grashof number, $Gr_C = g\beta_C \frac{(C_w - C_\infty)}{a^2 x}$ is the modified Grashof number, $Pr = \frac{\nu}{\alpha}$ is the Prandtl number, $N_R = \frac{16\sigma^* T_\infty^3}{3K^* k}$ is the thermal radiation parameter, $\Delta = \frac{Q_0}{\rho C_P a}$ and $\delta_x = \frac{\beta^* x}{\rho C_p}$ are heat generation/absorption coefficients, $Sc = \frac{\nu}{D}$ is the Schmidt number and $Kr_x = \frac{Kr'}{a}$ is the chemical reaction parameter, respectively.

6.4 Physical Parameters

The physical quantities of interest are the skin friction C_f, the local Nusselt number Nu_x and the local Sherwood number Sh_x which are given by

Shear stress,

$$\tau_w = \mu\left(\frac{\partial u}{\partial y}\right)\Big|_{y=0}$$

$$= \mu\frac{\partial}{\partial y}\{axf'(\eta)\}\Big|_{y=0}$$

$$= \mu ax\frac{\partial}{\partial \eta}\{f'(\eta)\}\frac{\partial \eta}{\partial y}\Big|_{y=0}$$

$$= \mu axf''(0)\sqrt{\frac{a}{\nu}}$$

The skin friction C_f is given by

$$C_f = \frac{1}{2}\frac{\tau_w}{\rho u^2}$$

$$= \frac{1}{2\rho u^2}\mu ax\sqrt{\frac{a}{\nu}}f''(0)$$

$$= \frac{1}{2\rho\{axf'(0)\}^2}\mu ax\sqrt{\frac{a}{\nu}}f''(0)$$

$$= \frac{1}{2\rho a^2x^2}\mu ax\sqrt{\frac{a}{\nu}}f''(0)$$

$$= \frac{1}{2}\frac{\nu}{ax}\sqrt{\frac{a}{\nu}}f''(0)$$

$$= \frac{1}{2}\frac{\sqrt{\nu}}{\sqrt{x}\sqrt{ax}}f''(0)$$

$$= \frac{1}{2}\frac{\sqrt{\nu}}{\sqrt{x}\sqrt{u}}f''(0)$$

$$C_f = \frac{1}{2}\frac{1}{\sqrt{Re_x}}f''(0) \quad (6.27)$$

The local Nusselt number Nu_x is given by

$$Nu_x = \frac{x}{T_w - T_\infty}\left(\frac{\partial T}{\partial y}\right)\Big|_{y=0}$$

$$= \frac{x}{T_w - T_\infty}(T_w - T_\infty)\theta'(0)\sqrt{\frac{a}{\nu}}$$

$$= x\theta'(0)\sqrt{\frac{a}{\nu}}$$

$$= \frac{\sqrt{x}\sqrt{ax}}{\sqrt{\nu}}\theta'(0)$$

$$= \frac{\sqrt{x}\sqrt{u}}{\sqrt{\nu}}\theta'(0)$$

$$Nu_x = \sqrt{Re_x}\,\theta'(0) \quad (6.28)$$

The local Sherwood number Sh_x

$$Su_x = \frac{x}{(C_w - C_\infty)}\left(\frac{\partial C}{\partial y}\right)\Big|_{y=0}$$

$$= \frac{x}{(C_w - C_\infty)}(C_w - C_\infty)\theta'(0)\sqrt{\frac{a}{\nu}}$$

$$= x\phi'(0)\sqrt{\frac{a}{\nu}}$$

$$= \frac{\sqrt{\mathrm{x}}\sqrt{\mathrm{ax}}}{\sqrt{\nu}}\phi'(0)$$

$$Su_x = \frac{\sqrt{\mathrm{x}}\sqrt{u}}{\sqrt{\nu}}\phi'(0) = \sqrt{Re_x}\,\phi'(0) \tag{6.29}$$

6.5 Finite Difference Method (FDM)

Our main goal in this article is to apply the finite difference method to solve the problems (6.22) -(6.24) with the boundary conditions (6.25) -(6.26). This method has been tested for accuracy and efficiency for solving different problems (Cheng and Liu [16] and Chamkha et al., [17]).

By using the transformation $f'(\eta) = z(\eta)$ to convert the system of equations (6.22) - (6.24) in the following form:

$$f' - z = 0 \tag{6.27}$$

$$z'' + fz' - z^2 - \frac{1}{Da}z + Gr_T\theta + Gr_C\phi = 0 \tag{6.28}$$

$$\theta'' + \frac{Pr}{1+N_R}[f\theta' + \Delta\theta - \delta_x z\theta] = 0 \tag{6.29}$$

$$\phi'' + Sc[f\phi' - Kr_x\phi] = 0 \tag{6.30}$$

Subject to the boundary conditions:

$$f(0) = R, \qquad z(0) = 1, \qquad \theta(0) = 1, \qquad \phi(0) = 1 \tag{6.31}$$

$$f(\infty) = 0, \qquad \theta(\infty) = 0, \qquad \phi(\infty) = 0 \tag{6.32}$$

The space of solution's domain is discretized in finite difference methods. By using the following notations: $\Delta\eta = h > 0$ to be the grid size in η-direction, $\Delta\eta = \frac{1}{N}$, with $\eta_i = ih$ for $i = 0, 1, 2, \ldots\ldots\ldots N$. Define $f_i = f(\eta_i)$, $z_i = z(\eta_i)$, $\theta_i = \theta(\eta_i)$, and $\phi_i = \phi(\eta_i)$. Let F_i, Z_i, Θ_i and ϕ_i represent the numerical values of f, z, θ and ϕ at the node i^{th} node, respectively. Then, we get

$$f'\big|_i \approx \frac{f_{i+1} - f_{i-1}}{2h}, \qquad z'\big|_i \approx \frac{z_{i+1} - z_{i-1}}{2h}, \tag{6.33}$$

$$\theta' \big|_i \approx \frac{\theta_{i+1} - \theta_{i-1}}{2h}, \qquad \phi' \big|_i \approx \frac{\phi_{i+1} - \phi_{i-1}}{2h}, \tag{6.34}$$

$$z'' \big|_i \approx \frac{z_{i+1} - 2z_i + z_{i-1}}{h^2}, \qquad \theta'' \big|_i \approx \frac{\theta_{i+1} - 2\theta_i + \theta_{i-1}}{h^2}, \tag{6.35}$$

$$\phi'' \big|_i \approx \frac{\phi_{i+1} - 2\phi_i + \phi_{i-1}}{h^2} \tag{6.36}$$

By using the FDM the main step is that the system of ordinary differential equations (6.27) -(6.30) is discretizes in space. Now, using the equations (6.33) -(6.36) into the equations (6.27) -(6.30) and omitting the truncation errors, finally we get the system of algebraic equations which are given for $(i = 0, 1, 2, \dots \dots \dots N)$:

$$F_{i+1} - F_{i-1} - 2hZ_i = 0 \tag{6.36}$$

$$Z_{i+1} - 2Z_i + Z_{i-1} + 0.5h[Z_{i+1} - Z_{i-1}] + h^2 \left[Gr_T \Theta_i + Gr_C \phi_i - Z_i^2 - \frac{1}{Da} Z_i\right] = 0 \tag{6.37}$$

$$\Theta_{i+1} - 2\Theta_i + \Theta_{i-1} + \frac{Pr}{1 + N_R} 0.5h[F_i(\Theta_{i+1} - \Theta_{i-1}) + 2h(\Delta\, \Theta_i - \delta_x\, Z_i \Theta_i)] = 0 \tag{6.38}$$

$$\phi_{i+1} - 2\phi_i + \phi_{i-1} + 0.5h\, Sc[F_i(\phi_{i+1} - \phi_{i-1}) - 2hKr_x \phi_i] = 0 \tag{6.39}$$

Also, the boundary conditions are:

$$F_0 = F_W, \qquad Z_0 = 1, \qquad \Theta_0 = 1, \qquad \phi_0 = 1 \tag{6.40}$$

$$F_N = F_{N-1}, \qquad Z_N = Z_{N-1}, \qquad \Theta_N = \Theta_{N-1}, \qquad \phi_N = \phi_{N-1} \tag{6.41}$$

The nonlinear system of algebraic equations are the system of equations (6.36) -(6.39) in the variables $F_i,\ Z_i,\ \Theta_i$ and ϕ_i. In our simulations we used the MATLAB package.

6.6 Numerical Results and Discussions

By using the similarity solution technique in MATLAB, the set of ordinary differential equations (6.22)- (6.23) with the boundary conditions (6.24)- (6.25) are solved numerically. Here the velocity, temperature and concentration are determined as a function of coordinate η. We have adopted a numerical procedure based on MATLAB for getting the solution of the differential equations (6.22)- (6.23) with the boundary conditions (6.24)- (6.25). The fundamental parameters that governed the flow are the Grashof number, Darcy number, Prandtl number, thermal radiation parameter, heat generation/absorption parameter, Schmidt number and chemical reaction parameter. According to study their effects, a

MATLAB programe is written to enumerate and produce the graphs for the velocity, temperature and concentration for different values of these parameters. Few delegate results are given in Figures 6.2-6.9.

6.6.1 Effect of Grashof Number Gr_T on Velocity, Temperature and Concentration Profiles

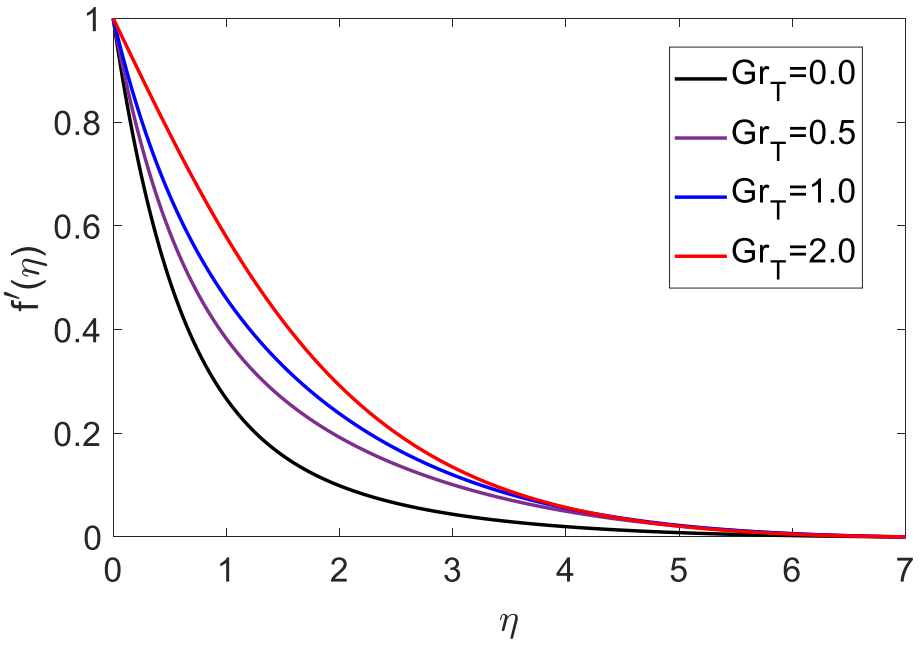

Figure 6.2: (a) Velocity profiles for different values of Grashof number Gr_T with fixed values of $Da = 0.8, F_W = 0.5,\ N_R = 1, \Delta = 0.5, Pr = 1.0, Sc = 0.5\ and\ Kr_x = 0.02$

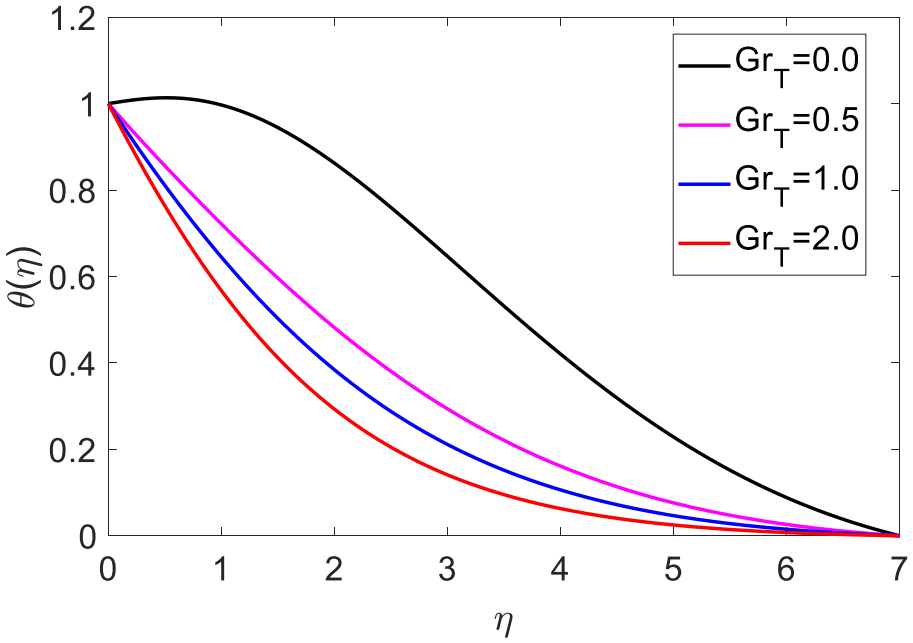

Figure 6. 2: (b) Temperature profiles for different values of Grashof number Gr_T with fixed values of $Da = 0.8, F_W = 0.5,\ N_R = 1,\ \Delta = 0.5, Pr = 1.0, Sc = 0.5\ and\ Kr_x =$

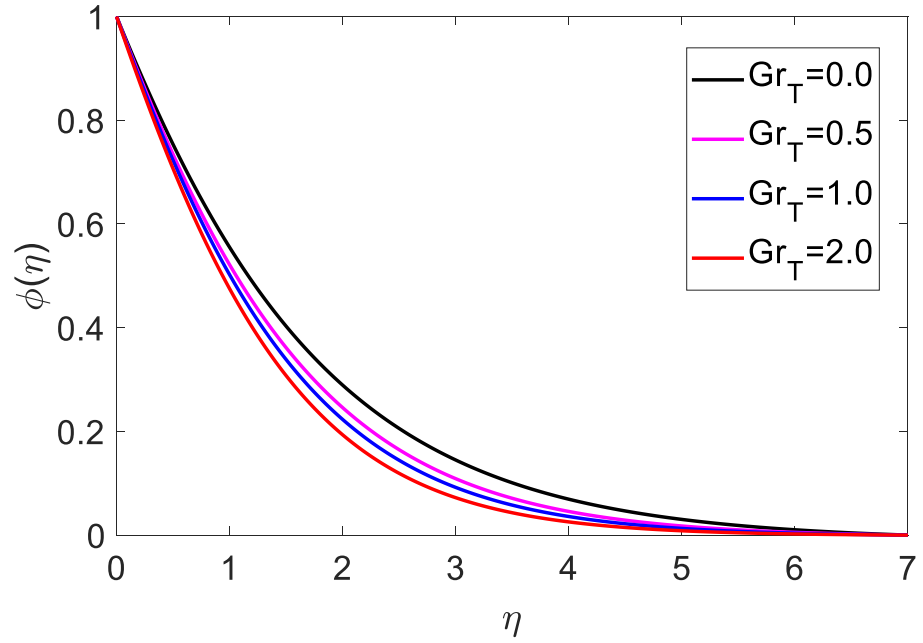

Figure 6.2: (c) Concentration profiles for different values of Grashof number Gr_T with fixed values of $Da = 0.8, F_W = 0.5,\ N_R = 1,\ \Delta = 0.5, Pr = 1.0, Sc = 0.5\ and\ Kr_x = 0.02$

Figures 6.2(a), (b) and (c) show the effects of the buoyancy force (Grashof number Gr_T) to the viscous forces of a typical velocity, temperature and concentration profiles in the

boundary layer, respectively. From Fig 6.2(a), it is clear that the momentum boundary layer thickness increases with increasing values of Gr_T enabling more flow. In Fig. 6.2(b), this figure represents increasing the value of Gr_T outcomes in thinning of thermal boundary layer associated with an increase in the wall temperature gradient and hence produces an increase in the heat transfer rate. It is noticed that the concentration boundary thickness decreases with an increase in the buoyancy force. It is due to fact that an increase in the values of the Grashof number has the tendency to increase the mass buoyancy effect. This gives rise to an increase in the induced flow and there by decrease the concentration which is shown in Figure 6.2(c).

6.6.2 Effect of Darcy Number *Da* on Velocity, Temperature and Concentration Profiles

The influence of Darcy number on velocity, temperature and concentration profiles are shown in Figure 6.3(a), (b) and (c), respectively. From Fig. 6.3(a), it is observed that the velocity increases with the increase of the Darcy parameter along the sheet and the reverse is true away from the sheet. The dimensionless temperature and concentration profiles are displayed in Fig. 6.3(b) and 6.3(c), respectively.

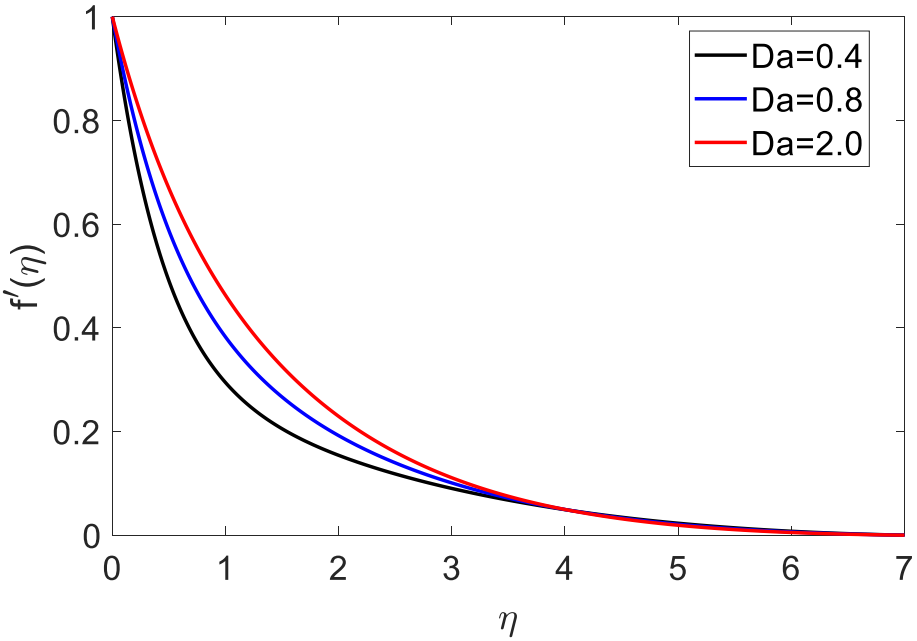

Figure 6.3: (a) Velocity profiles for different values of Darcy number *Da* with fixed values of $Gr_T = 0.5, F_W = 0.5,\ N_R = 1,\ \Delta = 0.5, Pr = 1.0, Sc = 0.5\ and\ Kr_x =$

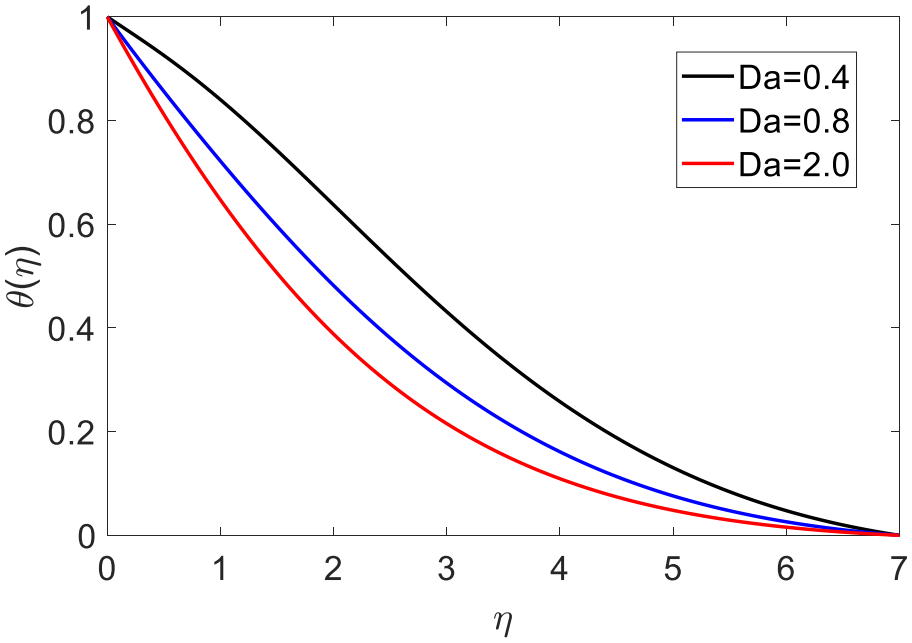

Figure 6.3: (b) Temperature profiles for different values of Darcy number *Da* with fixed values of $Gr_T = 0.5, F_W = 0.5,\ N_R = 1,\ \Delta = 0.5, Pr = 1.0, Sc =$

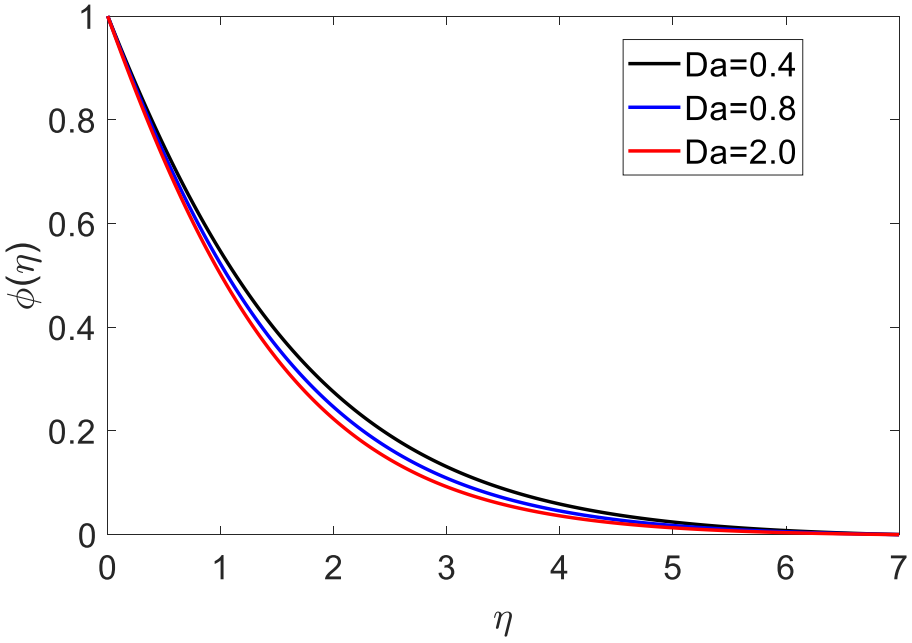

Figure 6.3: (c) Concentration profiles for different values of Darcy number *Da* with fixed values of $Gr_T = 0.5, F_W = 0.5,\ N_R = 1,\ \Delta = 0.5, Pr = 1.0, Sc = 0.5\ and\ Kr_x = 0.02$

6.6.3 Influence of Suction/Blowing F_W on Velocity, Temperature and Concentration Profiles

The influence of suction/blowing parameter F_W on velocity, temperature and concentration profiles is shown in Figures 6.4(a), (b) and (c), respectively. From Fig. 6.4(a) it is observed that the hydrodynamic boundary layer which shows an increase in the fluid velocity when the imposition of the wall fluid injection increases. However, the exact opposite behavior is produced by imposition of wall fluid suction. From Fig. 6.4(b), it is observed that with an increase the injection parameters the temperature increases, and the temperature decreases the suction parameter decreases. The same behavior arises for the concentration profiles which is shown in Fig. 6.4(c).

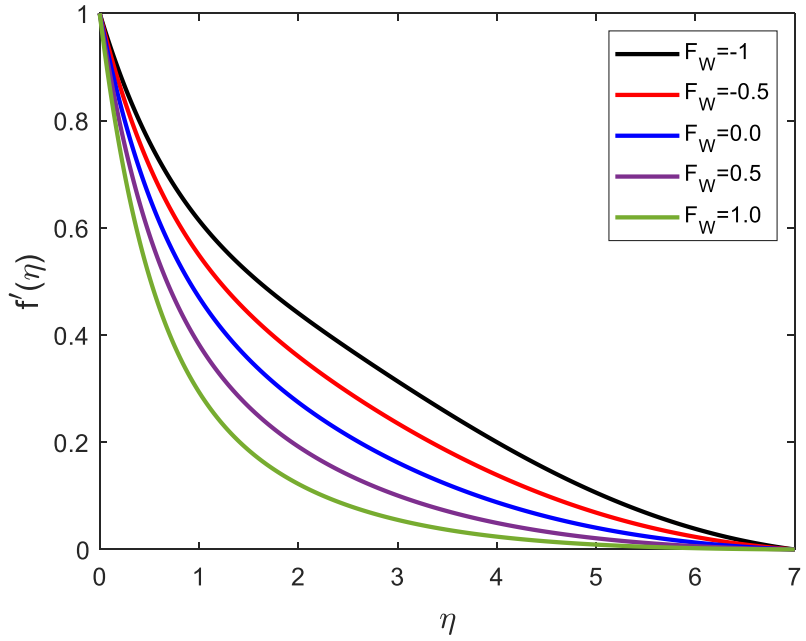

Figure 6.4: (a) Velocity profiles for different values of suction/blowing parameter F_W with fixed values of $Da = 0.8,\ N_R = 1, Gr_T = 0.5,\ \Delta = 0.5, Pr = 1.0, Sc = 0.5\ and\ Kr_x = 0.02$

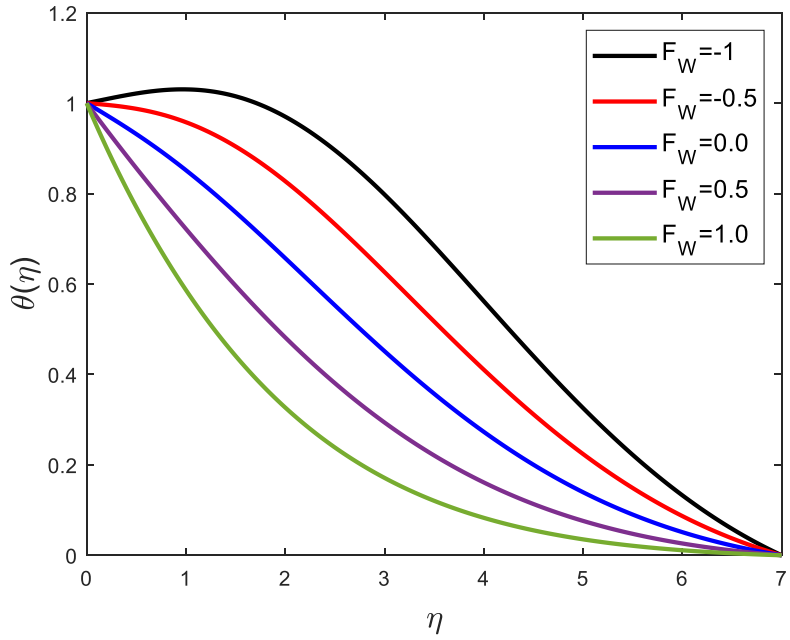

Figure 6.4: (b) Temperature profiles for different values of suction/blowing parameter F_W with fixed values of $Da = 0.8, Gr_T = 0.5,\ N_R = 1,\ \Delta = 0.5, Pr = 1.0, Sc = 0.5\ and\ Kr_x = 0.02$

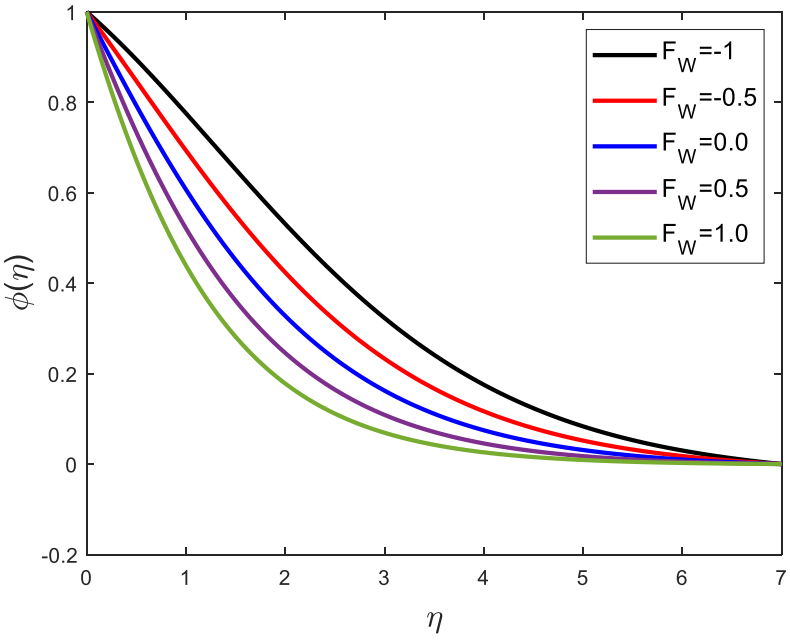

Figure 6.4: (c) Concentration profiles for different values of suction/blowing parameter F_W with fixed values of $Da = 0.8, Gr_T = 0.5,\ N_R = 1, \Delta = 0.5, Pr = 1.0, Sc = 0.5\ and\ Kr_x = 0.02$

6.6.4 Effect of Heat Generation ($\Delta > 0$) and Heat Absorption ($\Delta < 0$) on Velocity, Temperature and Concentration Profiles

Figures 6.5(a), (b) and (c) represent the effect of heat generation ($\Delta > 0$) or heat absorption ($\Delta < 0$) in the boundary layer on the velocity, temperature and concentration profiles. From Fig 6.5(a), it is observed that increasing the heat generation the fluid velocity increase and for the case of absorption parameter increases the velocity decrease. With an increase the heat generation the temperature increase. This increase in the fluid temperature causes more induced flow towards the plate through the thermal buoyancy effect which shown in Fig. 6.5(b). From Fig. 6.5(c) it is clearly observed that increasing the heat generation parameter the concentration decreases and for absorption increasing there is unchanged in concentration profile.

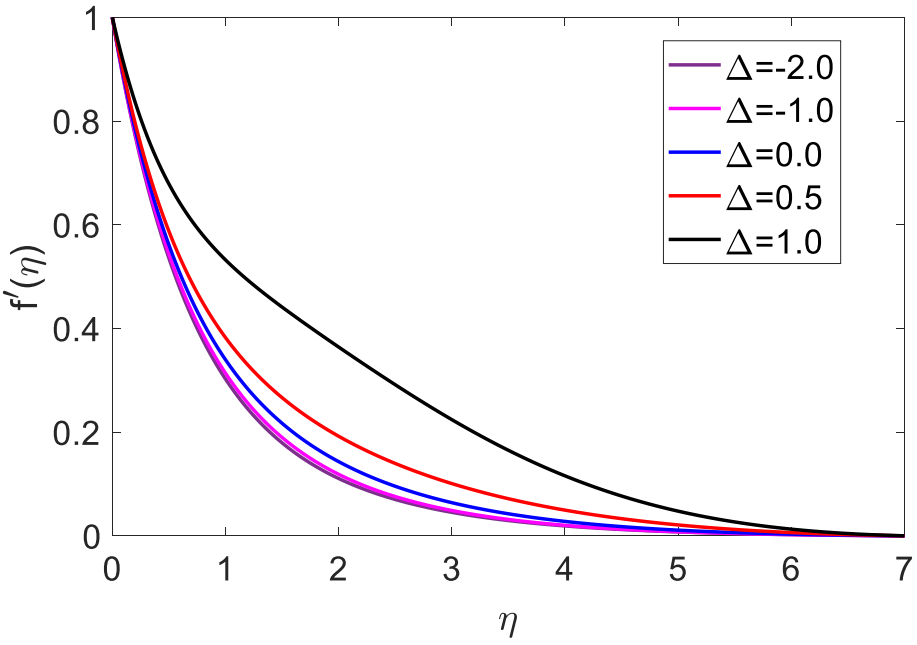

Figure 6.5(a): Velocity profiles for different values of heat generation/absorption parameter Δ with fixed values of $Da = 0.8, F_W = 0.5,\ N_R = 1,\ Gr_T = 0.5, Pr = 1.0, Sc = 0.5\ and\ Kr_x = 0.02$

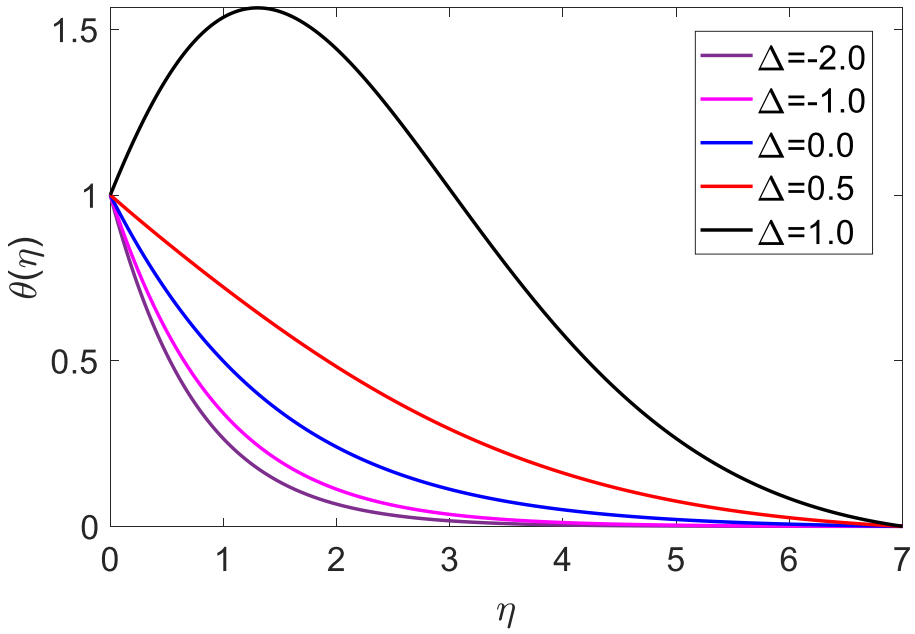

Figure 6.5 (b): Temperature profiles for different values of heat generation/absorption parameter Δ with fixed values of $Da = 0.8, Gr_T = 0.5, F_W = 0.5,\ N_R = 1,\ Pr = 1.0, Sc = 0.5\ and\ Kr_x = 0.02$

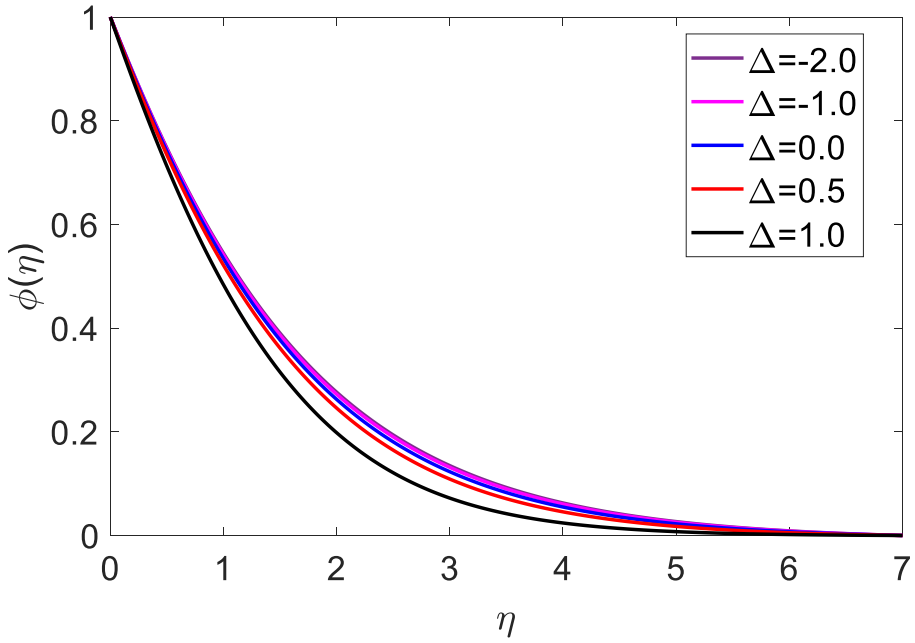

Figure 6.5(c): Concentration profiles for different values of heat generation/absorption parameter Δ with fixed values of $Da = 0.8, Gr_T = 0.5,\ F_W = 0.5,\ N_R = 1,\ Pr = 1.0, Sc = 0.5\ and\ Kr_x = 0.02$

6.6.5 Effect of Prandtl Number *Pr* on Temperature Profiles

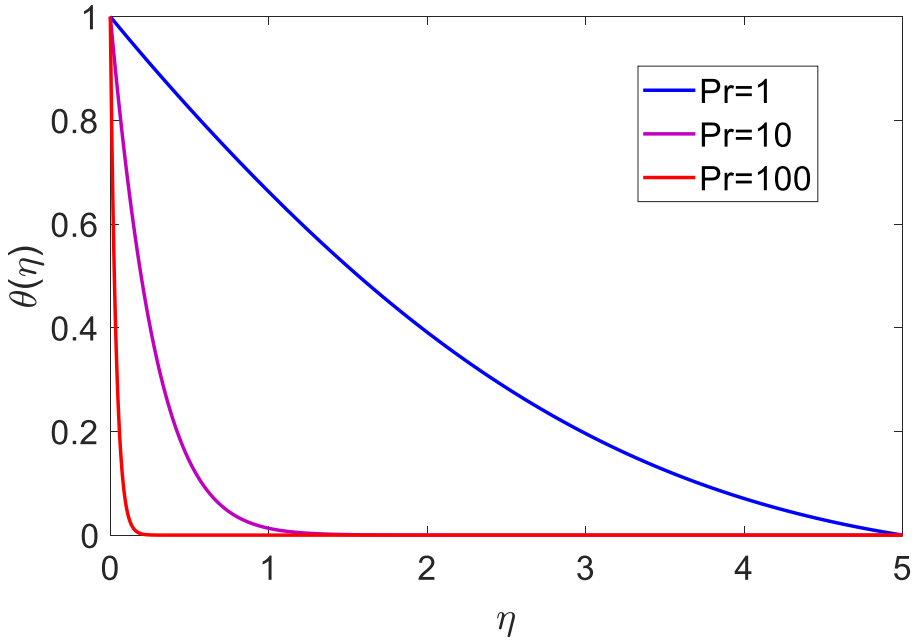

Figure 6.6: Temperature profiles for different values of Prandtl number *Pr* with fixed values of $Da = 0.8, Gr_T = 0.5,\ F_W = 0.5,\ N_R = 1,\ \Delta = 0.5, N_R = 1.0, Sc = 0.5\ and\ Kr_x = 0.02$

Figure 6.6 demonstrates the effect of the Prandtl number Pr on the temperature profile. It is observed that with the increase of Prandtl number the temperature decrease. This because a fluid with large Prandtl number possesses large heat capacity, and hence augments the heat transfer.

6.6.6 Effect of Radiation Parameter N_R on Temperature Profiles

Figure 6.7 represents the effect of the radiation parameter N_R on the dimensionless temperature $\theta(\eta)$. It is clearly noticed that the increase of the radiation parameter N_R leads an increase in the temperature at any point. This is due to fact that higher surface heat flux and thereby increasing the temperature of the fluid when the thermal radiation parameter increases.

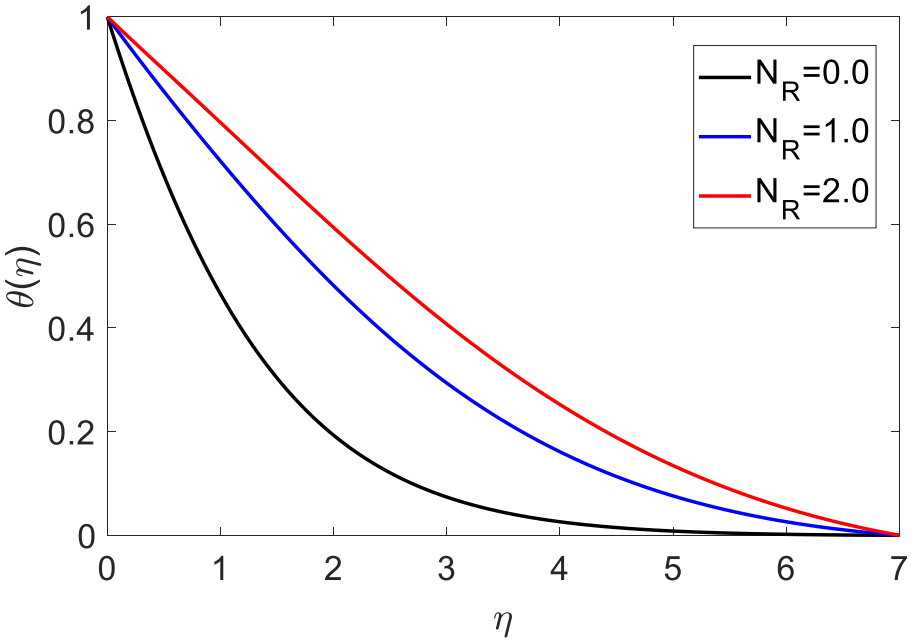

Figure 6.7: Temperature profiles for different values of radiation parameter N_R with fixed values of $Da = 0.8, Gr_T = 0.5, F_W = 0.5,\ \Delta = 0.5, Pr = 1.0, Sc = 0.5\ and\ Kr_x = 0.02$

6.6.7 Effect of Schmidt Number *Sc* on Concentration Profiles

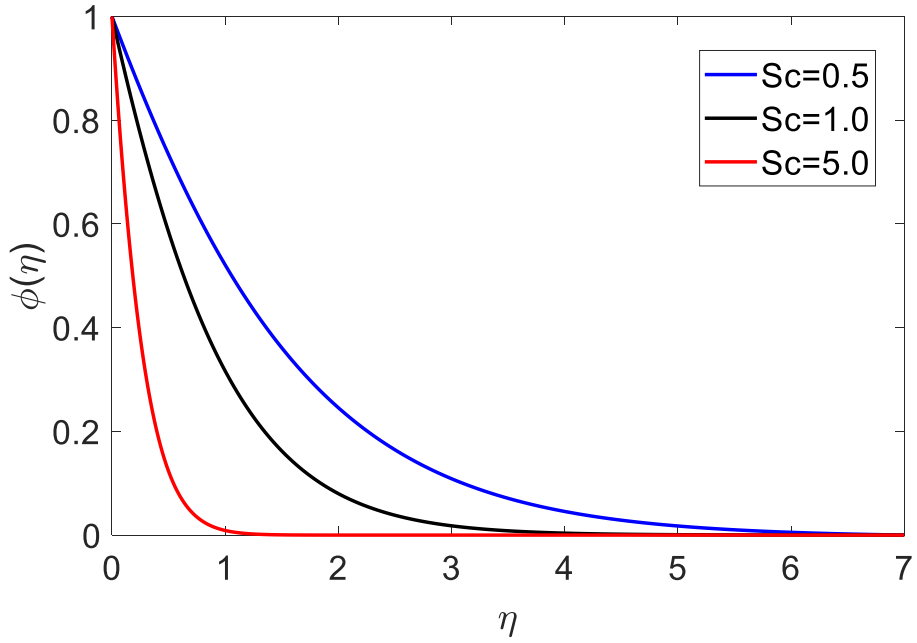

Figure 6.8: Concentration profiles for different values of Schmidt number Sc with fixed values of $Da = 0.8, Gr_T = 0.5, F_W = 0.5,\ N_R = 1,\ \Delta = 0.5, Pr = 1.0, N_R = 0.5\ and\ Kr_x = 0.02$

The variation of the dimensionless concentration against η for different values of the Schmidt number *Sc* are displayed in Figure 6. 8. It is clearly observed that with an increase the Schmidt number the concentration decreases. Diffusion coefficient is inversely proportional to the Schmidt number. A smaller diffusion coefficient corresponds to an increase in Schmidt number. Such smaller diffusion coefficient creates a reduction in the concentration.

6.6.8 Effect of Chemical Reaction Parameter Kr_x on Concentration Profiles

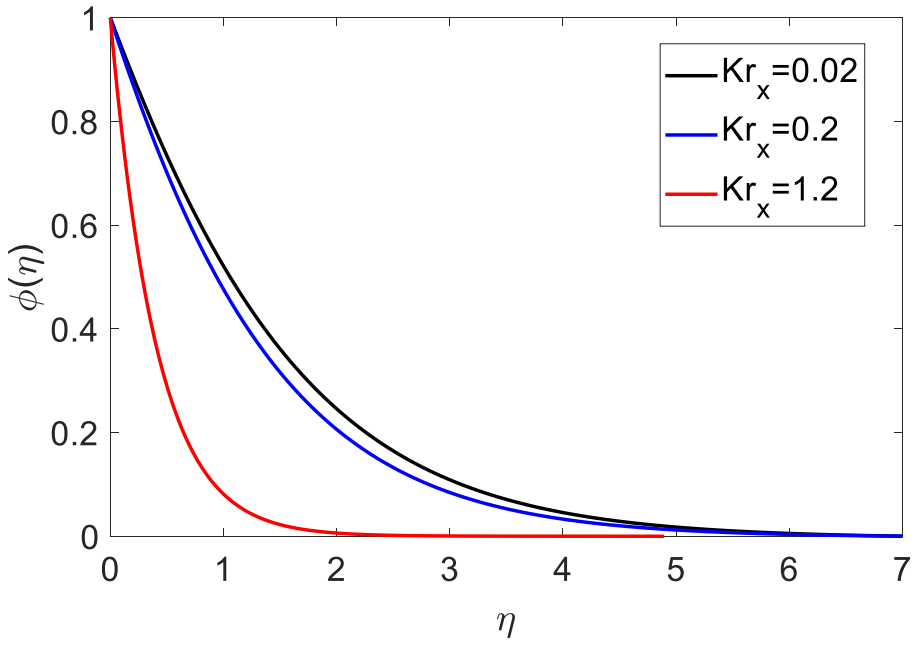

Figure 6.9: Concentration profiles for different values of chemical reaction Kr_x with fixed values of $Da = 0.8, Gr_T = 0.5,\ F_W = 0.5,\ N_R = 1,\ \Delta = 0.5, Pr = 1.0, N_R = 0.5\ and\ Sc = 0.5$

Figure 6.9 illustrate the effect of the chemical reaction parameter on the concentration profile. From Fig. 6.9, it is clearly seen that the concentration and its associated boundary layer thickness are decreasing functions of chemical reaction. Chemical reaction increases the rate of interfacial mass transfer. The concentration gradient and its flux increasing when the chemical reaction reduces the local concentration. Finally, with an increase in the chemical reaction parameter the concentration of the chemical species in the boundary layer decreases.

6.6.9 Variation of Physical Parameters

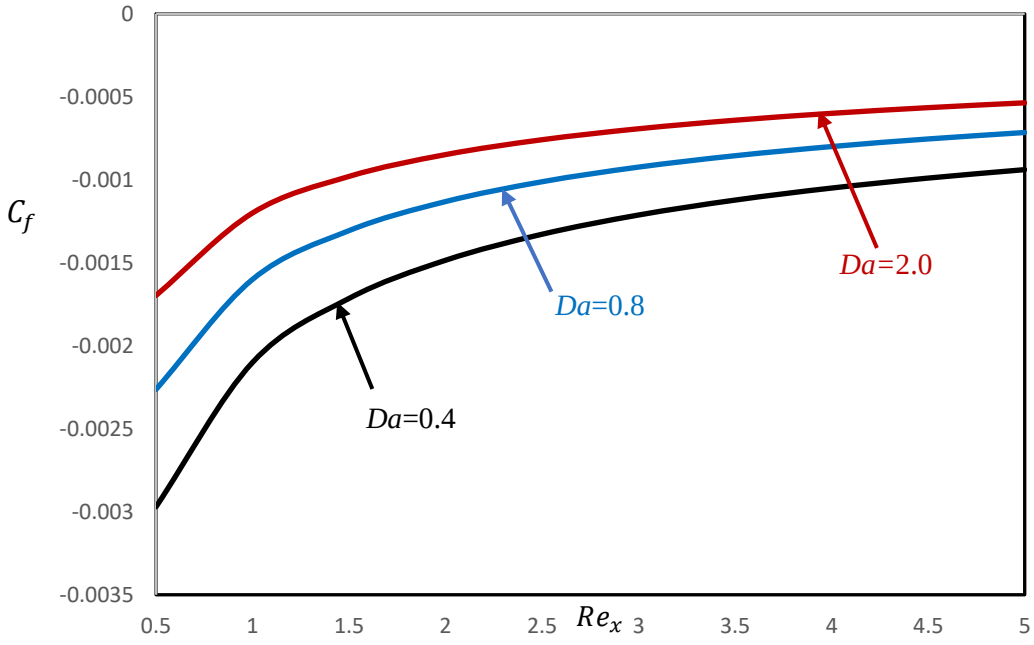

Figure 6.10: Variation of Skin-friction C_f with Local Reynolds number Re_x for various Darcy number *Da*

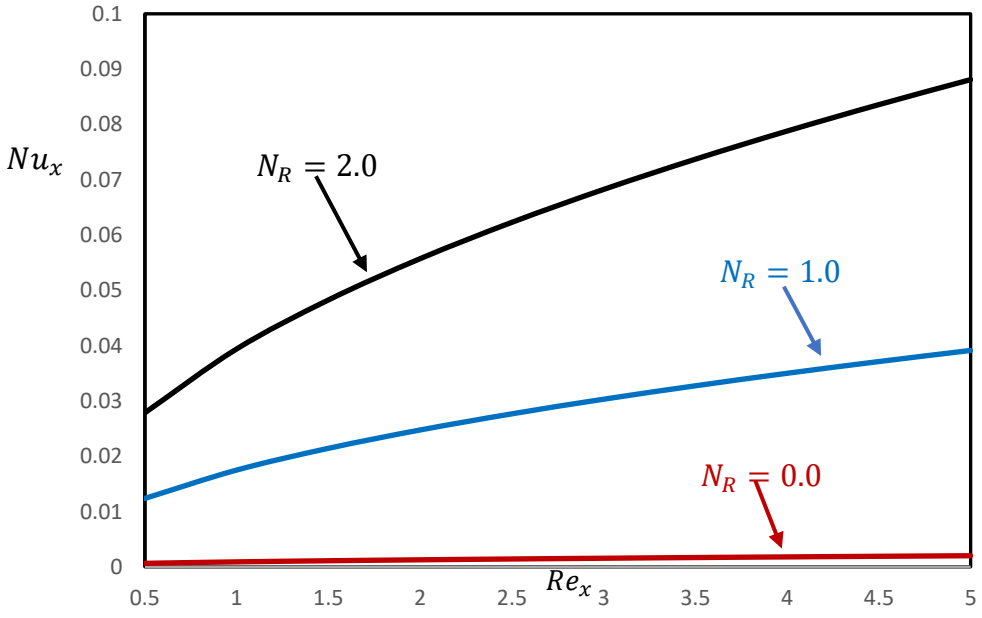

Figure 6.11: Variation of local Nusselt number Nu_x with Local Reynolds number Re_x for various thermal radiation parameter N_R

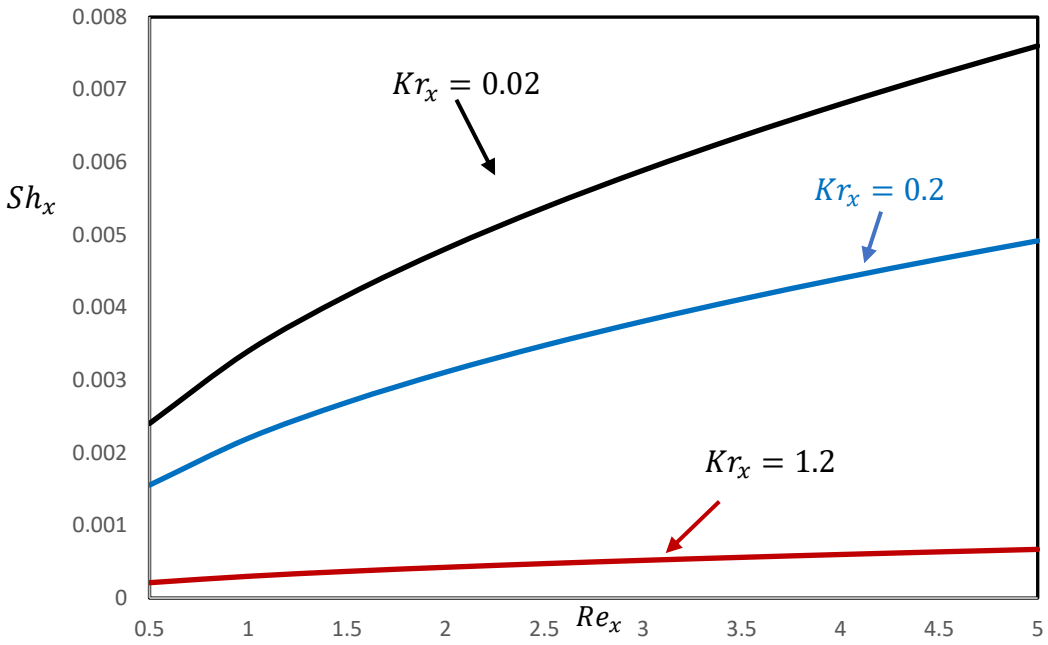

Figure 6.12: Variation of local Sherwood number Sh_x with Local Reynolds number Re_x for various thermal radiation parameter Kr_x

Figure 6.10 illustrates the effect of the Darcy number *Da* on the skin-friction versus the local Reynolds number. With an increase the Darcy number the skin-friction increase along the local Reynolds number. This is because that a porous media produces a resistive type of force which causes the increase of the skin-friction. Figure 6.11 represents the effect of the radiation parameter N_R on the Nusselt number Nu_x along the local Reynolds number Re_x. With an increase the thermal radiation parameter, the Nusselt number Nu_x increases along the local Reynolds number. This is due to fact that for increasing thermal radiation larger heat transfer rates are achieved. Also, with an increase the chemical reaction Kr_x the local. Sherwood number Sh_x decrease along the local Reynolds number Re_x.This is because, for increasing the Chemical reaction parameter smaller mass flow rates are achieved which is shown in Figure 6.12.

Table 6.1: Values proportional to the coefficients of skin-friction ($f''(0)$), rate of heat transfer ($-\theta'(0)$) and the magnitude of the local Sherwood number ($-\phi'(0)$) with the variation of Grashof number Gr_T (for fixed $Da = 0.8, Pr = 1, Kr_x = 0.02$ and $Sc = 0.5$)

Gr_T	$f''(0)$	$-\theta'(0)$	$-\phi'(0)$
0.0	-0.0014	-0.0650	-0.0072
0.5	-0.0032	-0.0175	-0.0034
1.0	-0.0029	-0.0096	-0.0022
2.0	-0.0023	-0.0044	-0.0013

Table 6.2: Values proportional to the coefficients of skin-friction ($f''(0)$), rate of heat transfer ($-\theta'(0)$) and the magnitude of the local Sherwood number ($-\phi'(0)$) with the variation of Darcy parameter Da (for fixed, S=0.8, Pr=1.0, $N_R = 1$ and Sc=0.5)

Da	$f''(0)$	$-\theta'(0)$	$-\phi'(0)$
0.4	-0.0042	-0.0334	-0.0052
0.8	-0.0032	-0.0175	-0.0034
2.0	-0.0024	-0.0101	-0.0023

Table 6.3: Values proportional to the coefficients of skin-friction ($f''(0)$), rate of heat transfer ($-\theta'(0)$) and the magnitude of the local Sherwood number ($-\phi'(0)$) with the variation of radiation parameter N_R (for fixed $Da = 0.8, Pr = 1, Kr_x = 0.02$ and $Sc = 0.5$)

N_R	$f''(0)$	$-\theta'(0)$	$-\phi'(0)$
0.0	-0.0012	-0.0009	-0.0052
1.0	-0.0032	-0.0175	-0.0034
2.0	-0.0052	-0.0394	-0.0028

Table 6.4: Values proportional to the coefficients of skin-friction ($f''(0)$), rate of heat transfer ($-\theta'(0)$) and the magnitude of the local Sherwood number ($-\phi'(0)$) with the variation of Chemical reaction Kr_x (for fixed $Da = 0.8, Pr = 1, Kr_x = 0.02$ and $Sc = 0.5$)

Kr_x	$f''(0)$	$-\theta'(0)$	$-\phi'(0)$
0.02	-0.0032	-0.0175	-0.0034
0.2	-0.0032	-0.0175	-0.0022
1.2	-0.0032	-0.0175	-0.0003

6.7 Conclusions

In this present research, we are tried to investigate the effect of various non-dimensional numbers on the non-dimensional velocity, temperature and concentration fields. The higher values of heat generation parameter result in higher velocity and temperature distributions and lower concentration distribution. For the higher absorption the velocity and temperature decrease. The concentration gradient and its flux increasing when the chemical reaction reduces the local concentration. Finally, with an increase in the chemical reaction parameter the concentration of the chemical species in the boundary layer decreases. A fluid with large Prandtl number possesses large heat capacity, and hence augments the heat transfer. Moreover, as the thermal radiation increase larger heat transfer rate is achieved as well as the chemical reaction increase smaller mass flow rate is achieved.

References

[1] L. J. Crane, "Flow past a stretching plate," Zeitschrift fur angewandte Mathematik und Physik", vol. 12, pp. 645–647, 1970.

[2] M. K. Laha, P. S. Gupta, and A. S. Gupta, "Heat transfer characteristics of the flow of an incompressible viscous fluid over a stretching sheet," Warme und Stoffubertrag, vol. 24, no. 3, pp. 151–153, 1989.

[3] N. Afzal, "Heat transfer from a stretching surface," International Journal of Heat and Mass Transfer, vol. 36, no. 4, pp. 1128–1131, 1993.

[4] K. V. Prasad, A. S. Abel, and P. S. Datti, "Diffusion of chemically reactive species of non-Newtonian fluid immersed in a porous medium over a stretching sheet," The International Journal of Non-Linear Mechanics, vol. 38, no. 5, pp. 651–657, 2003.

[5] M. S. Abel and N. Mahesha, "Heat transfer in MHD viscoelastic fluid flow over a stretching sheet with variable thermal conductivity, non-uniform heat source and radiation," Applied Mathematical Modelling, vol. 32, no. 10, pp. 1965–1983, 2008.

[6] P. G. Abel, Siddheshwar, and M. M. Nandeppanava, “Heat transfer in a viscoelastic boundary layer flow over a stretching sheet with viscous dissipation and non-uniform heat source,” International Journal of Heat and Mass Transfer, vol. 50, no. 5-6, pp. 960–966, 2007.

[7] R. Cortell, “Viscoelastic fluid flow and heat transfer over a stretching sheet under the effects of a nonuniform heat source, viscous dissipation and thermal radiation,” International Journal of Heat and Mass Transfer, vol. 50, no. 15-16, pp. 3152–3162, 2007. 8. C. Wang, “Analytic solutions for a liquid film on an unsteady stretching surface,” Heat and Mass Transfer, vol. 42, pp. 43–48, 2006.

[8] C. Wang, “Analytic solutions for a liquid film on an unsteady stretching surface,” Heat and Mass Transfer, vol. 42, pp. 43–48, 2006.

[9] M. A. Hossain, M. A. Alim, and D. A. S. Rees, “The effect of radiation on free convection from a porous vertical plate,” International Journal of Heat and Mass Transfer, vol. 42, no. 1, pp. 181–191, 1999.

[10] H. I. Andersson, J. B. Aarseth, N. Braud, and B. S. Dandapat, “Flow of a power-law fluid film on an unsteady stretching surface,” Journal of Non-Newtonian Fluid Mechanics, vol. 62, no. 1, pp. 1–8, 1996.

[11] H. I. Andersson, J. B. Aarseth, and B. S. Dandapat, “Heat transfer in a liquid film on unsteady stretching surface,” International Journal of Heat and Mass Transfer, vol. 43, no. 1, pp. 69–74, 2000.

[12] B. S. Dandapat, B. Santra, and H. I. Andersson, “Thermocapillary in a liquid film on an unsteady stretching surface,” International Journal of Heat and Mass Transfer, vol. 46, pp. 3009–3015, 2003.

[13] R. Tsai, K. H. Huang, and J. S. Huang, “Flow and heat transfer over an unsteady stretching surface with non-uniform heat source,” International Communications in Heat and Mass Transfer, vol. 35, no. 10, pp. 1340–1343, 2008.

[14] E. M. A. Elbashbeshy and M. A. A. Bazid, “Heat transfer over an unsteady stretching surface with internal heat generation,” Applied Mathematics and Computation, vol. 138, no. 2-3, pp. 239–245, 2003.

[15] Yahaya Shagaiya Daniel and Simon K. Daniel, “Effects of buoyancy and thermal radiation on MHD flow over a stretching porous sheet using homotopy analysis method”, Alexandria Engineering Journal, Vol. 54, pp. 705-712.

[16] Cheng, W.T., Liu, C.H., “Unsteady mass transfer in mixed convective heat flow from a vertical plate embedded in a liquid saturated porous medium with melting effect”, Int. Commun. Heat Mass Transfer Vol. 35, pp. 1350–1354, 2008.

[17] Chamkha, A.J., Ahmed, S.A., Aloraier, A.S., 2010. Melting and radiation effects on mixed convection from a vertical surface embedded in a non-Newtonian fluid saturated non-Darcy porous medium for aiding and opposing eternal flows, Int. J. Phys. Sci. Vol. 5, pp. 1212–1224.

[18] Md. Hasanuzzaman and Akio Miyara, 2017. Similarity solution of natural convective boundary layer flow around a vertical slender body with suction and blowing, J. Mech. Cont. & Math. Sci., 11, 8-22.

CHAPTER SEVEN

CONCLUSIONS AND RECOMMODATION

7.1 Conclusions

A two-dimensional numerical simulation of wavy liquid film flowing along an inclined porous wall has been performed. We investigated the effect of several parameters on the film thickness. In solid substrate, a small disturbance generated at the inflow grows to a solitary wave consisting of a big-amplitude roll wave and the small-amplitude short capillary waves, where as in porous wall only the solitary waves are observed and in low frequency, wave front is steeper than wave rear. Moreover, symmetrical waves are observed in the case of high frequency. For the low porosity the wave front is steeper than the wave rear. The principal effect of the porous substrate on the film flow is to displace the liquid-porous interface to an effective liquid-solid interface located at the lower boundary of the upper momentum boundary layer in the porous medium.

In chapter four, the analytical and numerical solutions of the considered problems which have been obtained by using similarity solution technique in MATLAB. Similarity transformations were used to convert the partial differential equations describing the problem into a system of ordinary differential equations. In liquid film region, with an increase of the gravitational force the velocity decrease and enhancing the temperature. Also, a fluid with large Prandtl number possesses small heat capacity, and hence reduce the heat transfer. The velocity decreases with an increase of the Darcy number. This is due to fact that the porous medium produces a resistive type of force which causes a reduction in the fluid velocity. Where as in gas stream region, large Prandtl fluids possess lower thermal diffusivity and smaller Prandtl fluids have higher thermal diffusivity. The concentration decreases with an increase of the Lewis number. This is because with decrease diffusivity the concentration decrease. Moreover, the Prandtl number in liquid region increase the larger heat transfer rate is achieved and the Lewis number increase the smaller mass transfer rate is achieved.

Influence of triple stratification in the falling film flow on a porous medium with heat generation and absorption, thermal radiation and chemical reaction are examined in Chapter Five. The velocity and concentration increase as well as temperature decreases with an

increase in Froude number. This is due to fact that influence of the gravitation force enhancing the velocity and concentration as well as reduce the temperature of the fluid. With an increase the heat generation the temperature increases. This increase in the fluid temperature causes more induced flow towards the plate through the thermal buoyancy effect. For the case of absorption, the temperature decreases with an increase the absorption. The increase in the radiation parameter implies higher surface heat flux and there-by decreasing the temperature of the fluid. An increase in the chemical reaction effects increases the concentration within the thermal boundary layer region. This is because increasing the chemical reaction rate causes a thickening of the mass transfer boundary layer. In addition, for the absorption and Schmidt number increase, larger heat transfer rate and mass flow rate are achieved.

In chapter six, we are tried to investigate the effect of various non-dimensional numbers on the non-dimensional velocity, temperature and concentration fields. The higher values of heat generation parameter result in higher velocity and temperature distributions and lower concentration distribution. For the higher absorption the velocity and temperature decrease. The concentration gradient and its flux increasing when the chemical reaction reduces the local concentration. Finally, with an increase in the chemical reaction parameter the concentration of the chemical species in the boundary layer decreases. A fluid with large Prandtl number possesses large heat capacity, and hence augments the heat transfer. Moreover, as the thermal radiation increase larger heat transfer rate is achieved as well as the chemical reaction increase smaller mass flow rate is achieved.

7.2 Recommendation

Recommendations for future work based on the present study are:

Numerical simulations are performed for two-dimensional falling film along an incline porous wall as shown in chapter 2. It is necessary to carry out three-dimensional simulations with larger simulation domain. Characteristics of these types of waves are required to investigate. Energy analysis of 3D simulation may reveal the characteristics of various energies in the transformation from 2D to 3D waves.